ELUCIDATION OF SPECIFIC CYTOTOXIC EFFECTS OF β-β -DIMETHYLACRYLSHIKONIN IN MELANOMA AND CHORDOMA CELLS

DISSERTATION

Submitted by
Alexander STALLINGER, MSc.

for the Academic Degree of
Doctor of Medical Science
(Dr. scient. med.)

at the
Medical University of Graz
Department of Biomedical Research

under the Supervision of
Assoc. Prof. Dr. Beate RINNER

2019

„Ich kam, sah, und traute meinen Augen nicht“

Julius Cäsar in Asterix bei den Briten

Statutory Declaration

I hereby declare that this thesis is my own original work and that I have fully acknowledged by name all of those individuals and organisations that have contributed to the research for this thesis. Due acknowledgement has been made in the text to all other material used. Throughout this thesis and in all related publications I followed the "Standards of Good Scientific Practice and Ombuds Committee at the Medical University of Graz".

Date, Place Signature

Disclosures

Part of this thesis was published in Jahanafrooz Z, Stallinger A, Anders I, Kleinegger F, Lohberger B, Durchschein C, Bauer R, Deutsch A, Rinner B, Kretscher N. 2018. Influence of silibinin and β-β-dimethylacrylshikonin on chordoma cells. Phytomedicine. 2018;49:32–40.

Part of this thesis is currently submitted for publication as Stallinger A, Kleinegger F, Brvar L, Liegl-Atzwanger B, Prokesch A, Durchschein C, Bauer R, Deutsch A, Kretschmer N, Rinner B. β-β-Dimethylacrylshikonin induces Apoptosis in Melanoma Cell Lines by NOXA Upregulation, manuscript submitted

Author affiliations:
Anders Ines[a], Bauer Rudolf[b], Brvar Luka[a], Deutsch Alexander[c], Durchschein Christin[b], Jahanafrooz Zohreh[d], Kleinegger Florian[e], Kretschmer Nadine[b], Liegl-Atzwanger Bernadette[e], Lohberger Birgit[f], Prokesch Andreas[g,h], Rinner Beate[a]

[a]Division of Biomedical Research, Medical University Graz, Graz, Austria
[b]Department of Pharmacognosy, Institute of Pharmaceutical Sciences, University of Graz, Graz, Austria
[c]CBmed Center for Biomarker Research in Medicine, Division of Hematology, Medical University of Graz, Graz, Austria
[d]Immunology Research Center, Tabriz University of Medical Sciences, Tabriz, Iran;

Department of Biotechnology, Higher Education Institute of Rab-Rashid, Tabriz, Iran.
[e]Institute of Pathology, Medical University of Graz, Graz, Austria
[f]Department of Orthopedics and Trauma, Medical University Graz, Graz, Austria.
[g]Gottfried Schatz Research Center for Cell Signaling, Metabolism & Aging, Medical University of Graz, Graz, Austria
[h]BioTechMed-Graz, Graz, Austria

Acknowledgements

First of all, I would like to thank Beate Rinner for her supervision and guidance throughout my thesis.

My special thanks goes to the members of the Core Facility APCI, namely Luka Brvar, Silke Schrom, Ines Anders, Katharina Meditz, Marie Therese-Frisch, and Stefanie Wallner, for helping me with the experiments. Furthermore, I would like to thank Alexander Deutsch and Rudolf Bauer for their guidance as dissertation committee members. Andreas Prokesch, Birgit Lohberger, Heike Kaltenegger and Dietmar Glänzer have my gratitude for helping with - and partly performing - the western blot experiments. I would further like to convey my thanks to Georg Singer who provided the foreskin samples needed for melanocyte primary cultures. My thanks also goes to Nadine Kretschmer and Christin Durchschein, who provided DMAS for all experiments.

Last but not least I would like to thank Amby, Arik and my parents for supporting me throughout my thesis.

Doctoral student Alexander Stallinger received funding from the Austrian Science Fund (FWF, P 27505-B31) and the Medical University of Graz through the Doctoral School Molecular Medicine and Inflammation.

Table of Contents

Abbreviations

°C	Degree Celsius
µg	Micro Gram
µl	Micro Litre
µM	Micro Molar
2D	Two-dimensional
ACS	American Cancer Society
ACTB	Actin Beta
AF488	Alexa Fluor 488
AKT	AKT Serine/Threonine Kinase
AMA	American Medical Association
BAD	BCL2 associated Agonist of Cell Death
BAK	BCL2 Antagonist/Killer
BAX	BCL2 associated X Protein
BCA	Bicinchoninic Acid Assay
BCC	Basal Cell Carcinoma
BCL2	B cell Leukaemia/Lymphoma 2
BH	Benjamini-Hochberg
BH3	BCL2 Homology 3
BRAF	B-Raf Proto-oncogene
BSA	Bovine Serum Albumin
C	Control
CCS	Chordoma Cancer Society
CD	Circular Dichroism
CDK4	Cyclin dependent Kinase 4
CDKN2A	Cyclin dependent Kinase 2A
cDNA	Complementary Deoxyribonucleic Acid
c-MYC	MYC Proto-Oncogene
CO2	Carbon Dioxide
Cq	Quantitation Cycles

CRAF	Raf-1 Proto-Oncogene, Serine/Threonine Kinase
CYC	Cytochrome C
DMAS	β-β-Dimethylacrylshikonin
DMEM	Dulbecco's Modified Eagle Medium
DMSO	Dimethyl Sulfoxide
DNA	Deoxyribonucleic Acid
DNase-I	Deoxyribonuclease I
EDTA	Ethylenediaminetetraacetic Acid
ERK	Extracellular Signal-regulated Kinase
Ex/EM	Extinction/Emission
EZ4U	EZ4U Cell Proliferation and Cytotoxicity Assay
f	Fold Change
FACS	Fluorescence activated Cell Sorting
FBS	Fetal Bovine Serum
FGF2	Fibroblast Growth Factor 2
FTI	Farnesyltransferase Inhibitors
g	Gravitational Force
GAPDH	Glyceraldehyde 3-phosphate Dehydrogenase
GO	Gene Overrepresentation
GOI	Gene of Interest
h	Hours
H&E	Haematoxylin & Eosin
HPLC	High-performance Liquid Chromatography
IC_{50}	Half maximal inhibitory Concentration
IMDM	Iscove´s modified Dulbecco´s medium
kD	Kilo Dalton
kg	Kilo Gram
KI67	Marker Of Proliferation Ki-67
LE	Lithospermum erythrorhizon
MAP	Mitogen-activated Protein
MAPK	Mitogen-activated Protein Kinase
MCL1	Myeloid Cell Leukemia Sequence 1
MEK	Mitogen-activated Protein Kinase Kinase
Mg	Milligram
Min	Minutes
ml	Millilitre
mM	Millimolar

Mm	Millimetre
MRC-5	Medical Research Council Cell Strain 5
mRNA	Messenger Ribonucleic Acid
mTOR	Mammalian Target of Rapamycin
MTS	3-(4,5-dimethylthiazol-2-yl)-5-(3-carboxymethoxyphenyl)-2-(4-sulfophenyl)-2H-tetrazolium
MTT	3-(4,5-dimethylthiazol-2-yl)-2,5-diphenyltetrazolium
MUG-CC1	Medical University Graz Clival Chordoma 1
MUG-Chor1	Medical University Graz Chordoma 1
MUG-Mel1/MUG-Mel2	Medical University Graz Melanoma 1/ Melanoma 2
NC	No Transfection, no DMAS Treatment
NF-kB	Nuclear Factor Kappa B Subunit 1
nm	Nanometre
nM	Nanomolar
NMR	Nuclear Magnetic Resonance
NOXA	NADPH Oxidase Activator
NRAS, HRAS, KRAS	N-Rat Sarcoma/ H-Rat Sarcoma/ K-Rat Sarcoma
NRT	No reverse Transcriptase
NT	No Transfection, DMAS Treatment
OP	Onosma Paniculata
P	P-value
p38	Tumour Protein P38
p53	Tumour Protein p53
PBS	Phosphate Buffered Saline
PCR	Polymerase Chain Reaction
PDK1	Phosphoinositide-dependent Kinase-1
PI3K	Phosphatidylinositol-3-kinases
PTCH	Patheched 1
PTEN	Phosphatase and Tensin Homolog
PUMA	p53 upregulated Modulator of Apoptosis
RAF	Rapidly accelerated Fibrosarcoma
RAS	Rat Sarcoma
RC	NOXA siRNA transfected, no DMAS Treatment
RPMI	Roswell Park Memorial Institute
RT	Room Temperature
RT (only NOXA knockdown	NOXA siRNA transfected, DMAS Treatment

experiments)	
RT-qPCR	Real Time quantitative Polymerase Chain Reaction
s	Seconds
Sbcl2	No extension available
SC	Scrambled siRNA transfected, no DMAS Treatment
SCC	Squamous Cell Carcinoma
SCF	Skin Cancer Foundation
SD	Standard Deviation
SEM	Standard Error of the Mean
siRNA	Small interfering RNA
SMARCB1	SWI/SNF Related, Matrix Associated, Actin Dependent Regulator Of Chromatin, Subfamily B, Member 1
SMO	Smoothend
ST	Scrambled siRNA transfected, DMAS Treatment
STAT	Signal Transducer and Activator of Transcription Proteins
T	Treated
TBS	Tris Buffered Saline
TBST	Tris Buffered Saline with Tween
TNF	Tumour Necrosis Factor
Tyr705	Tyrosine on Position 705
U-CH2	University of Ulm Chordoma 2
UM-Chor1	University of Michigan Chordoma 1
UV/UVA/UVB	Ultraviolet/ Ultraviolet A/ Ultraviolet B
V	Volt
WM164, WM793	Wistar Institute Melanoma 164/793
WNT	Wingless/Integrated

ZUSAMMENFASSUNG

Chordom und Melanom, eine Knochentumorart und eine Hautkrebsart, werden mit schlechten Prognosen und geringen Überlebensraten assoziiert, was vor allem auf fehlende Behandlungsmöglichkeiten zurückzuführen ist. Daher ist die Entwicklung neuer Therapeutika dringend notwendig. β-β-Dimethylacrylshikonin (DMAS), ein Shikonin Derivat, hat sich als vielversprechendes neues Medikament in Pilot Experimenten mit mehreren Krebsarten erwiesen. Dennoch sind die von DMAS induzierten Effekte in Melanom- und Chordomzellen bis heute unbekannt.

Inhalt dieser Arbeit ist die Erörterung von DMAS induzierten Effekten in Melanom- und Chordom Zelllinien sowie die Untersuchung der beeinflussten Signalwege. DMAS Effekte auf die Zell Viabilität wurden mit MTS und EZ4U Analysen untersucht, von DMAS ausgelöste Apoptose mit Annexin V / SYTOX Green sowie Caspase-3 Färbungen. RT-qPCR und Western Blots wurden zur Bestimmung der Expressions-Levels von Apoptose Genen und/oder Genen, die für das Überleben der Zellen bedeutend sind, durchgeführt. Bei den Melanom Ziellinien wurden zudem mRNA Sequenzierung zur Auffindung neuer Kandidaten Gene sowie NOXA Knockdown zur Erläuterung von NOXA abhängigen, DMAS induzierten Effekten durchgeführt. Außerdem wurden in-vivo Experimente gemacht, um einen Vergleich von DMAS Effekten zwischen in-vivo und in-vitro Experimenten zu ermöglichen.

Dabei reduzierte DMAS die Zell Viabilität bei beiden Krebsarten dosisabhängig, in Melanom Zellen zusätzlich zeitabhängig. Weiter wurde DMAS induzierte Apoptose in-vitro bei Melanom- und Chordom Zelllinien nachgewiesen, wohingegen Apoptose, Nekrose und Fibrose in Melanomen in-vivo beobachtet wurde. Bezüglich der beeinflussten Signalwege wurde NOXA als einziges auf genetischer als auch auf Protein Ebene als signifikant überreguliert gefunden. NOXA knockdown reduzierte die Effizienz von DMAS Behandlungen, daher ist DMAS induzierte Apoptose abhängig von NOXA. Zusammenfassend kann man sagen, dass DMAS eine vielversprechende neue Therapiemöglichkeit für Chordome als auch Melanome darstellt. Es sind jedoch noch weitere Studien erforderlich, um die DMAS induzierten Effekte und die beeinflussten Signalwege in beiden Krebsarten vollends zu verstehen.

ABSTRACT

Chordoma and melanoma, one a bone tumour, the other a skin cancer type, are both associated with poor prognosis and low overall survival rates, which is due to missing treatment options. Therefore, the development of novel therapeutics is urgently necessary. β-β-Dimethylacrylshikonin (DMAS), a shikonin derivative, has proven to be a promising new candidate for treatment of several cancer types in preliminary experiments, including melanoma. However, the mechanism of DMAS induced effects on melanoma and chordoma cells are still unknown.

In this work, the effects of DMAS on melanoma and chordoma cell lines as well as the affected pathways are elucidated. The influence of DMAS on cell viability was examined with MTS and EZ4U assays and DMAS induced apoptosis was analysed with Annexin V / SYTOX Green staining as well as the active caspase-3 assay. RT-qPCR and Western blots were performed to investigate expression levels of apoptosis and/or survival genes under DMAS treatment. For melanoma cell lines, mRNA sequencing was performed to find potential new candidate genes. Additionally, NOXA knockdown was carried out to show NOXA dependent DMAS treatment effects. Finally, *in-vivo* studies with melanoma cell lines were conducted to elucidate whether DMAS induced effects *in-vitro* can also be observed *in-vivo*.

DMAS was found to reduce cell viability in both cancer types in a dose-dependent manner, in melanoma additionally in a time dependent one. Furthermore, DMAS induced apoptosis in melanoma and chordoma cells *in-vitro*, but apoptosis, necrosis and fibrosis in melanoma derived tumours *in-vivo*. Concerning affected pathways, only NOXA was significantly upregulated in both cancer types on genetical as well as protein level. NOXA knockdown diminished DMAS treatment efficiency, therefore DMAS induces apoptosis *in-vitro* in a NOXA dependent manner. Taken together, DMAS is a possible new cancer therapeutic for both chordoma and melanoma. However, further studies need to be conducted to fully understand DMAS induced effects and influenced pathways in both cancer types.

1 INTRODUCTION

1.1 Cancer

All cells within the human body share certain mechanisms or programs regulating important functions like proliferation, metabolism and cell death. In cancer cells, genetical changes lead to disorganisation of those programs, resulting in abnormal traits of cells and ultimately to indefinite cell growth. Cancer arises when genetically altered cells with indefinite proliferation potential start to invade distinct sites within the body and form metastasis (1).

Patients suffering from cancer die of a variety of complications associated with this abnormal cell growth. It is estimated that more than 8.8 million people died of cancer in 2015, making it the second most common cause of death worldwide according to the world health organisation (2). The global cancer burden is increasing at a steady rate and is expected to from rise from 14.1 million new diagnosis and 8.2 million deaths in 2012 to 21.6 million new diagnoses and 13 million deaths by 2030. The reasons for this increase are mainly population growth and higher life expectancy (3,4). However, about 40% - 50% of all diagnosed cancers are believed to be caused by external factors such as smoking, UV radiation and in general an unhealthy lifestyle with high calorie diets and physical inactivity. Thus, active cancer prevention strategies and avoiding external risk factors could significantly lower the worldwide cancer burden (5).

Cancer is a diverse disease, with more than 100 cancer types currently distinguished (6). Cancer types are usually identified histologically by their tissue of origin and can roughly be divided into five different types namely, Carcinoma, tumours originating from epithelial tissues, make up the majority (85%) of all cancers, followed by sarcoma, which arise from muscle, bone- or connective tissue. Further categories are Leukemia, arising from blood cells, and Lymphoma as well as myeloma, originating from the immune system. The rarest category of cancers are brain and spinal tumour coming from the nervous system (7).

Cancer types and incidence rates are unevenly spread between genders as well as countries. In women, breast cancer is most common with 24.2%, followed by colorectal cancer with 9.5% of all cases and lung cancer with 8.4%. In contrast, the most common cancer types in males are lung (14.5%), prostate (13.5%) and colorectal cancer (10.9%)

(8). However, those values represent worldwide cancer incidence and mortality rates, and therefore convey only an abstract view on cancer burden. To get a more detailed picture, cancer statistics need to be specific for countries or even regions to really represent the risk of individuals for developing certain tumour types. For instance, in males, lung cancer is predominant in most parts of Asia, while in Europe or in America prostate cancer is more common. Additionally, in several countries people have a unique high risk of developing a certain type of cancer, like in Mozambique, where the most common tumour type is Kaposi sarcoma in males and cervix cancer for females (3). Notably, cancer mortality is not directly linked to cancer incidence rates, but rather to possible screening programs and available treatments. Due to significantly better treatment and screening options, only 30% of all cancer deaths occur in countries with high human development index, while cancer incidence rates are up to three-fold higher than in countries with low human development index (2,9).

Compared to the above mentioned cancer types, melanoma and chordoma, one a subtype of skin cancer, the other a bone cancer, have small incidence- and death rates. Melanoma make up about 1.6% (8) of all cancers. Chordoma, being part of the rare cancers, account for about 3% of all bone tumours (10), which only make up about 0.2% of all cancer cases (11). Therefore, those cancer types are less investigated in comparison to the most common cancers, resulting in fewer treatment options and low survival rates. As the focus of this work is on testing a new substance on both cancer types, the following sections will introduce melanoma and chordoma in the context of skin and bone tumours.

1.2 Skin Cancer

Skin cancer is currently divided into non-melanoma skin cancer and melanoma. If both are taken together, they make up the largest group of malignancies in Caucasian people (12), with incidence rates higher than those of lung or any other cancer type. The reason for this is the large amount of newly diagnosed non-melanoma skin cancers each year (13). However, non-melanoma skin cancers hardly metastasize and therefore have low mortality rates. The American Cancer Society as well as other organisations exclude non-melanoma skin cancers from their yearly reports to provide a more relevant image of cancer cases in terms of mortality rates (14–16).

Non-melanoma skin cancers can be divided, amongst others, into basal cell carcinoma (BCC), squamous cell carcinoma (SCC) and Bowen’s disease (13). In contrast to

melanoma, those types arise from skin cells other than melanocytes and are not pigmented, therefore being usually referred to as “white” skin cancer. BCC arise from basal cells, which normally form the basal laminar of epithelial tissues and are responsible for replenishing squamous cells on the skin surface. Therefore, basal cells form the border between epidermis and dermis. BCC make up about 70%-80% of all non-melanoma skin cancer cases. SCC, in contrast, develop from squamous cell which form the biggest part of the epidermis (17,18). Due to the low metastasis rate ofless than 0.1% for BCC and 0.3%-3.7% for SCC, non-melanoma skin cancers can usually be completely removed by resection or icing, therefore the mortality rates are lower than for most other cancer types (19,20).

Sun exposure is the predominant risk factor for development of all skin cancer types. UVA and UVB radiation damages cells and leads to DNA mutations, which subsequently can lead to cancer development (21). Approximately 90% of all non-melanoma (22) and 86% of melanoma (23) are associated with accumulated sun exposure. Not surprising, skin and hair colour is a major indicator for skin cancer risk, with Caucasian and fair-haired people having significantly higher risks of developing any kind of skin cancer. In contrast, a family history of melanoma with inherited risk factors only play a minor role, resulting in only 2% of all patients having a close relative which also suffers from this disease (24).

The cancer type and its cellular origin is only one factor defining tumour progression and mortality rates. Another, however, is the genetical difference between cancer types, which may be the major reason for the low metastasis rates of BCC and SCC. More than 70% of all BCC share mutations in patheched1 (PTCH) or smoothened (SMO) genes, which are drivers of uncontrolled proliferation when not functional or overexpressed. Due to these mutations, BCC may grow slowly over time, but more mutations would be necessary to develop metastatic potential, hence BCC rarely spreads to other parts of the body (25,26). SCC, in contrast, develop usually from actinic keratosis or Bowen´s disease and display a multitude of different genetical changes, which are accumulated over a longer time period (27). Apart from p53, which is mutated in up to 90% of all SCC, also RAS, c-MYC, WNT and other driver mutations have been found in SCC, often in combination. This makes SCC a more diverse, and potentially more dangerous cancer type then BCC, and is one possible explanation for the increased metastasis rates (21). However, none of the non-melanoma skin cancer types is nearly as dangerous as melanoma, which is the focus of this study.

1.3 Melanoma

Melanoma arise from melanocytes within the epidermis and present the most dangerous skin cancer type. Despite of only accounting for approximately 2%-3% of all skin cancer cases, they cause about 75% of all skin cancer associated deaths (24). Global melanoma incidence rates are rising faster than those of any other cancer, making melanoma an increasing problem (28). However, it is controversial whether this increase is due to prolonged sunbathing and tanning, representing a real increase, or whether it is an artefact of better screening and prevention methods. Evidence was provided for both arguments, with critics pointing out that the increased incidence rates were not accompanied by increased mortality rates (29,30), while epidemiologists argue that the increases are spread over all socio-economic classes and skin types, which makes it unlikely that the screening alone is responsible for the higher incidence rates (31,32). The problem of possible rising melanoma incidences is accompanied by the fact that little progression was made in melanoma treatment in the last years, leaving melanoma, and especially late stage melanoma, as one of the most incurable types of cancer known. The main reason for the high mortality rates associated with melanoma are the aggressiveness of the tumour, leading to early metastasis, and fast growth rates. In general, if melanoma is found before it reaches the vertical growth phase (stage one or two), it can be surgically removed and therefore often cured. However, as melanoma usually obtain the ability to spread above a diameter of 1mm², the tumour is often diagnosed too late. Once melanoma has spread to the lymph nodes (stage three), the 5-year survival rates drop to 63%, and to 17% if the tumour has already metastasised (stage four) (4,14,24).

1.4 Melanoma Treatment

Once melanoma was diagnosed, there are limited treatment options, depending on grading, staging as well as the mutational profile of the tumour. Surgery remains the method of choice, however, success rates are limited in late stage melanoma. This leaves classical radio- and chemotherapy as options pre- and postoperative. As melanoma are fast spreading and show high proliferation rates, chemotherapy looks promising, as many therapeutics like cisplatin, vinblastine or dacarbazine target especially fast proliferating cells (24,33). However, statistically, treatment success is also limited with this method. One major reason is chemoresistance, another recurrence rates. In recent years, targeted- and immunotherapies (e.g. PDL1/2-, CTLA4- or BRAF inhibitors) have gained in popularity, as they are more specific towards certain tumour types and have better

prognosis (34). Although these therapies have better response rates than traditional drugs like cisplatin and fewer side effects, they are still more of a palliative care than a real cure. For instance, vemurafenib, the currently most commonly used targeted therapy against melanoma featuring BRAF mutations, is only able to increase 5-year survival rates of patients by 20%. Side effects often include the development of squamous cell carcinoma or keratoacanthoma but are still less severe than with traditional chemotherapy with cisplatin and comparable drugs (24,35). Furthermore, melanoma often acquire resistances against targeted therapies, caused for instance by mutations within tumour cells or changes in the tumour microenvironment. Resistances have been observed in all major targeted therapies, from MAPK inhibitors (BRAF and MEK inhibitors) to immunotherapeutic drugs like CTLA4 inhibitors (36).

Taken together, the recent advances in melanoma therapy yielded only small benefits for melanoma patients, leaving early diagnosis and surgical resection the only real cure. Acquired tumour resistances, severe side effects and high recurrence rates diminish treatment success with anti-cancer drugs, be it with chemotherapeutics, targeted- or immunotherapies (28,37).

1.5 Melanoma Genetics

Underlying the entire process of melanomagenesis, staging, grading, diagnosis as well as the prognosis is the mutational profile of tumours, which harbours individual mutations or combinations thereof for each patient. The understanding of tumour mutations and their influence on the disease is therefore crucial for treatment as well as research.

In all tumour types, irrespective of their origin, two groups of genes can be distinguished harbouring all important driver mutations namely, oncogenes and tumour suppressor genes. Although many tumour types share common driver mutations, the mutational profile of each tumour is different, thereby defining the disease. Colon carcinoma has a different mutational profile in comparison to pancreatic cancer or melanoma. Furthermore, within a cancer type, common mutations are only shared to a certain percentage, thus the exact determination of mutations, defining the cancer subtype, is crucial for every single tumour. Dysregulation of oncogenes and tumour suppressors leads to certain hallmarks of cancer, which are cell self-sufficiency in signalling, insensitivity to growth inhibitory signals, invasion and metastasis, limitless replicative potential, evading apoptosis and the potential to induce angiogenesis (1,38). These hallmarks were increased by four more defining characteristics by Hanahan and Weinberg in 2011(39), however, the original six

are at the core of each tumour.

In melanoma, efforts undertaken in the last decades concerning tumour sequencing and determination of mutational profiles revealed a landscape of driver mutations including common pathways (40). The most commonly mutated oncogenes are: RAF, RAS, KIT, CDK4, CCND1, ERBB4, AKT1/2/3, NEDD9, GNAQ, GNA11, PI3K, MEK, EGFR, MET, HGF, MITF, MYC and ETV1. In contrast to this vast amount, only a few tumour suppressor genes are mutated in a significant number of tumours, namely CDKN2A, TP53, BAP1 and PTEN. Additionally, new upcoming driver mutations occur in PPP6C, RAC1, SNX31, TACC1, STK19 and ARID2 (38,40,41). Although all these mutations are important for melanoma development, emphasis in this work is put on the most frequent driver mutations in melanoma, namely RAF and RAS, and their respective pathway.

1.5.1 The MAP-Kinase Signalling Pathway

Arguably one of the most important pathways in all cancer types, be it lung adenocarcinoma, hepatocarcinoma or melanoma, is the mitogen activated protein kinase (MAPK) pathway. External growth signalling molecules which bind to cell surface receptors lead over a signalling cascade to RAS activation, which then activates RAF, followed by MEK and ERK. This cascade ends by induction of cell proliferation due to activation of several pathways (42). Each of the key players RAS-RAF-MEK-ERK can be mutated, rendering it constantly active and making the cell independent of external growth signals, which is one of the hallmarks of cancer (1). However, dependent on which gene is mutated, cancer prognosis and treatment options vary dramatically. BRAF mutations, for instance, can be treated with vemurafenib and other BRAF inhibitors, while NRAS mutations cannot be directly targeted, thus MEK inhibitors are used (34).

In contrast to many other cancer types like colon carcinoma, a relatively small amount of melanoma (10%-15%) feature RAS mutations. NRAS (Q61K or Q61L) is the most commonly found type of RAS mutation in melanoma, partly showing high incidence rates in certain subtypes. For instance, 56% of all congenital nevi show a NRAS mutation, and about 25% of all primary melanoma (43,44). In contrast, HRAS has rarely been found in melanoma (45) and no cases of KRAS mutations have been reported in melanoma lesions till date. This stands in strong contrast to other tumour types like colon carcinoma, were KRAS mutations play a pivotal role, with 30%-45% of all cancer cases harbouring this mutation (46). However, recent studies suggest that also wild-type KRAS might play a vital role in melanoma development and could be a promising target for therapy (47),

therefore the importance of KRAS for melanoma research might change in the near future. In contrast to BRAF, NRAS mutation in melanoma is believed to activate the PI3K pathway additionally to the MAP kinase pathway, which may be the reason why NRAS mutated melanoma are in general more aggressive than BRAF mutated ones (48). Efforts for developing RAS inhibitors led to the development of farnesyltransferase inhibitors (FTI), which were believed to block the post translational modification of RAS, hence rendering the protein unfunctional. However, due to lack of treatment success, FTI clinical trials were discontinued after phase two, thus leaving again MEK inhibitors as the only possible treatment alternative (49).

Taking over the normally primary role from RAS in cancer development, RAF mutations, especially BRAF V600E, are made responsible for at least half of the melanoma cases. In average, about 50% of all tumours feature this mutation, making it the primary target for targeted therapies (40).

BRAF mutations are commonly divided into two categories: mutations that constitutively activate BRAF (like V600E), making BRAF independent of RAS signalling, and those that lead to direct activation of CRAF by BRAF instead of MEK. CRAF is closely related to BRAF and equally capable of activating MAPK signalling (50). Interestingly, wild-type BRAF has solely MEK as substrate, while CRAF is usually activated by RAS, therefore the second category of BRAF mutations is indirectly substituting RAS activity by BRAF signalling (51). However, mutations resulting in constant activation make up about 90% of all changes in BRAF, therefore, the second category plays a minor role in cancer development (52). Furthermore, BRAF and NRAS mutations hardly occur within the same primary tumour, therefore cases can roughly be divided into BRAF driven and NRAS driven ones, with the latter having a poorer prognosis (53).

1.5.1.1 The role of UV light in melanoma associated mutations

BRAF and NRAS, being the most common driver mutations in melanoma, have led to a controversy about the role of sunlight in melanoma development. Excessive sun exposure, sunburns and UV radiation in general are commonly associated with melanoma development (54–56). UV damage is known to induce either C>T (UVB) or G>T (UVA) exchanges. The most common mutations in BRAF, however, are T>A (e.g. V600E) exchanges and for NRAS A>T or A>G (40,57), therefore those mutations cannot be directly linked to sun exposure. Interestingly, BRAF mutated tumours usually occur on the torso or arms, regions associated with extended sun exposure (58). Hodis et al 2012(40) proposed that exceptions from the rule of UV induced mutations are possible, leading to

C>T transitions, enabling V600E mutations. However, in their study, they could not find sufficient evidence for this hypothesis. Interestingly, UV induced mutations in tumour suppressor genes like p53 and PTEN are more common in melanoma than oncogene driver mutations. Furthermore, benign nevi and moles often feature BRAF (59,60) mutations and higher skin cancer risk is associated with higher nevi and mole numbers. This could lead to the assumption that latent BRAF and NRAS mutations, together with acquired sun damage induced mutations of tumour suppressor genes are needed in combination to induce melanoma development. However, only 20% of all melanoma arise from existing moles (61), and BRAF as well as NRAS driven melanoma do not exclusively arise on areas with high sun exposure (58,62).

Taken together, UV radiation cannot be directly linked to the two most abundant mutated genes BRAF and NRAS. Therefore, the role of sunlight in melanoma development needs further investigation. Concerning melanoma treatment, NRAS or BRAF mutated melanoma in stage three or four have poor prognosis and low overall survival rates. Therefore, new treatment options are urgently needed.

1.6 Melanoma Cell Lines

The use of cell lines for research purposes, also including drug discovery research, has been controversially discussed over the years (63–67). Arguments against the feasibility of cell lines as tumour models are mainly based on genetical as well as phenotypical changes within the cell lines over long culture periods. In long term culture, genetical expression and mutational profiles are changing, thereby increasing the differences between cell lines and original tumours. Additionally, cell culture leads over time to selection of more aggressive, faster growing cell lines. Further arguments against the use of cell lines are their susceptibility to cross contamination and the diversity of tumours. Concerning tumour diversity, authors argue that cell lines derived from primary tumours or metastasis are differing in aggressiveness and other phenotypical features, making them hardly feasible for drug discovery research. Furthermore, several studies conducted comparing the experimental outcomes of the same cell lines in different laboratories show clear differences in cell behaviour (64,65,67). In contrast, publications promoting the use of cell lines claim that the overall cell behaviour can be maintained in cell culture, mimicking the differences between cell lines and the original disease (63). A major argument for this hypothesis are studies comparing genetical profiles of cell lines and primary tumours, showing that mutational as well as transcriptional profiles suffer minimal changes over time, with the exception of immune system related changes (66).

Taking those arguments into consideration, five melanoma cell lines with different characteristics were chosen for this work (Tab. 1). To be able to differentiate between BRAF and NRAS mutated melanoma cell lines, two cell lines each featuring one of those driver mutations have been chosen. MUG-Mel2 and Sbcl2 both feature NRAS mutations, while WM164 and WM793 are both BRAF mutated cell liens. MUG-Mel1 has neither BRAF nor NRAS mutation and is therefore used as a wild-type control. To consider problems associated with cell line age, two relatively new cell lines (MUG-Mel1 and MUG-Mel2) were included in the study for comparability. Problems arising from differences between metastasis and primary tumours are addressed, as MUG-Mel1, MUG-Mel2 and WM164 are derived from metastasis, while Sbcl2 and WM793 resemble primary tumours. To compare cell lines and healthy primary cells, juvenile melanocytes and MRC-5 fibroblasts were included as control cells. Therefore, possible issues occurring due to the above mentioned changes in cell behaviour during cell culturing are addressed by the choice of cell lines for this study.

Table 1: Used melanoma cell lines and their core driver mutations

Cell Line	NRAS	BRAF
MUG-Mel1	WT	WT
MUG-Mel2	Q61K	WT
Sbcl2	Q61I	WT
WM164	WT	V600E
WM793	WT	V600E

1.7 Bone Cancer

Bone cancers, malignant neoplasms originating from bone tissue, account for approximately 0.2% of all tumours (11). The most common bone cancer is osteosarcoma, making up 35.1% of all cases, followed by chondrosarcoma with 25.8%, Ewing sarcoma with 16% and chordoma with 8.4%. Other types like spindle cell sarcoma, adamantinoma, angiosarcoma and giant cell tumours, are less common (68,69). Survival rates differ widely between the various bone cancer subtypes, which is mainly due to different behaviour and aggressiveness of the tumour. For instance, in chondrosarcoma, the 5-year overall survival rate is 72.7%, while for chordoma it is at 63.6% and for osteosarcoma it drops to 41% (70). In contrast to many other cancer types, bone cancer does not primarily

occur in older people, but has two predominant time periods in life: teenage and young adult years between 15 - 25 or above 50 years (71,72). However, the age in which bone cancer is most likely diagnosed is strongly dependent on the subtype of bone cancer and the site of origin. Osteosarcomas and Ewing sarcoma usually developed under 20 years of age and occur mainly in long bones or the knee region, respectively (73,74), while chondrosarcomas are often found in patients older than 40 years and at similar sites like osteosarcoma (75). Possible causes of bone cancer have not been elucidated completely till date. Commonly, radiation and chronic inflammation are accepted as causes, however, also incorporation of heavy metals, as well as the influence of certain prosthetics might cause bone cancer. Notwithstanding, many patients develop bone cancer without the involvement of any of the assumed causes. Furthermore, inheritance seems to play a minor role in bone cancer development, and most of the found driver mutations are somatic (76). Treatment of bone cancers is primarily done by surgery, chemotherapy and radiotherapy. After diagnosis of the tumour via x-ray, magnetic resonance imaging and histological methods, the primary objective is to remove as much of the tumour as possible. In many bone tumour types like osteosarcoma or Ewing sarcoma, surgery is accompanied by chemotherapy, while chondrosarcomas or chordomas are often chemoresistant and therefore subjected to other methods like radiotherapy. In all bone cancer types, radiotherapy is used as palliative care method, or if there is no option for surgical removal of the tumour. However, the optimal treatment is different for each tumour patient, therefore only rough guidelines are available on how to manage bone cancer in the clinic (72). The focus of this work is on testing a possible new drug on chordoma cells, therefore this bone cancer type will be introduced in the following section.

1.8 Chordoma

Chordoma are rare cancers arising from undifferentiated remnants of the notochord and can be found throughout the axial skeleton, from the sacrum up to the skull base (77). Although the notochord disappears in foetuses after eight weeks, some elements persist, with the proposed potential for chordoma development. This theory is strengthened by physaliferous cells found in the notochord and throughout chordoma tumours as well as the expression of the transcription factor brachyury and certain cytokines in both chordoma as well as notochord cells (78). The combination of brachyury, cytokeratin and vimentin is unique for chordoma and is therefore being used for tumour identification. Chordoma make up approximately 1% - 4% of all bone tumour cases, therefore less than one in a million develop this disease (79,80). The exact percentage distribution of chordoma locations on the mobile spine is still under debate, with some suggesting a 50%

/ 30%/ 20% distribution for sacrum, skull base and spine (81), while others propose a more equal distribution of 32%/ 32.8% and 29.2%, respectively (82). Compared to other tumour types like melanoma or colon carcinoma, chordoma are slow-growing, locally aggressive and hardly metastasise (83). Furthermore, most chordomas are rather chemoresistant. Chordoma form metastasis predominantly after tumour recurrence, which happens in approximately 30% - 40% of all cases. Therefore, the major effects of chordoma are caused by its local aggressiveness. Despite characteristically slow-growing, chordoma have 5-year survival rates of 67.7% and 10-year survival rates of around 40%, which is mainly due to missing treatment options (76,81,84).

1.9 Chordoma Treatment

As chordoma are rather rare tumours, less case studies are available, and less research is conducted in this field compared to other areas of cancer research, therefore knowledge concerning treatment options are limited. The Chordoma Global Consensus Group tried to define standards for chordoma therapy with position papers from 2015 (81) and 2017 (84). The presented consensus was that the best treatment of chordoma was en-bloc surgery with wide margins, followed normally by radiotherapy with the goal of complete removal of the tumour. This is difficult due to the location of the tumour, which is potentially always located near or around nervous or brain tissue. Especially in clival chordoma, located at the skull base, tumours often grow into the skull, thereby making resections without destruction of neuronal tissue almost impossible. Hence, emphasis is laid on upholding brain tissue functions, and margins are made as small as possible, risking incomplete tumour removal (85). This might be one reason for the high relapse rates, which are often beyond 90% (86). However, in case of possible en-bloc resections with large margins, relapse rates are still 50%, therefore surgery is often only a temporary solution. Radiotherapy is usually the method of choice following surgery, as chordoma have proven to be rather chemoresistant (81). However, radiotherapy usually only enables tumour control over a short time period. No targeted therapies are currently available for chordoma treatment. However, several drugs are currently tested in clinical trials. For instance, imatinib, a tyrosine kinase inhibitor, has successfully passed several phase two clinical trials (87,88), and a phase two clinical trial is currently conducted with afatinib, an EGFR inhibitor (89). Therefore, targeted therapies might become available for chordoma patients in several years.

Taken together, chordoma have a high recurrence rate, and the main treatment options currently available, namely surgery and radiotherapy, lead only to short term relief of

tumour burden. As knowledge of this tumour is limited as well as treatment options, chordoma still have a rather poor prognosis.

1.10 Chordoma Genetics

Chordomas were found to be genetically heterogeneous, with various karyotypes, chromosomal aberrations and changed regions throughout the genome (90). The molecular basis of chordoma has not been completely understood till date, with many gains and losses found in different loci, but no conclusive mechanism. However, several genes and pathways have been proposed to play a major role in chordomagenesis. Choy et al 2014(91) found that losses of CDKN2A, PTEN and SMARCB1 are predominant in more than 70% of all chordoma cases, therefore making their associated pathways promising candidates for driving tumour growth. Loss of function in CDKN2A, deregulating the cell cycle, together with disfunction of PTEN, a prominent tumour suppressor that should send cells into apoptosis or senescence in case of cell cycle problems, may play a crucial role in tumour development. Mutation of SMARCB1 might further aid to tumourigenesis. CDKN2A was further reported to negatively interfere with MDM2 ubiquitylation, which leads to higher p53 and CDK4 levels in chordoma. Interestingly, this was found to correlate with a poor prognosis, with only 39% 5-year survival rate for patients showing p53 overexpression, in contrast to a 79% 5-year survival rate for patients with normal p53 levels. Thus, CDKN2A might play a crucial role for chordoma development (92). Another driver pathway of chordoma formation might be the MEK/ERK pathway in association with brachyury and FGF2. Brachyury, unique for chordoma and notochordal cells, as well as FGF2, is directly linked to MEK/ERK and crucial for chordoma growth and survival, as found by Hu et al in 2014(93). In their study, inhibition of FGF2 lead to decrease of MEK/EKR phosphorylation, followed by lower brachyury expression and subsequently apoptosis of chordoma cells. Furthermore, receptor tyrosine kinases play a crucial role in many cancer types and could also be responsible for chordoma growth. Different studies have shown involvement of PI3K/AKT, c-MET and mTOR, as well as dysregulation of several genes of the PI3K/RAS/AKT/mTOR pathways (94,95). However, BRAF and NRAS, playing a pivotal role in many tumours like in melanoma, were not found to be predominant in chordoma. Taken together, many potential pathways are proposed to be main drivers of chordomagenesis, but none has yet been proven to play a predominant role in most chordoma cases. Therefore, it is likely that a combination of several pathways, rather than one, is responsible for chordoma development.

1.11 Chordoma Cell Lines

For this work, four different chordoma cell lines were chose. As the focus was not on specific mutational differences as in the melanoma part of this project, the aim was to choose cell lines with vast differences to obtain a representative cell line population. Therefore, two clival (MUG-CC1, UM-Chor1) and two sacral (MUG-Chor1, U-CH2) cell lines were chosen. MUG-CC1 and UM-Chor1 are novel chordoma cell lines, while MUG-Chor1 and U-CH2 are seven and nine years old, respectively. The problems and pitfalls concerning cell line usage described for melanoma cell lines count for chordoma cell lines as well and are therefore described only in section 1.6. However, as all cell lines, including MUG-Chor1 and U-CH2, are relatively young, no changes concerning cell behaviour are expected.

1.12 Natural Drugs

As described in the previous sections, treatment efficiency for chordoma and melanoma is limited. In case of chordoma, this is due to the location of the tumour, high recurrence rates and limited knowledge concerning the molecular basis of the disease resulting in only few available treatment options (81,84,85). Melanoma, although intensely researched by many groups, has proven to be challenging due to limited surgical options at advanced stages, combined with high aggressiveness and metastasis rates, the ability to develop drug resistances, and the severe side effects of known chemo- as well as targeted therapies (24,28,33,35). Therefore, new treatment options with long term efficiency and fewer side effects are urgently needed for both cancer types.

Concerning the search for novel cancer therapeutics, natural products derived from plants have always played a crucial role. Reports estimating the amount of new therapeutics hitting the market show that more than 80% of available small-molecule tumour therapeutics were either natural products or derived therefrom. Overall, about 75% of all drugs licenced between 1840 and 2014 were non-synthetic, including 49% natural products. Additionally, many synthetic drugs have been inspired or were directly derived from natural drugs. Most commonly, structures and mechanisms of natural products are adapted and slightly changed by addition or deletion of side chains during chemical synthesis, yielding therapeutics with novel anti-cancer traits. Commonly used plant derived drugs in cancer therapy include vinblastine, doxorubicin and paclitaxel, underlining the crucial role of natural products in drug development (96–98).

In the search for new therapeutics, one approach is to look for plants commonly used in folk medicine, like the traditional Chinese medicine. Two rather popular plants, used for the treatment of a variety of diseases from measles over skin infections up to cancer, are *Lithospermum erythrorhizon* (LE) and *Onosma paniculata* (OP) Bureau & Franchet (Boraginaceae). The main ingredients harbouring the therapeutic potential of these plants are shikonin/alkanin in LE and *β-β*-Dimethylacrylshikonin (DMAS), a shikonin derivative, in OP (99–101). The structures of shikonin and alkanin, two chiral molecules, as well as DMAS, are shown in Figure 1.

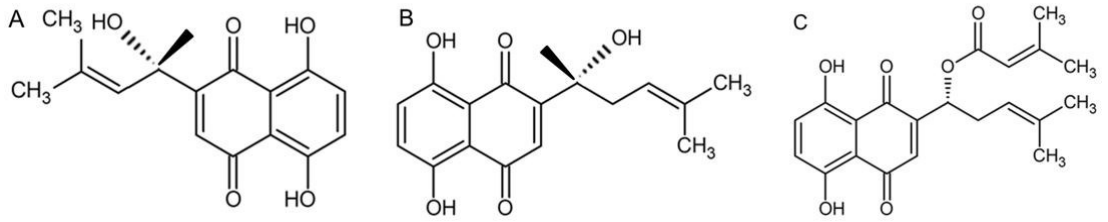

Figure 1: Chemical structures of A) shikonin, B) alkanin and C) DMAS. Reproduced with modifications from (122) with permission of publisher Elsevier.

Shikonin and alkanin are chiral molecules, with skikonin being the right confirmation and alkanin the left. Both enantiomers have different pharmacological properties. Shikonin seems to have more beneficiary properties and has been shown to harbour anti-inflammatory, wound healing and antimicrobial effects, among others. Alkanin, in contrast, seems to have a minor therapeutic potential. Therefore, shikonin has been researched with great interest, not just for traditional uses but also in cancer research (102). Positive influences of shikonin were reported for several cancer types, including non-small cell lung cancer (103), leukaemia (104) and colon carcinoma (105). However, the efficiency of shikonin as cancer therapeutic is limited and therapeutic effects temporary, therefore a more potent shikonin derivative, leading to possibly lower treatment concentrations and better prognosis, is needed. In a previous study performed by our group (106,107), a petrol-ether extract of OP was tested on a panel of eight cancer cell lines, with promising results especially on melanoma cells, and DMAS confirmed as the main therapeutic compound. Therefore, DMAS, a possible more potent candidate than shikonin for cancer therapy, was investigated in this work to determine its anti-cancer properties.

In previous studies investigating DMAS induced effects in various cancer types (108–110), DMAS was found to induce apoptosis *in-vitro* and *in-vivo* over different mechanisms like the p38 MAPK pathway (111) or BCL2 upregulation (112).

1.12.1 Apoptosis

Apoptosis is induced via two major pathways, namely the intrinsic or mitochondrial apoptosis pathway and the extrinsic or death-receptor pathway (113,114). Both pathways are largely independent from each other, but join when cleaving/activating caspase-3. Once cleaved, caspase-3 initiates fragmentation of the DNA, the cytoskeleton as well as major nucleic proteins, which then activates proteases for degradation of the fragments. Subsequently, cellular parts are released enveloped in apoptotic bodies, and ultimately destroyed by phagocytic cells (115).

The extrinsic apoptosis pathway starts on the cell surface, with activation of death receptors which are part of the tumour necrosis factor superfamily (TNF). TNF receptors build clusters upon activation, to which adapter proteins bind on the cytosolic side. Afterwards, a signalling pathway is activated that ultimately leads to dimerization and activation of caspase-8, which initiates caspase-3 cleavage (116).

However, concerning DMAS, several papers (109,112,117) have shown that the drug induces apoptosis primarily over the intrinsic apoptosis pathway. In contrast to the extrinsic pathway, the intrinsic one is activated as a result of cellular stress like DNA damage. Within a healthy cell, cell survival factors like growth factors, inhibitors of cell death or certain cytokines are balanced with apoptosis inducing factors. Cellular stress leads to a disbalance, either by reduction of growth factors, inhibition of survival factors or upregulation of apoptosis genes. The dysregulation leads to disruption of the inner mitochondrial membrane potential, resulting in membrane pore formation. Subsequently, cytochrome-c is released, caspase-9 activated and caspase-3 cleavage initiated, leading to apoptosis (114).

Crucial for the intrinsic apoptosis pathway are members of the BCL2 protein family and p53 (118). While relatively low expressed in healthy cells, p53 is activated upon cellular stress like DNA damage, and activates the BCL2 family members NOXA, PUMA, BAX and BAK. BAK and BAX activation is further facilitated by PUMA activation. Once activated, BAX and BAK lead to disruption of the mitochondrial membrane potential, resulting in apoptosis as described above. To prevent apoptosis in healthy cells, BAX and BAK are usually inhibited by BCL2, a survival factor. NOXA, PUMA and BAD, however, inhibit BCL2, thereby facilitating apoptosis (113).

1.13 Hypothesis and Study Aims

The main hypothesis followed in this thesis for chordoma and melanoma consisted of three statements:

1. DMAS reduces cell viability in chordoma and melanoma cells
2. The mode of cell death induced by DMAS in chordoma and melanoma cells is apoptosis
3. DMAS influences distinct pathways that, once activated, lead to apoptosis induction

Concerning melanoma, another hypothesis was added:

4. DMAS efficacy differs between *BRAF* and *NRAS* mutated melanoma cell lines

Based on the hypothesis, the **first aim** of this work was to determine the necessary concentration to significantly lower cell viability, also in comparison with non-tumourigenic cells.

For chordoma cell lines, two clival (MUG-CC1 and UM-Chor1) as well as two sacral (MUG-Chor1 and U-CH2) were chosen. As the molecular mechanisms of chordoma are not fully understood, as described in the previous sections, emphasis was on the location of the tumours rather than their mutational profiles. By selecting both clival and sacral chordoma cell lines, a more comprehensive image of DMAS induced effects should be obtained compared to studies focussing on a single chordoma site. Adult human fibroblasts were used as healthy control cells.

Concerning melanoma, five different cell lines with different mutational profiles were chosen with emphasis on *BRAF* and *NRAS* mutations. MUG-Mel1, featuring neither mutation, served as wild type control. Sbcl2 and MUG-Mel2, one derived from a primary tumour, the other from a metastasis, were representatives of *NRAS* mutated melanoma. Furthermore, WM164 and WM793 harboured *BRAF* mutations. Juvenile melanocytes and MRC-5 fibroblasts were used as healthy control cells.

The **second aim** of this work was to investigate the mode of cell death, which was done with Annexin V (apoptosis) and SYTOX Green (necrosis) staining after DMAS treatment. The results were confirmed with caspase-3 staining.

The **third aim** was to select possible candidate pathways and genes effected by DMAS. Therefore, mRNA sequencing was performed in two chosen melanoma cell lines, one with

a BRAF (WM164), the other with an NRAS (Sbcl2) mutation. Subsequently, DMAS effects on the chosen genes were investigated on genetic (RT-qPCR) as well as protein (Western blot) level. Concerning melanoma cells, the most promising candidate gene was chosen for knockdown experiments to confirm the effect.

The **fourth aim**, only planned with the chosen cell lines (Sbcl2 and WM164), was the confirmation of the cytotoxic effects of DMAS *in-vivo*. Therefore, human melanoma xenograft mouse experiments were performed.

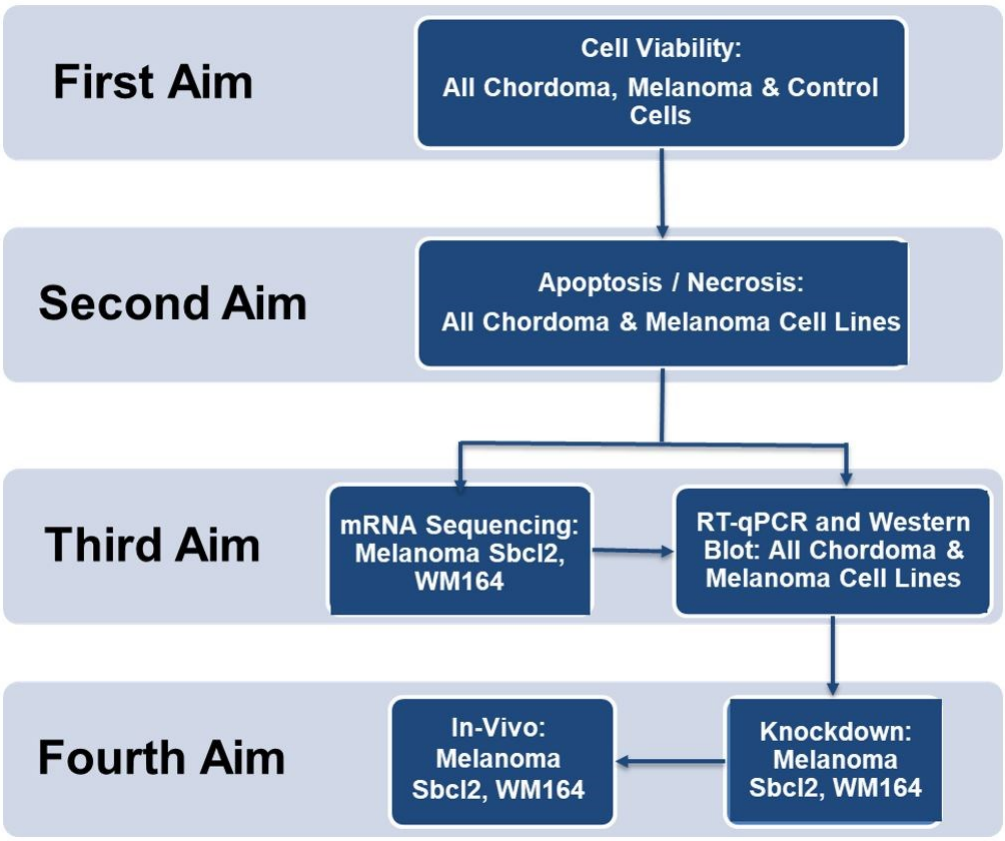

Figure 2: Dissertation aims and structure

2 MATERIAL AND METHODS

The elucidation of DMAS induced effects in melanoma and chordoma was initially separated into two independent projects, which were only partly combined after the viability assays. Therefore, several assays were either performed differently for chordoma and melanoma or were just conducted for one of the projects. Concerning the cell viability assay, different reagents were used for chordoma and melanoma, while western blot experiments were conducted for different proteins. Additionally, cell cycle experiments, mRNA sequencing, NOXA knockdown and mouse experiments were only performed with melanoma cell lines. Furthermore, all chordoma experiments after the cell viability assay were conducted using 2.2µM DMAS concentration, while the respective DMAS IC_{50} concentration of each cell line was used for melanoma experiments. Therefore, whenever applicable, melanoma and chordoma experiments are described separately.

2.1 Cell Culture

2.1.1 Chordoma

MUG-CC1 (119) and MUG-Chor1 (120) cell lines were isolated from chordoma samples by our group. UM-Chor1 were donated by the Chordoma Foundation (Durham, USA) and U-CH2 were obtained from Silke Brüderlein (University of Ulm, Germany). All chordoma cell lines were cultivated in a mixture of 4:1 IMDM/RPMI (both Gibco, Thermo Fisher Scientific, Carlsbad, USA) medium containing 2mM L-glutamine (Invitrogen, Thermo Fisher Scientific), 10% fetal bovine serum (FBS) (Biochrom, Berlin, Germany), 1% penicillin/streptomycin and 1% insulin-transferrin-selenium (both Invitrogen).

2.1.2 Melanoma

MUG-Mel1 (unpublished) and MUG-Mel2 (121) cell lines were isolated by our group from melanoma samples. Cells were cultivated with RPMI, including 10% FBS, 2mM L-glutamine and 1% penicillin/streptomycin. Sbcl2, WM164 and WM793 (all obtained from Dr. Helmut Schaider, Wistar Institute, Philadelphia, USA) were grown in RPMI, containing 2% FBS, 2mM L-glutamine and 1% penicillin/streptomycin.

2.1.3 Primary Cells and MRC-5 Fibroblasts

Adult human fibroblasts were isolated from the chordoma MUG-Chor1 patient by our group and grown using DMEM (Gibco) containing 10% FBS, 2mM L-glutamine and 1%

penicillin/streptomycin. MRC-5 fibroblasts were obtained from the ATCC (Manassas, USA) and grown under the same conditions and in the same medium as adult human fibroblasts.

To obtain primary melanocytes, juvenile foreskin samples were collected from donors below six years of age at the children´s hospital of the University Hospital Graz. Then, foreskin samples were incubated for 24h with Dispase-2 (Hoffmann - La Roche, Basel, Switzerland). Afterwards, the epidermis was removed with forceps and cut into 1mm² pieces. Samples were grown in melanocyte growth medium M2 with supplements (Biomedica, Vienna, Austria) for several days until the amount of the primary melanocytes was sufficient for subculturing. For identification, melanocytes were seeded into chamber slides (BD Biosciences Franklin Lakes, USA) and subsequently stained with Melan-A, HMB45, S100 (all Dako, Agilent Technologies, Santa Clara, USA). To rule out fibroblast contamination, slides were additionally stained with SMA (Sigma-Aldrich, St. Louis, USA).

2.1.4 Culture Conditions

Incubation of all cell lines as well as primary cells was done at 37°C, 90-95% humidity and 5% CO_2. The cell culture medium was changed periodically every three days for all cell lines. Cells were passaged whenever they reached over 70% confluency.

2.2 Isolation of DMAS

For DMAS isolation, roots of *Onosma paniculata* Bureau & Franchet (Boraginaceae) were bought at the medicinal plant market in Kunming (China). For identification, the plants were subjected to genomic analysis of the ITS2 region of nuclear DNA as well as plasmid DNA and the trnL-F region as reported previously (107). Then the roots were grinded and extracted with Soxhlet extraction using petroleum ether. Afterwards, DMAS was isolated by preparative HPLC consisting of a Varian R PrepStar SD-1 (Agilent Technologies, USA) with Dynamax R solvent delivery system and an absorbance detector model UV-1 and by using a VDSpher 100 RP18 column (250 × 25 mm, 10 µm). Gradient elution was performed for 45min, using a 70−100% acetonitrile (Sigma-Aldrich) in water gradient, followed by a second step of 15min with 100% acetonitrile. Afterwards, DMAS purity and identity was determined with nuclear magnetic resonance and circular dichroism measurements. DMAS purity was found to be 95%. The substance was dissolved in 100% ethanol for all cell culture experiments (106).

2.3 Harvesting and Cell Seeding for Cell Culture Experiments

2.3.1 Harvesting

Cell harvesting and seeding followed the same workflow for all cells and all experiments. Differences occurred only in seeding densities with respect to different cell lines and cell culture vessels. For harvesting, the cell culture medium was first aspirated, then the cells were washed once with PBS. Subsequently, cells were detached with TrypLE Express (Gibco) by incubation at 37°C and 90-95% humidity for 3min. New medium containing 10% FBS was added in a 10:1 (FBS/TrpLE Express) ratio to deactivate the trypsin. The cell solution was then transferred into a 15ml or 50ml centrifuge tube (VWR, Radnor, USA) and centrifuged at 125g for 4min at RT.

The above described method of harvesting was used whenever cells needed to be seeded into cell culture vessels. However, in experiments were harvesting occurred after DMAS treatment; the medium was not aspirated but transferred into the same falcon after the cells were dissociated with trypsin. This was done to include the floating cells aswell.

2.3.2 Seeding

After aspiration of the supernatant, cells were re-suspended in PBS and counted with CASY TT (Omni Life Science, Bremen, Germany). Following another centrifugation step at 125g for 4min at RT, cells were re-suspended in the appropriate amount of cell culture medium, counted again with the CASY TT and seeded into various cell culture vessels. The seeded cell amount was optimised for all experiments to obtain 70% confluency 24h after seeding.

2.4 Short Tandem Repeat Analysis

Regular analysis of cell line identity was performed by short tandem repeat analysis (STR) using PCR. First, cells were dissociated using trypsin, washed once with phosphate buffered saline (PBS, Lonza, Basel, Switzerland) and the cell pellet frozen at -20°C for later analysis. Once an appropriate amount of cell pellets was obtained, the DNA was isolated using the QIAamp DNA Mini Kit (Qiagen, Hilden, Germany). First, cell pellets were re-suspended in 200µl PBS, then 20µl Proteinase K and 200µl Buffer AL (both from Qiagen) were added and the cell solution incubated for 10min at 56°C. Subsequently,

200µl of 100% ethanol (Merck, Darmstadt, Germany) were added and the mixture loaded onto spin columns (Qiagen). After centrifugation with 6000g at room temperature (RT) for 1min, the flow through was discarded and 500µl Buffer AW1 (Qiagen) were added to the columns and the procedure repeated once. Then, Buffer AW2 (Qiagen) was added and the columns centrifuged with 20,000g at RT for 3min. The columns were loaded onto 1.5ml DNA low bind collection tubes (Eppendorf, Hamburg, Germany) and 50µl Buffer AE (Qiagen) were added. Following 5min incubation time at RT, DNA was eluted by centrifugation at 6000g, RT for 1min. DNA quality and quantity was assessed using NanoDrop 2000 (Thermo Fisher Scientific, Waltham, USA) and samples were subsequently analysed using the PowerPlex 16HS System (Promega, Fitchburg, USA). First, cells were diluted to a concentration of 0.5ng/µl DNA. Per sample, one 0.2ml PCR tube (Eppendorf) was prepared containing 1µl DNA (0.5ng/ml), 1µl 10x Primer Stock, 2µl 5x Master Mix (all Promega) and 6µl dH_2O. A positive control provided in the kit and dH_2O as negative control were prepared for all experiments. PCR was carried out on the T100 Thermal Cycler (Bio-Rad Laboratories Laboratories Inc, Hercules, USA) using the following program: For initialisation, samples were heated to 96°C for 2min. Then the samples were cooled to 94°C for 30s for denaturation, followed by gradual cooling down to 60°C with a slope of 0.5°C/s. Samples were annealed at 60°C for 30s before being gradually heated up to 70°C with a slope of 0.2°C/s. Samples were elongated at 70°C for 45s. This cycle was repeated ten times. Subsequently, the samples were subjected to a second cycle spanning 22 cycles and featuring the same slopes, temperatures and times, except for a different denaturation temperature of 90°C. Following this second cycle, samples were cooled down to 60°C for 30s and then stored at -20°C. Afterwards, sample measurement was performed with the ABI3730 Genetic Analyzer (Applied Biosystems, Thermo Fisher Scientific) at the Institute of Human Genetics of the Medical University of Graz. The raw data files were analysed using the ABI Genemapper Software Version 4.0 (Applied Biosystems, Thermo Fisher Scientific). STR analysis was periodically performed with all cell lines.

2.5 Mycoplasma Detection

Cell lines and primary cultures were periodically checked for mycoplasma contamination with the VenorGeM Mycoplasma Detection Kit for conventional PCR (Minerva Biolabs, Berlin, Germany). First, cells were grown to 100% confluency without antibiotics to prepare them for mycoplasma detection. The medium was not changed for three consecutive days, then 1ml cell culture supernatant was taken and stored at -20°C until use for mycoplasmas detection. For detection, samples were first centrifuged at 200g for

4min at RT. Then, 100µl supernatant was transferred to a 1.5ml reaction tube and incubated at 95°C for 5min. Additionally, PCR kit components were rehydrated by adding 65µl PCR grade water to the Primer/Nucleotide mix, and 300µl PCR grade water to the positive- and the internal control DNA tubes. Then, master mix was prepared containing 15.3µl PCR grade water, 2.5µl 10x reaction buffer, 2.5µl Primer/Nucleotide mix, 2.5µl internal control DNA and 0.2µl of MB Taq hot start polymerase (5U/µl) (all Minerva Labs) per reaction. From this master mix, 23µl were transferred into 0.2ml PCR reaction tubes and mixed with 2µl of the prepared sample supernatant. The supplied positive control DNA was used as positive control, PCR grade water as negative control. The reaction tubes were subsequently loaded onto the T100 Thermal Cycler (Bio-Rad Laboratories) and run with the following program: For initialisation, samples were heated to 94°C for 3min. To start the cycle, samples were kept at 94°C for 30s for denaturation. Afterwards, samples were cooled to 55°C for 30s to allow annealing, followed by heating up to 72°C for 1min for elongation. After 35 cycles, samples were kept at 72°C for 4min for final elongation, and then stored at -20°C until further use. To analyse the amplified samples, agarose gel electrophoresis was performed. First, a 1.5% Seakem LE agarose (Lonza) solution in 1x Tris-acetate-EDTA electrophoresis buffer (Thermo Fisher Scientific) was prepared by heating it in the microwave until the agarose was completely dissolved. Then, SybrGold (Thermo Fisher Scientific) was added in a 1:10,000 ratio, the gel poured into a cassette and after solidifying loaded with the prepared samples. Per slot, 10µl sample mixed with 2µl 6x MassRuler DNA loading dye (Thermo Fisher Scientific) were loaded. Fast Ruler Low Range DNA Ladder (Thermo Fisher Scientific) was used as lane marker. The gel was run at 90V for 40min, then band measurement and data read out was performed with the ChemiDoc Touch (Bio-Rad Laboratories). All cell lines and primary cells were periodically checked for mycoplasma contamination.

2.6 Cell Viability Assay

For chordoma cells and adult human fibroblasts, the Cell Titer 96® Aqueous Non-Radioactive Cell Proliferation Assay Kit (Promega, Madison, USA) was performed for viability determination, while for melanoma cells, MRC-5 fibroblasts and juvenile melanocytes the EZ4U cell proliferation and cytotoxicity assay (Biomedica) was conducted.

Concerning chordoma cells and adult human fibroblasts, 100µl medium containing 8,000 (U-CH2) or 10,000 (MUG-CC1, MUG-Chor1, UM-Chor1) cells were seeded into 96-well cell culture plates and incubated for 24h. Following incubation, the cell culture medium

was aspirated and new medium containing various DMAS concentrations added. The DMAS concentrations were 0µM (control), 2.2µM, 4.4 µM, 8.6 µM, 17.3 µM, 25.9 µM and 34.6 µM. After 48h DMAS treatment, 20µl of mixed reagent from the Cell Titer 96® Aqueous Non-Radioactive Cell Proliferation Assay Kit was applied per well and incubated for one to four hours. Optical density was measured at 490nm using the Omega SPECTROstar photometer (BMG Labtech., Ortenberg, Germany). SigmaPlot 13.0 (Systat Software GmbH, Germany) was used to determine IC_{50} values for the various cell lines using a four-parameter logistic curve. Culture medium was used as background value and ethanol as solvent control. Results were normalised to control cells. Three independent biological replicates, each consisting of six technical replicates, were made. The results were visualised in Excel 16.0 (Microsoft, Washington, USA). All incubations steps were done at 37°C, 90-95% humidity and 5% CO2 (122).

Melanoma cells, adult human fibroblasts and MRC-5 cells were seeded into 96-well plates in the following concentrations: 5,000 cells/well for MUG-Mel1 and MUG-Mel2, 3,000 cells/well for WM164 and 7,000 cells/well for Sbcl2 and WM793, each seeded in 200µl per well. Cells were incubated for 24h, then treated with a DMAS concentration gradient of 0µM (control), 0.3µM, 0.5µM, 1.1µM, 2.2µM, 4.3 µM, 6.5 µM, 8.6µM, 12.9µM, 17.3µM and 34.5µM DMAS. MRC-5 cells and adult human fibroblasts which served as control cells were treated for 24h. Melanoma cell lines were treated for 24h, 48h and 72h. Subsequently, 20µl of EZ4U reagent (Biomedica) were added to each well and the cells incubated for 3h. Then, optical density was determined at the Omega SPECTROstar photometer at 492nm with a reference wavelength of 620nm. IC_{50} calculation was done with Sigma Blot 13.0 and the results visualized with Excel 16.0. Three independent experiments were conducted in triplicates. All incubations steps were done at 37°C, 90-95% humidity and 5% CO2 (123).

2.7 Apoptosis / Necrosis Determination

To analyse the type of cell death, cells were first seeded into six-well plates to obtain a cell confluency of about 70%, incubated for 24h, and then treated either with DMAS or vehicle (100% ethanol). For chordoma cells, 2.2µM DMAS were applied for 24h, while for melanoma the respective IC_{50} DMAS concentrations were used for 6h or 24h incubation. After DMAS incubation, cells were stained with Annexin V Pacific Blue (BioLegend, San Diego, USA) for apoptosis and SYTOX Green (Life Technologies) for necrosis determination using the following protocol: First, cells were harvested as described in section 2.5. Instead of TrypLE Express (Gibco), 700µl Accutase (Gibco) were used per

well to detach the cells. The obtained cell pellet after centrifugation was washed once with 2ml cold (4°C) Cell Staining Buffer (Biolegend). Subsequently, cells were re-suspended in 120µl 1x Annexin V Binding Buffer and transferred into 1.4ml Mirconic tubes (Micronic, Lelystad, The Netherlands). SYTOX green was diluted 100:1 with PBS, then 5µl were applied per tube, together with 5µl Annexin V Pacific Blue. Micronic tubes were vortexed and then incubated for 20min at RT in darkness. Subsequently, 150µl Annexin V Binding Buffer were added per sample. Measurement were performed at the CytoFLEX flow cytometer (Beckman Coulter, Brea, USA) at Ex/Em: 405nm / 455nm for Annexin V Pacific Blue (PB450 channel) and Ex/Em: 504nm／523nm for SYTOX Green (FITC channel). No compensation experiments were performed as no spectral overlap could be observed between the PB450 channel and the FITC channel. Data readout was done using the CytExpert 1.2.10.0 software (Beckman Coulter). Two independent experiments were conducted per cell line.

2.8 Caspase-3 Assay

Validation of the Annexin V Pacific Blue / SYTOX Green apoptosis / necrosis assay results was done with the anti-active caspase-3 assay. Cells were seeded to obtain a confluency of 70% after 24h incubation, then treated with 2.2µM DMAS for chordoma or the respective IC_{50} DMAS concentrations for melanoma. Control cells were treated with vehicle (100% ethanol). Following another 24h incubation step, cells were harvested using TrypLE Express. Subsequently, cells were stained for active caspase-3 using the Fixation / Permeabilization Solution Kit and Alexa Fluor® 647 Rabbit Anti-Active Caspase-3 (both BD Biosciences, Franklin Lakes, USA). After harvesting, the cell pellet was re-suspended in 1ml PBS and the cell solution transferred to 1.4ml micronic tubes. Cells were then centrifuged at 16,000g for 4min at RT and the supernatant was discarded. Hereafter, 100µl Cytofix / Cytoperm (BD Biosciences) solution were added to the samples, followed by incubation for about 20min at 4°C in the dark to fix and permeabilise the cells. Wash buffer was prepared by diluting the 10x BD Biosciences wash buffer 10:1 with dH_20. After fixation and permeabilization of the cells, 500µl of 1x wash buffer were added to the samples. The samples were then centrifuged at 16,000g for 4min at RT and the supernatant was discarded. Subsequently, the pellet was re-suspended in 50µl wash buffer, then 5µl Alexa Fluor® 647 Rabbit Anti-Active Caspase-3 antibody were added to the cells and incubated for 30min at RT in the dark. Afterwards, the samples were diluted with 500µl wash buffer, and then spun down at 16,000g for 4min at RT and the supernatant was discarded. The cell pellet was re-suspended in 100µl wash buffer and measured at the LSRII flow cytometer (BD Biosciences) at Ex/Em: 650nm / 668nm (APC

channel). Data readout was performed with the FACS Diva 1.0 software (BD Biosciences). Two independent experiments were conducted per cell line.

Validation of DMAS induced caspase-3 activity was done with MUG-Mel1 and WM793 cells. Apart from the control and treated sample, an additional sample was made by adding pan-caspase inhibitor 30min before DMAS treatment.

2.9 Cell Cycle Analysis

To analyse the type of cell death, cells were first seeded into six-well plates to obtain a cell confluency of about 70%, incubated for 24h, and then treated either with DMAS or vehicle (100% ethanol). DMAS treatment was performed for 24h or 48h, then the cells were harvested using trypsin. Then, the cell pellets were re-suspended in 4°C cold PBS and centrifuged at 200g for 4min at 4°C. The supernatant was discarded, then the cells were re-suspended in 500µl of 4°C cold PBS. Subsequently, 5ml of 4°C cold 70% ethanol were added and the samples fixed for 10min at 4°C. Cell solutions were then stored at 4°C for a maximum of two weeks before use. Afterwards, the cell solution was centrifuged at 1,000g for 4min at RT and the supernatant was discarded. The cell pellet was re-suspended in 5ml PBS containing 0.5% FBS, centrifuged at 1000g for 4min at RT and the supernatant was aspirated. This step was repeated once. Then, the cell pellets were re-suspended in 200µl lysis buffer consisting of 0.1% sodium citrate, 0.1% Triton X-100, 50µg/ml propidium iodide (all from Sigma-Aldrich), and 100µg/ml RNAse A (Fermentas, Thermo Fisher Scientific) in dH_2O. Cells were subsequently measured at the LSRII flow cytometer with Ex/Em: 535nm / 617nm. Data readout was performed with the FACS Diva 1.0 software. Two independent experiments were performed per cell line. Cell cycle analysis was only performed with melanoma cell lines.

2.10 RNA Extraction

For RNA extraction, cells were first seeded into 60mm petri dishes to reach a confluency of approximately 70% after 24h incubation. Cells were then treated with the respective DMAS IC_{50} concentrations for 6h or 24h for melanoma cell lines and with 2.2µM DMAS for 24h for chordoma cell lines. Then, total RNA was extracted from cells using the miRNeasy Mini Kit (Qiagen, Hilden, Germany). For that, the supernatant was transferred into 15ml centrifugation tubes (VWR). Then, 5ml PBS were added per petri dish and subsequently transferred to the same centrifugation tubes (washing step). After that, 500µl TrypLE Express were added per petri dish and incubated at 37°C and 90-95% humidity for 3min.

The detached cells were transferred into the same falcon as the supernatant, then the falcon was centrifuged at 1,500g for 4min at RT. The supernatant was discarded, the cell pellet re-suspended in 1ml Qiazol (Qiagen) and transferred into 1.5ml reaction tubes, followed by 5min incubation at RT. Subsequently, samples were vortexed for 1min, then incubated for five more minutes at RT. After this step, cell lysates were frozen at -80°C until further use. Upon usage, samples were rapidly thawed in a water bath at 37°C, then 200µl chloroform (Sigma-Aldrich) were added to each sample, followed by vigorous shaking for 15s. Subsequently, cell lysates were incubated for another 3min at RT, after which they were centrifuged at 13,000g for 4min at 4°C. The cell solution was thereby separated into three layers, of which the top layer was taken for further processing. The volume of the obtained sample was then determined and 1.5x volumes of 100% ethanol were added. Afterwards, 700µl of sample were added onto RNeasy mini spin columns (Qiagen), centrifuged at 10,000g for 15s at RT and the flow through was discarded. This step was repeated until the entire sample was spun down.

Potential DNA contamination was then eliminated by subjecting the samples to DNase-I digestion using the RNase free DNase Kit (Qiagen). Preparation of the DNase solution was done by mixing 10µl DNase-I stock with 70µl RDD Buffer (both Qiagen) per sample to obtain a DNase working solution.

After all samples were collected in RNeasy mini spin columns, 700µl Buffer RWT (Qiagen) were added to the column, centrifuged for 15s at 10,000g, and the flow through was discarded. Then, 80µl of DNase-I working solution were added per sample and incubated at 25°C for 15min in a heating block. Afterwards. 350µl Buffer RWT were added to the column and centrifuged for 15s at 10,000g. The flow through was discarded.

Then, 700µl Buffer RPE (Qiagen) were added to the spin column, centrifuged at 10,000g for 15s at RT, and the flow through was discarded. Then, the procedure was repeated with 500µl Buffer RPE, but with a centrifugation time of 2min to dry the spin column filter. The collection tube was changed to a new one to remove residual contaminants, then another centrifugation step followed at 12,000g for 2min at RT. The spin columns were then transferred into new 1.5ml reaction tubes, 30µl RNase-fee water were added directly to the filter and the samples eluted at 10,000g for 1min. The eluent was measured at the NanoDrop 2000 as well as the 2100 Bioanalyzer (Agilent) to asses quantity and purity of the sample. Samples were stored at -80°C until further use.

2.10.1 Inhibitor Removal in RNA Samples

To eliminate melanin in MUG-Mel2 cells which would otherwise inhibit the PCR reaction, MUG-Mel2 RNA samples were processed using the OneStep PCR Inhibitor Removal Kit (Zymo Research, Irvine, USA). First, 600µl preparation solution were loaded onto Zymo-Spin™ III-HRC Columns (both Zymo Research) and centrifuged at 8,000g for 3min. Then, the spin columns were transferred into new 1.5ml reaction tubes. The entire RNA eluent of MUG-Mel2 samples was subsequently added to the spin columns and centrifuged at 16,000g for 3min. The eluent was stored at -80°C until further use.

2.11 cDNA Synthesis

cDNA synthesis was carried out using the High-Capacity cDNA Reverse Transcription Kit (Applied Biosystems, Thermo Fisher Scientific). Before performing cDNA synthesis, RNA sample concentrations were used to calculate the amount of RNA needed per sample to obtain 2µg cDNA. In accordance with the results, the following cDNA mixture was prepared for each individual sample: 2µl 10x RT Buffer, 25x dNTP Mix, 10x RT Random Primers, 1µl MultiScribe Reverse Transcriptase (all Applied Biosystems) and 5.2µl dH_2O nuclease free water were prepared per sample to obtain 10µl transcription solution. For No-Reverse-Transcriptase (NRT) control samples, the same mixture was used, but without the MultiScribe Reverse Transcriptase. RNA samples were diluted with the calculated amount of nuclease free water to obtain 10µl of a 0.2µg RNA/µl solution. The RNA solutions were then heated to 70°C for 2min in a thermal cycler (Bio-Rad Laboratories). Subsequently, 10µl of transcription solution were added to each RNA sample, then the samples were put into a thermal cycler (VWR) and the following program was applied: Samples were kept at 25°C for 10min, then the lid was heated to 37°C (Lid heating and sample heating was done separately). Samples were heated to 37°C for 120min, then the lid was heated to 110°C. Samples were then heated to 85°C for 5s, after which they were stored at -20°C until further use.

2.12 RNA Sequencing

To get an idea of DMAS affected pathways and genes, mRNA sequencing was performed with Sbcl2 and WM164 cell lines. Therefore, cells were seeded into six-well plates, incubated for 24h, and then treated for 24h either with DMAS IC_{50} concentrations or vehicle. Subsequently, RNA was extracted, quality and quantity analysed using NanoDrop 2000 and 2100 Bioanalyzer. Three independent replicates were made per cell line. The RNA samples were then sent for library preparation with the TruSeq stranded mRNA Kit

(Illumina, San Diego, USA) and sequencing using the Illumina HiSeq2500 (Illumina). Measurements were performed as single-read with 1x100bp and two HiSeq Rapid v2 SR runs. Processing of the raw data was performed with DeSeq2 3.6 (124). After obtaining differential expression data of both cell lines, further data read out was performed using DAVID 6.8 (125) and WebGestalt 2017 (126). First, differentially expressed genes were sorted out according to p-value, fold changes and IDs. Genes with p-values higher than 0.01 were discarded as well as genes exhibiting fold changes between minus one and one. Furthermore, all genes which were not identifiable by the entrez database were discarded. The remaining gene set was uploaded to DAVID 6.8 and WebGestalt 2017. Gene overrepresentation (GO) analysis was performed individually for each cell line in respect to biological processes, molecular functions and cellular distributions of genes. Gene sets with positive and negative fold changes were analysed first separately, then in combination. The resulting GO terms were uploaded in GO View (126) and overlapping GO terms between both software packages were chosen for further analysis. Hereafter, the chosen GO terms of both cell lines were uploaded to GO View and only overlapping pathways considered for further processing. All genes within the pathways of the chosen overlapping GO terms were looked up in the original data set of each cell line. Then, genes were compared between both cell lines in Excel 16.0. The resulting gene list, only representing genes overexpressed in both cell lines and found by both software packages, were now run again in WebGestalt 2017 to sort them into GO terms. In a last step, the found GO terms were screened for relevant pathways and potential gene candidates for further analysis.

2.13 RT-qPCR

Based on the results obtained from RNA sequencing and previously conducted apoptosis assays, real time quantitative polymerase chain reaction (RT-qPCR) measurements of *BAD*, *BAX*, *BCL2*, *NOXA, PUMA* and the housekeeping genes *ACTB, GAPDH* and *HPRT* were performed (Tab. 2) for melanoma cells. For chordoma, *BAD*, *BCL2, NOXA, PUMA* and the housekeeping genes *ACTB and GAPDH were* examined. MUG-Mel2, which did not yield results in the first runs, was later only repeated with *BAD*, *BAX*, *BCL2 NOXA, PUMA, ACTB* and *GAPDH* instead of all genes. For RT-qPCR experiments, melanoma and chordoma cell lines were first seeded into six-well plates. Following 24h settling time in the incubator, chordoma cells were treated with 2.2µM DMAS or vehicle and melanoma cells with the respective IC_{50} concentrations or vehicle. Chordoma cells were harvested after 24h treatment, melanoma cells after 6h or 24h DMAS treatment. mRNA was extracted and reverse transcribed to cDNA performed with all cells as described above.

For amplification, master mix was prepared using the Hot FirePol Evagreen qPCR Supermix (Solis Biodyne, Tartu, Estland). Per reaction, 2µl 5xHot FirePol Evagreen qPCR Supermix were mixed with the respective primers to reach a concentration of 150nM, then the solution was diluted with nuclease free H_2O to 6µl. cDNA was diluted with nuclease free H_2O to a concentration of 2.5ng/µl. Master Mix and cDNA were mixed at the Hamilton STARLet (Hamilton Robotics, Bonaduz, Switzerland) at a 6:4 ratio (Master Mix / cDNA) in a 384-well plate. The plate was then centrifuged at 200g for 1min at RT and run at the CFX384 real time thermal cycler (Bio-Rad Laboratories) using the following cycler protocol: For initialisation, samples were heated up to 95°C for 12min before starting the cycle. Then, samples were kept at 95°C for 20s (denaturation), followed by cooling down to 57°C for 20s (annealing) and heating up 72°C for 30s (elongation). Measurements were performed after the elongation step. This cycle was repeated for 40 times, after which a melting curve protocol was run: Samples were heated up to 95°C for 15s, then cooled down to 50°C. Afterwards, samples were heated up to 95°C for 0.5s. Throughout the heating, measurements were conducted. For relative quantification of the results, the ΔΔCt method based on the geometric mean of the internal controls ACTB and GAPDH was used. The values were obtained by first calculating the arithmetic mean of all quantitation cycles (Cq) values of all technical replicates of each housekeeping gene, then combining the gene Cq values using the geometric mean. Concerning the genes of interest (GOI), the arithmetic means of all technical replicates of the respective quantitation cycles (Cq values) were calculated. Then, the Cq values of the respective housekeeping genes were subtracted from the Cq values of the GOI to determine ΔCt. Subsequently, the untreated Cq values of each gene were subtracted from the treated Cq values to get ΔΔCt. The negative logarithmic value on base two of the determined ΔΔCt values was then calculated. Three independent experiments were conducted in triplicates.

2.14 Western Blot

2.14.1 Sample Preparation

Validation of qPCR derived overexpression results was done by western blot. First, cells were seeded in 60mm (melanoma cells) or 100mm (chordoma cells) petri dishes and incubated for 24h. Chordoma cells were treated with 2.2µM DMAS or vehicle and melanoma cells with the respective IC_{50} concentrations or vehicle for 24h.

Hereafter, western blots of chordoma cells were outsourced. The received densitometric raw data was analysed with ImageLab 5.2 (Bio-Rad Laboratories). Primary antibodies

against ACTB, AKT/pAKT, BCL2, BAX, BAK, ERK/pERK, PUMA, STAT3/pSTAT3 (Tyr705), (all from Cell Signaling Technology Technology, Danvers, Netherlands) cytochrome C (Santa Cruz Biotechnology, Santa Cruz, USA) and NOXA (Thermo Fisher Scientific) were used. Signal intensities were analysed densitometrically and expressed relative to ACTB, and the values were expressed relative to the control (mean ± SD).

Concerning melanoma cells, the cell culture medium was transferred into 15ml falcons and centrifuged at 1,500g for 4min at RT. The supernatant was then discarded. In the meanwhile, 100µl of RIPA lysis buffer (Thermo Fisher Scientific) containing protease inhibitor cocktail and PhosSTOP (both Sigma-Aldrich) was applied to the petri dishes. Following lysis, the cell solutions from the petri dishes were used to re-solubilise the cell pellets in the 15ml centrifugation tubes. They were then incubated for 10min at 4°C. Cell lysates were then centrifuged at 14,000g for 15min. Subsequently, the supernatant was obtained and stored at -80°C until further analysis.

2.14.2 Protein Concentration Determination with the Bicinchoninic Acid Assay (BCA)

Protein concentrations were determined from cell lysates using the Pierce BCA Protein Assay Kit (Thermo Fisher Scientific). First, a standard row containing bovine serum albumin (BSA, Thermo Fisher Scientific) concentrations of 0.01mg/ml to 1mg/ml was made in a 96-well plate. Per well 25µl of BSA in RIPA buffer were used. Then, 5µl of cell lysate and 20µl RIPA buffer were added into sample wells. Per well, 200µl of BCA working reagent (50:1 mixture of bottles A and B in the kit) (Thermo Fisher Scientific) were added and the solution incubated for 30min at 37°C. Afterwards, optical density was measured at the Omega SPECTROstar photometer at 562nm. Protein concentration was determined using the standard curve.

Hereafter, BAK, BAX, BCL2, GAPDH, PUMA (all Cell Signaling Technology), cytochrome C (Santa Cruz Biotechnology, Santa Cruz, USA), and NOXA (Thermo Fisher Scientific) were analysed by western blot using the below described method. Additionally, p53 (Cell Signaling Technology) was outsourced for western blotting and the received raw data interpreted using ImageLab 6.0.1.

2.14.3 Sodium Dodecyl Sulphate Polyacrylamide Gel Electrophoresis (SDS-Page) and Western Blot

After determination of protein concentrations, samples were diluted to a concentration of 1µg/µl. Samples were then mixed in a 1:1 ratio with 2x Laemmli sample buffer (Bio-Rad Laboratories) and loaded onto 4% – 12% Criterion XT Bis-Tris Protein Gels (Bio-Rad Laboratories). Page Ruler Plus Prestained Protein Ladder (Thermo Fisher Scientific) was used as band marker. Criterion XT mes 20x running buffer (Bio-Rad Laboratories) was diluted 20-fold with dH_2O and filled into the gel electrophoresis chamber. The gels were run at 40V for 20min, then at 180V for another 40min, until the loading buffer front reached the bottom of the gels. Subsequently, gels were blotted onto Immobilon-P PVDF 0.45µM nitrocellulose membranes (Merck) using the Trans-Blot SD Semi-Dry Transfer Cell (Bio-Rad Laboratories): First, membranes were activated in 100% methanol, and then submersed in dH_2O. Filter papers (Bio-Rad Laboratories) were soaked in transfer buffer (formula in Appendix). The blotting sandwich, consisting of filter paper on the bottom, then the membrane, followed by the gel and another filter paper, was placed on the semidry transfer system and the proteins were blotted at 180mA for 45min. Subsequently, membranes were submersed in PonceauS solution (Sigma-Aldrich) for 5min, and then the membranes cut above 10kd and below 35kd. Membranes were then de-colorized with water. Following cutting, membranes were blocked for 1h at RT using 5% skim milk powder (Sigma-Aldrich) in 1x TBST solution (formula in Appendix). Afterwards, membranes were washed with 1x TBST for 5min. Primary antibodies were dissolved in a 5% BSA in 1x TBST solution, applied to the respective membranes and incubated overnight at 4°C. For melanoma cells, BAK, BAX, BCL2, GAPDH, PUMA (all Cell Signaling Technology), cytochrome C (Santa Cruz Biotechnology, Santa Cruz, USA), and NOXA (Thermo Fisher Scientific) were used (Antibody details in Appendix). Following primary antibody incubation, membranes were washed three times with 1x TBST, then secondary antibodies were applied. Secondary antibodies were dissolved in a 5% skim milk powder in 1x TBST. After 1h incubation at RT, membranes were again washed 3 times with 1x TBST, then developed using Femto Maximum Sensitivity Reagent (Thermo Fisher Scientific). Chemiluminescence was measured with the ChemiDoc Touch and data readout was performed with the ImageLab 6.0.1 software. Results were depicted as relative protein expression of each sample compared to the respective GAPDH expression.

2.15 *NOXA* Knockdown

Transient *NOXA* knockdown was done in Sbcl2 and WM164 cells, then caspase-3 assays and western blots were performed.

2.15.1 Establishment of NOXA siRNA and Transfection Reagent Amounts

For establishment of DharmaFECT-2 (Dharmacon, Lafayette, USA) concentrations via FACS analysis, MUG-Mel1, MUG-Mel2, Sbcl2 and WM164 cells were seeded into 24-well plates and incubated for 24h. Then, 20µM or 80µM AllStars negative control siRNA AF488 (Qiagen) were added to all wells. Additionally, a concentration gradient of 5µM, 10µM, 20µM and 40µM DharmaFECT-2 was applied to the wells. A negative control containing no siRNA, but 40µM DharmaFECT-2 was used, as well as a negative control containing no DharmaFECT-2 but 20µM siRNA. Transfection was done for 24h or 48h, then samples were harvested and analysed on the CytoFLEX flow cytometer at Ex/Em: 495nm/519nm (FITC Channel) and data readout performed with the CytExpert 1.2.10.0 software.

Establishment of optimal *NOXA* siRNA amounts for highest transfection efficiency was done by western blotting. After seeding of Sbcl2 and WM164 cells in antibiotic free medium into 12-well plates and incubation for 24h, cells were transfected with 10µM DharmaFECT-2 and a *NOXA* siRNA concentration gradient of 10µM, 25µM, 50µM and 75µM. After 24h or 48h incubation, cells were treated with the respective DMAS IC_{50} concentrations for 24h and *NOXA* protein expression was determined using western blots. A negative control containing no DharmaFECT-2 nor DMAS treatment, and a control containing no siRNA while being DMAS treated, were used for comparison.

2.15.2 NOXA Knockdown Experiments

After determination of the optimal siRNA and DharmaFECT-2 concentrations, cells were seeded into 6-well plates and incubated for 24h. Then, 40µM DharmaFECT-2 were added to each well together with 20µM siRNA. Before that, siRNA and DharmaFECT-2 were diluted 1:10 with antibiotic free medium, then mixed and incubated for 20min at RT. Afterwards, medium was added to reach the needed total medium volume for treatment. The medium from the wells was then aspirated and the 6-well plates treated with 1ml transfection solution per well. Subsequent to 24h transfection, cells were treated with the respective DMAS IC_{50} concentrations for 24h, followed by active caspase-3 and western blot experiments were performed. Three biological replicates were made for both

experiments (123).

2.16 *In-Vivo* Experiments

2.16.1 Establishment

Melanoma cell concentrations ($2.5x10^6$ - $1x10^7$) needed for successful xenotransplantation were established on NU-Fox nu immunodeficient mice (Charles River Laboratories, Wilmington, USA). For Sbcl2 transplantation establishment, five mice were injected with 10^7 cells in the neck, $5x10^6$ cells in the right flank and $2.5x10^6$ cells in the left flank. For WM164 xenotransplants, the same cell amounts were injected at the same positions into five mice. Tumour size was measured by calliper every three days and DMAS injections started after the tumour reached a size of 5mm². Hereafter, 100µl of 1mM DMAS were injected directly into the tumours every 24h for four consecutive days. Tumour sizes were monitored throughout the treatment. Mice were subsequently sacrificed, then tumours (Sbcl2, WM164) and organs (only WM164) obtained for further analysis. WM164 tumours were embedded into paraffin (Sanova, Vienna, Austria) and 4µm slices stained with haematoxylin (Merck) and eosin (Gatt-Koller, Absam, Austria). All studies were conducted in accordance with the ethics committee vote BMWFW-66.010/0046-WF/V/3b/2016 (123).

2.16.2 In-Vivo Experiments

After completion of initial mouse trials, 40 NU(NCr)-Foxn1 immunodeficient mice (Charles River Laboratories, Wilmington, USA), 20 each for Sbcl2 and WM164, were injected with $5x10^6$ cells in both flanks for Sbcl2 and $2.5x10^6$ cells in both flanks for WM164. The change of mouse strain was necessary as Charles River Laboratories discontinued breeding of NU-Fox nu mice. Mouse tumour sizes were measured every three days and DMAS treatment started after the tumours reached sizes of approximately 5mm². DMAS was applied every 24h for three consecutive days, then paused for one day before starting a new cycle. In total, four cycles were made. In Sbcl2 tumour mice, one tumour was treated with 4mg/kg DMAS, the other one with PBS, while in WM164, mice were treated with a concentration gradient, with one tumour treated either with 1mg/kg, 2mg/kg or 4mg/kg per mouse and the other one with PBS. During treatment, mice were weighed, and the tumour sizes monitored. Mice were subsequently sacrificed, tumours and organs harvested and embedded into paraffin. Additionally, blood was taken from all mice and analysed. Paraffin blocks of all tumours and several organs were cut into 4µm slices and stained with haematoxylin and eosin (H&E) or KI67 (DAKO). All studies were conducted in

accordance with the ethics committee vote BMWFW-66.010/0046-WF/V/3b/2016 (123).

3 RESULTS

As Chordoma and Melanoma were largely examined independently from each other, the results chapter will be divided into those two tumour types. Chordoma- and melanoma cells will not be compared directly as each cancer type was handled like a single project.

3.1 Isolation of DMAS

DMAS was isolated as reported previously (Kretschmer et al., 2012) from roots of *Onosma paniculata* Bureau & Franchet (Boraginaceae) with 95% purity according to HPLC (Fig. 3). The HPLC chromatogram is shown below.

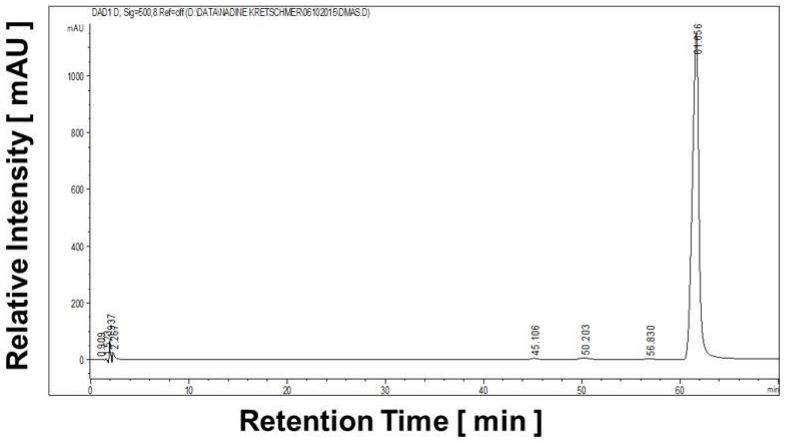

Ret. Time	Area
0.909	103.1
1.523	205.6
1.937	685.1
2.267	887.3
45.106	221.2
50.203	430
56.83	181.7
61.656	54302.1

Figure 3: HPLC chromatogram of the purification of a petrol-ether extract from Onosma paniculata Bureau & Franchet (Boraginaceae). The y-axis depicts the relative peak intensity in mAU, the x-axis the retention time for elution. DMAS purity was determined with 95% at a retention time of 61,7min. Reproduced from (122) with permission of publisher Elsevier.

3.2 CHORDOMA

3.2.1 Influence of DMAS Treatment on Chordoma Cell Viability

To determine the effects of DMAS on chordoma cell viability, two sacral (MUG-Chor1, U-CH2) and two clival (MUG-CC1, UM-Chor1) chordoma cell lines (App. Tab. 1) as well as adult human fibroblasts isolated from the MUG-Chor1 patient were treated with a DMAS concentration gradient and cell viability was measured after 48h incubation time using the Aqueous Non-Radioactive Cell Proliferation Assay Kit (Promega). Adult human fibroblasts

were chosen as control cells as there are currently no available non-tumourigenic cell lines originating from the notochord.

Hereby, it was found that chordoma cell viability decreased in a dose dependent manner, with DMAS efficacy varying among different cell lines, leading to different IC_{50} values (Tab. 1). Among the tested chordoma cell lines, U-CH2 depicted the highest susceptibility towards DMAS with an IC_{50} value of 1.9µM. MUG-Chor1, being next in line, needed to be treated already with twice the amount of DMAS to kill 50% of all cells, leading to an IC_{50} value of 3.5µM. This was followed closely by MUG-CC1 with 4.9µM IC_{50} value. UM-Chor1 DMAS susceptibility could not be determined due to a too high error bar, therefore the calculated IC_{50} value of 21.4µM was not significant. Thus, this value was not taken into consideration for decisions concerning DMAS treatments in further experiments. In comparison to the tested chordoma cell lines, adult human fibroblasts exhibited an IC_{50} value of 10.2µM, which was more than double the amount needed for MUG-CC1, the cell line depicting the lowest susceptibility to DMAS treatment. Therefore, DMAS treatment has a stronger influence on chordoma cell lines then on fibroblasts. Based on this assay, the treatment concentration for further experiments was set at 2.2µM DMAS. The graphs represent three independent experiments, performed in sextuplicate. Interestingly, the graphs formed a sigmoidal shape only for adult human fibroblasts, while MUG-CC1, MUG-Chor1 and UM-Chor1 graphs were closer to a linear course. U-CH2, in contrast, could even be approximated using an exponential equation (Fig. 4) (122).

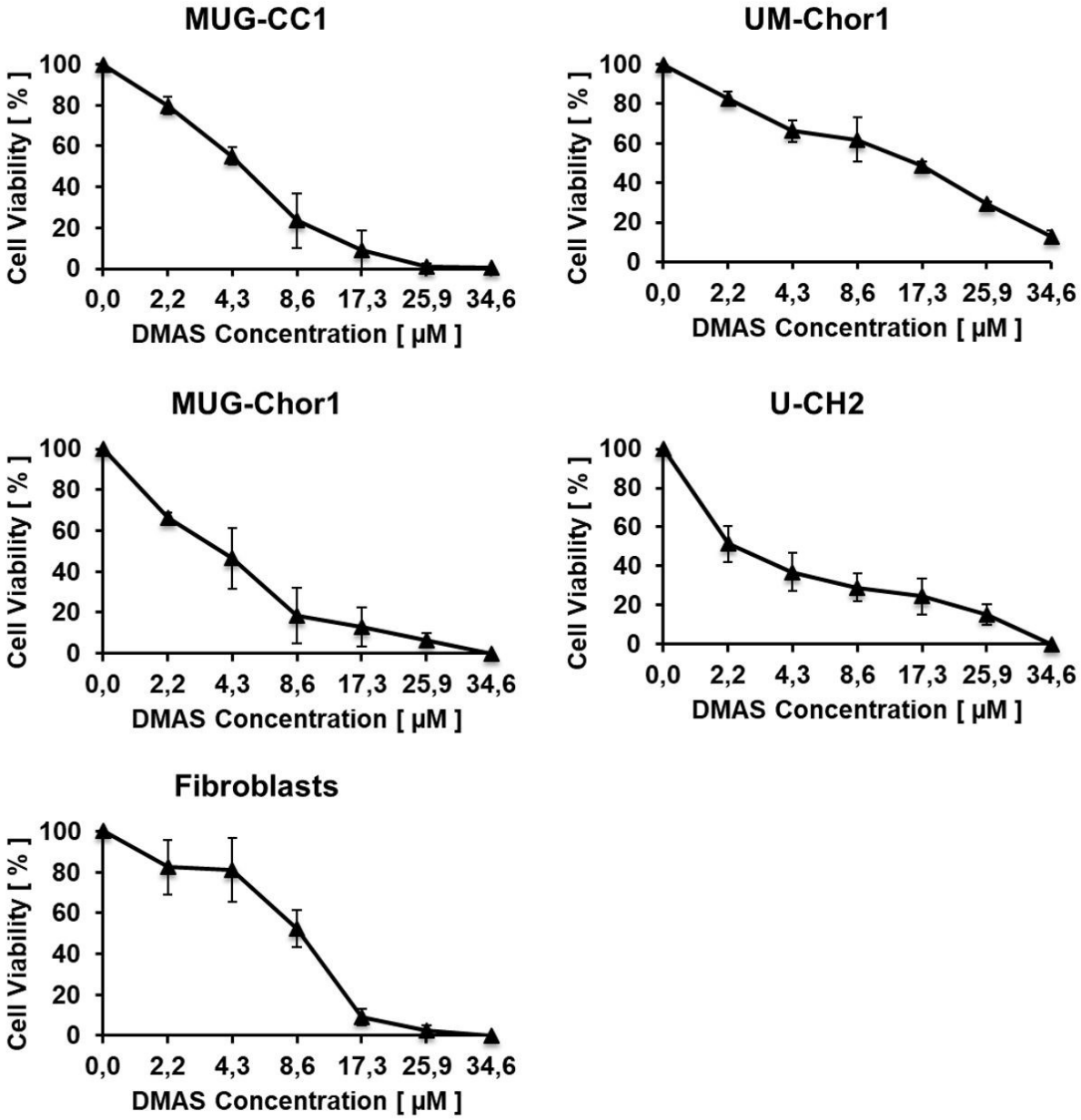

Figure 4: MTS viability assay of MUG-CC1, UM-Chor1, MUG-Chor1, U-CH2, and fibroblasts after DMAS treatment for 48h. The dot blot shows the cell viability at different DMAS concentration for the different cell lines. The x-axis represents cell viability in percent, the y-axis the various DMAS concentrations, with the error bars showing standard deviations Reproduced with modifications from (122) with permission of publisher Elsevier.

Table 2: DMAS IC_{50} values including standard deviations. Values represent three independent experiments in sextuplicate.

Cell Line	DMAS IC_{50} [µM]
MUG-CC1	4.9 ± 0.2
MUG-Chor1	3.5 ± 0.5
UM-Chor1	21.4 ± 44.9
U-CH2	1.9 ± 0.9
Adult Human Fibroblasts	10.2 ± 3.1

3.2.2 Apoptosis Induction by DMAS in Chordoma Cells

3.2.2.1 Annexin V / SYTOX Green Assay

To determine the DMAS induced type of cell death, Annexin V / SYTOX Green staining was performed on all used chordoma cell lines after 24h of 2.2µM DMAS treatment. Thereby, it was found that DMAS induced early- as well as late apoptosis in all used cell lines. Additionally, none of the cell lines exhibited significant amounts of necrosis. U-CH2, which showed the highest susceptibility in MTS assays, also displayed the strongest response to DMAS treatment in the Annexin V / SYTOX Green assay. For this cell line, 34% of all cells were stained Annexin V positive, depicting early apoptosis, while another 37% were stained positive for Annexin V and SYTOX Green, representing late apoptotic cells. The second most affected cell line was UM-Chor1, with 23.1% early and 8.7% late apoptotic cells, followed by MUG-CC1 with 24.7% early- and 5% late apoptotic cells. MUG-Chor1 was the least affected cell line in this assay, with 27.6% apoptotic cells, separated into 16% early- and 11.6% late apoptotic cells. The summary of all cell lines is shown in Figure 5A, while representative FACS dot blots are depicted in Figure 5B. The calculated amounts of apoptotic cells in percent are shown in Table 3 (122).

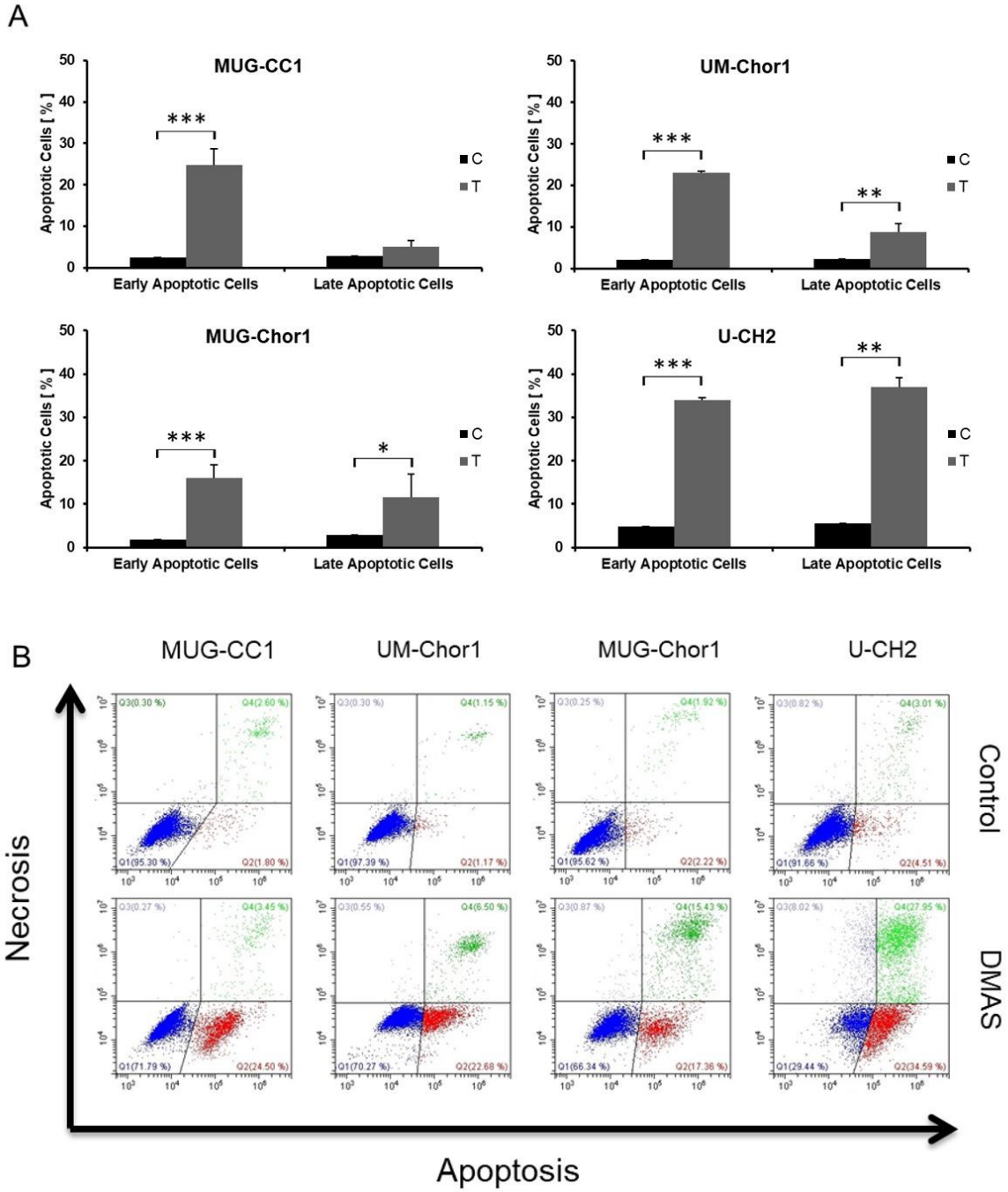

*Figure 5: Annexin V / SYTOX Assay of chordoma cell lines after 24h treatment time. Figure 5A shows the summary of the calculated early- and late apoptotic cells for each cell line, with the x-axis displaying the percentage of effected cells. Control cells are depicted in black, treated cells in dark grey. *p<0.05, **p<0.01, ***p<0.001, Error bars represent the standard deviation, C = control, T = treated Figure 5B shows representative FACS dot blots of all used chordoma cell lines. The x-axis displays Annexin V pacific blue staining, the y-axis SYTOX green staining. Blue coloured cells are Annexin V and SYTOX Green negative viable cells, red coloured cells are Annexin V positive early apoptotic cells. Green coloured cells depict Annexin V and SYTOX Green positive late apoptotic cells and purple coloured cells show SYTOX Green positive necrotic cells. Reproduced with modifications from (122) with permission of publisher Elsevier.*

Table 3: Calculated averages of viable cells, early apoptotic cells, late apoptotic cells, necrotic cells and overall apoptotic cells of 2.2µM DMAS treated and untreated chordoma cells after 24h incubation time

Cell Line	Treatment	Viable Cells	Early Apoptotic Cells	Late Apoptotic Cells	Necrotic Cells	Apoptotic Cells Overall
MUG-CC1	Control	94.5 ± 1.6	2.4 ± 0.5	2.8 ± 1.3	0.3 ± 0.1	5.2
	Treated	70 ± 5.1	24.7 ± 4	5 ± 1.6	0.3 ± 0	29.7
MUG-Chor1	Control	95 ± 1.6	1.8 ± 0.5	2.9 ± 1.4	0.3 ± 0.1	4.7
	Treated	71.6 ± 4.8	16 ± 3	11.6 ± 5.3	0.9 ± 0.1	27.6
UM-Chor1	Control	95.2 ± 2.2	2.1 ± 0.9	2.3 ± 1.1	0.4 ± 0.1	4.4
	Treated	67.3 ± 2.9	23.1 ± 0.4	8.7 ± 2.2	0.9 ± 0.4	31.8
U-CH2	Control	88.8 ± 3.7	4.8 ± 0.3	5.5 ± 3.4	0.9 ± 0.2	10.3
	Treated	22.9 ± 5.8	34 ± 0.6	37 ± 8.4	6.1 ± 2.3	71

3.2.2.2 Caspase-3 Assay

To verify the apoptosis inducing effect of DMAS on chordoma cells, cells were stained after 24h treatment with 2.2µM DAMS with fluorophore conjugated anti active caspase-3 antibodies and measured by flow cytometry. All samples were found to express active caspase-3 upon DMAS treatment, in contrast to untreated cells, which depicted no caspase-3 activity. As would be expected after the Annexin V / SYTOX Green assay, U-CH2 showed by far the strongest response to DMAS treatment, with 52.4% of all cells exhibiting active caspase-3. The second most effected cell line was MUG-CC1 with 18.9%, closely followed by UM-Chor1 with 16.2%. The cell line displaying the least amount of active caspase-3 was MUG-Chor1 with 6.5% (Fig. 6A, B and Tab. 4) (122).

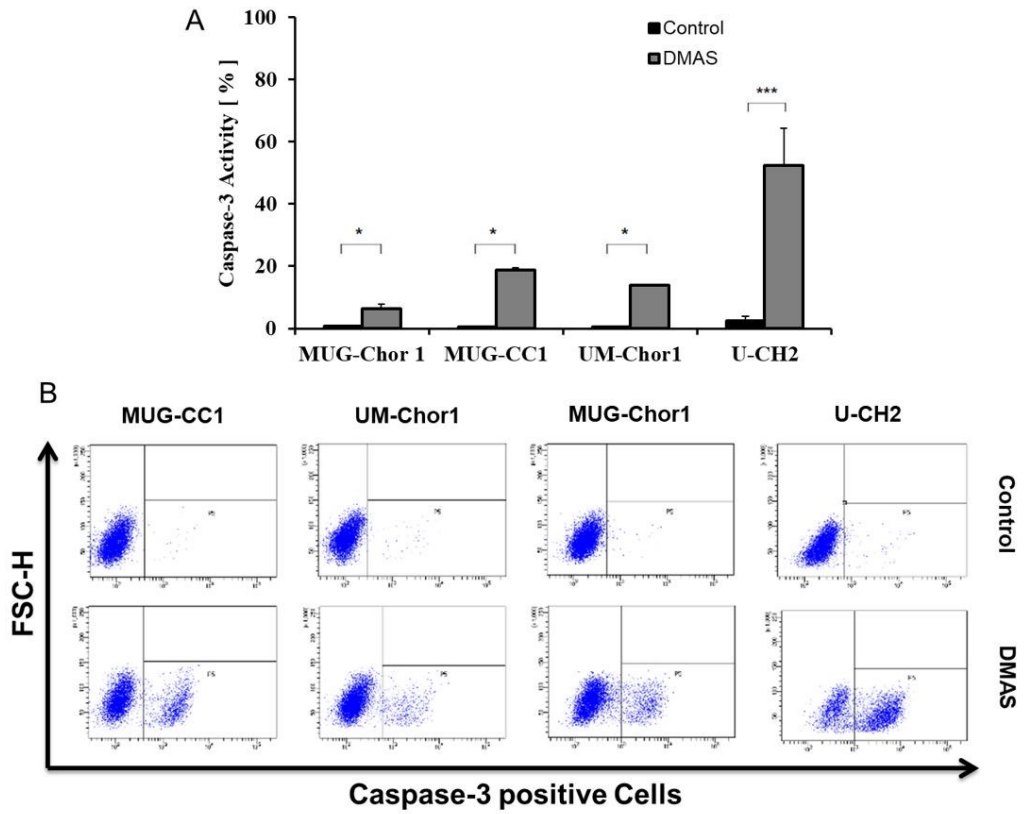

*Figure 6: Active caspase-3 assay after 24h DMAS treatment. Figure 6A shows the overview of all four used chordoma cell lines. The x-axis displays the cell lines, the y-axis the percentage of active caspase-3. Control cells are depicted in black, treated cells in grey. *p<0.05, ***p<0.001. Figure 6B shows representative caspase-3 FACS dot plots with caspase-3 positive cells on the x-axis and forward scatter height on the y-axis. The upper row shows untreated control cells, the lower row 2.2µM DMAS treated cells Reproduced from (122) with permission of publisher Elsevier.*

Table 4: Summery of the calculated averages of caspase-3 positive cells in percent including the standard deviation.

Cell Lines	Treatment	Caspase-3 Positive Cells
MUG-CC1	Control	0.4 ± 0.1
	Treated	18.9 ± 0.6
MUG-Chor1	Control	0.7 ± 0
	Treated	6.5 ± 1.3
UM-Chor1	Control	0.5 ± 0.1
	Treated	16.2 ± 3.3
U-CH2	Control	2.1 ± 2.1
	Treated	52 ± 11.4

3.2.3 DMAS changes Expression Levels of Apoptosis Genes in RT-qPCR Experiments

Examination of DMAS influence on apoptosis gene expression levels in chordoma cells was done using RT-qPCR. After 24h of 2.2µM DMAS treatment, RNA was isolated from cells, reverse transcribed into cDNA and RT-qPCR experiments were performed with primers for *BAD, BCL2, NOXA* and *PUMA*. *ACTB* and *GAPDH* were used as housekeeping genes (App. Tab. 2). Thereby, *BAD* did not exhibit any differences between control and treated cells, independent of the cell line. Furthermore, *BCL2* was only significantly overexpressed in *U-CH2*, depicting a 2.3-fold change compared to control cells. *PUMA* was overexpressed in all cell lines, however, only MUG-Chor1 showed a significant overexpression of 3.6 times compared to the untreated value. In contrast, significant differences in *NOXA* gene expression under DMAS treatment were observed in all four used cell lines. The strongest influence was seen with MUG-Chor1 with 6-fold overexpression, followed by U-CH2 with a 3.6-fold change and UM-Chor1 with a 3.4-fold overexpression. MUG-CC1 displayed the smallest change with 1.8-fold overexpression of DMAS treated cells in comparison to control cells (Fig. 7 and Tab. 5) (122).

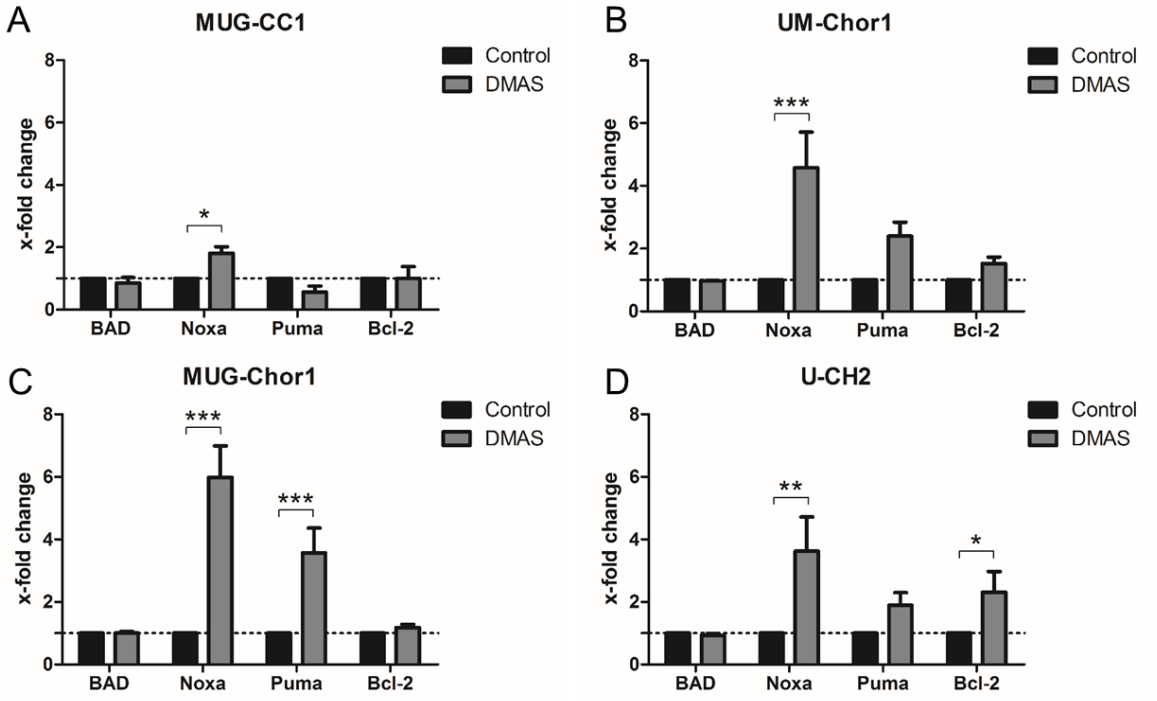

*Figure 7: mRNA expression levels, determined with RT-qPCR in chordoma cell lines after 24h of 2.2µM DMAS treatment. Overexpression levels of the apoptosis genes BAD, BCL2, NOXA and PUMA are displayed between control (black) and treated (grey) samples. The x-axis shows the genes, the y-axis the respective x-fold changes *p<0.05, **p<0.01, ***p<0.001. Reproduced from (122) with permission of publisher Elsevier.*

Table 5: Overexpression levels of BAD, BCL2, NOXA and PUMA after 24h 2.2µM DMAS treatment, with standard deviations.

Cell Lines	BAD	BCL2	NOXA	PUMA
MUG-CC1	0.9 ± 0.3	1.0 ± 0.7	1.8 ± 0.4	0.6 ± 0.3
MUG-Chor1	1.0 ± 0.1	1.2 ± 0.2	6.0 ± 1.7	3.6 ± 1.4
UM-Chor1	1.0 ± 0.0	1.5 ± 0.4	3.4 ± 0.0	2.4 ± 0.8
U-Ch2	0.9 ± 0.1	2.3 ± 1.1	3.6 ± 1.9	1.9 ± 0.7

3.2.4 DMAS Treatment influences Protein Expression Levels of Apoptosis and Survival / Proliferative Genes

Verification of DMAS induced overexpression of apoptosis genes was done with western blots. Similar to RT-qPCR experiments, BCL2, NOXA and PUMA were examined. BAD western blots were not performed as BAD did not show overexpression in RT-qPCR experiments in any cell line under DMAS treatment. Apart from verification of the RT-qPCR genes, BAK, BAX and CYC western blots were also made. All assessed protein expressions were calculated as ratios to the respective ACTB expression levels (Tab 6). Hereby, differences in protein expression levels were found between the used cell lines. Concerning BCL2/ACTB (Fig. 8A), expression levels were relatively similar, ranging from 0.43 to 1.0, while BAK/ACTB (Fig. 8C) expression levels changed drastically, from 0.37 to 1.48. However, none of these two proteins exhibited significant changes between control and treated cells. Similar results were obtained with BAX (Fig. 8B) and CYC (Fig. 8D). While BAX displayed relatively stable amounts between all cell lines except MUG-Chor1, which seemed to be BAX deficient, CYC displayed bigger differences between the cell lines. None of the changes, however, could be linked to DMAS treatment of the cells. In contrast, NOXA (Fig. 8E) and PUMA (Fig. 8F) showed strong DMAS dependent differences in protein expression levels. PUMA was marginally, but significantly overexpressed in MUG-Chor1, and strongly overexpressed in UM-Chor1 with a 0.07/1.82 ratio between control and treated cells. The other two cell lines displayed no significant changes of PUMA expression levels. NOXA, however, showed significant overexpression in all cell lines. The lowest NOXA overexpression was found in MUG-Chor1 with a 0.08/0.64 (C/T) ratio, followed by U-CH2 with 0.05/0.73 (C/T) ratio. UM-Chor1 showed

with 0.07/1.24 (C/T) ratio strong overexpression of NOXA, while the biggest change was seen in MUG-CC1 with 0.54/2.72 ration between control and treated cells. The blots representing protein expression levels between control and treated cells of the different cell lines are shown in Fig. 8G and Fig 8H (122).

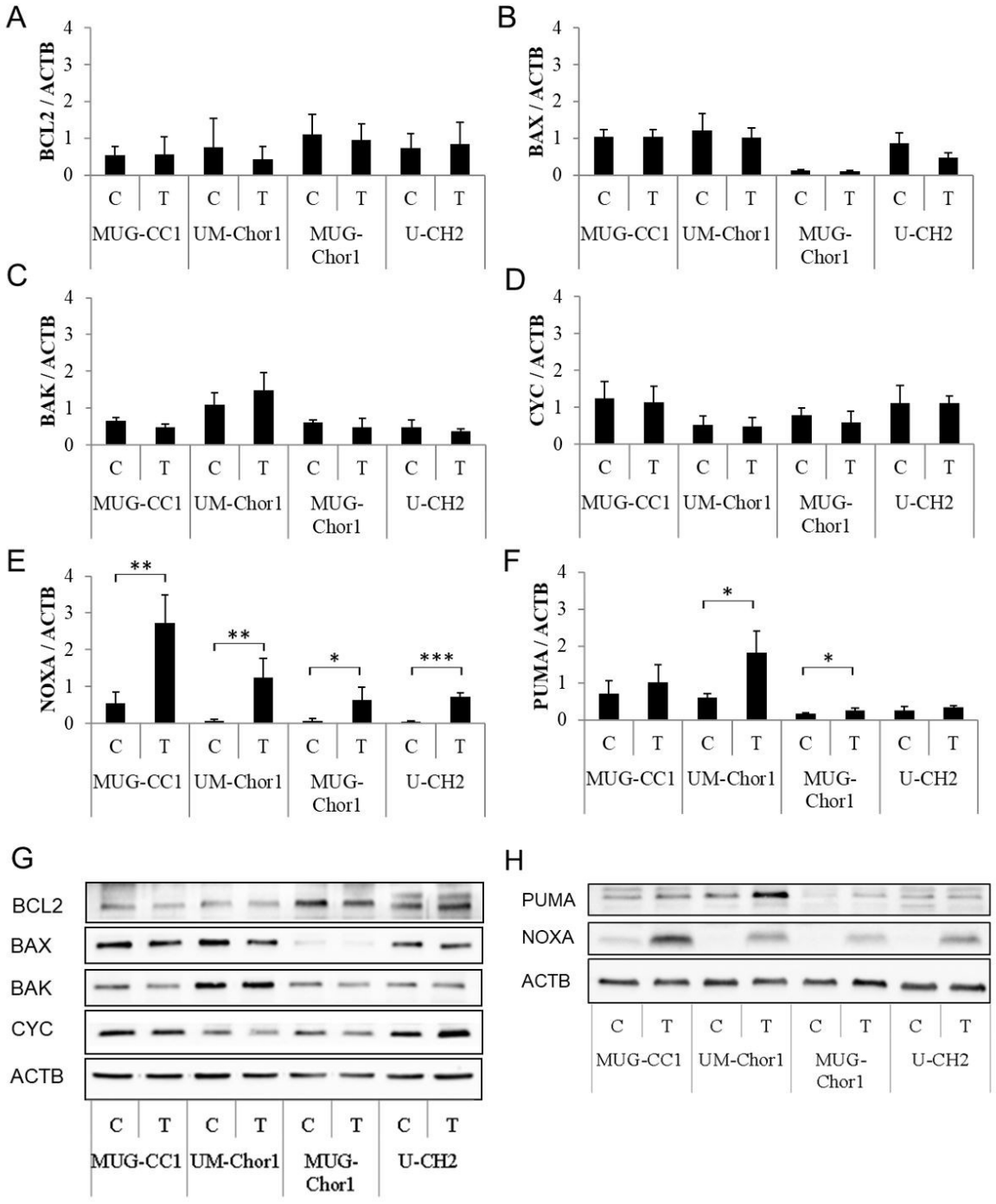

*Figure 8: Western blots of apoptosis proteins after 24h DMAS treatment. Densitometric analysis of the apoptosis related proteins A) BCL2, B) BAX, C) BAK, D) CYC, E) NOXA and F) PUMA in respect to ACTB. G) and H) show representative western blot membranes of the apoptotic proteins. The x-axis shows the different cell lines. the y-axis depicts the ratio between protein expression and ACTB as housekeeping gene, (C = control, T = treated). *p<0.05, **p<0.01, ***p<0.001. Reproduced from (122) with permission of publisher Elsevier.*

Table 6: Summary of all expression level ratios of the examined proteins including standard deviations after 24h DMAS treatment.

		BAK / ACTB	BAX / ACTB	BCL2 / ACTB	CYCS / ACTB	NOXA / ACTB	PUMA / ACTB
MUG-CC1	Control	0,66 ± 0,08	1,04 ± 0,19	0,55 ± 0,24	1,25 ± 0,45	0,5 ± 0,3	0,7 ± 0,4
	Treated	0,48 ± 0,09	1,04 ± 0,19	0,56 ± 0,48	1,14 ± 0,43	2,7 ± 0,8	1 ± 0,5
MUG-Chor1	Control	1,1 ± 0,32	1,21 ± 0,46	0,76 ± 0,78	0,52 ± 0,25	0,1 ± 0	0,2 ± 0
	Treated	1,48 ± 0,49	1,02 ± 0,27	0,43 ± 0,35	0,48 ± 0,25	0,6 ± 0,3	0,3 ± 0
UM-Chor1	Control	0,61 ± 0,07	0,13 ± 0,01	1,1 ± 0,55	0,78 ± 0,2	0,1 ± 0	0,6 ± 0,1
	Treated	0,48 ± 0,25	0,1 ± 0,04	0,96 ± 0,44	0,59 ± 0,29	1,2 ± 0,5	1,8 ± 0,6
U-CH2	Control	0,47 ± 0,2	0,87 ± 0,27	0,73 ± 0,4	1,11 ± 0,48	0 ± 0	0,3 ± 0,1
	Treated	0,37 ± 0,08	0,47 ± 0,13	0,84 ± 0,6	1,11 ± 0,2	0,7 ± 0,1	0,3 ± 0

To elucidate whether DMAS also has an influence on proliferative or survival proteins, AKT/pAKT, ERK/pEKR and STAT/pSTAT (Tyr705) were examined using western blots (Fig. 9 and Tab. 7). Phosphorylated and un-phosphorylated forms of each protein were measured under DMAS or vehicle treatment and the ratios between them was calculated. Ratios of untreated cells were set to 1 (= 100%) to enable better comparison between samples. The protein expression levels of all three proteins did not change under DMAS treatment, however, the ratios between the un-phosphorylated and the phosphorylated form did, indicating DMAS induced inhibition of protein activation. The ratio of ERK/pEKR (Fig. 9A) was strongest influenced in MUG-CC1, with values going down to 0.04 after treatment. This was followed by MUG-Chor1 with 0.46 ratio, then U-CH2 with 0.6 ratio and UM-Chor1 with the smallest effect of 0.67. Transferring to percent, even UM-Chor1 with the lowest susceptibility would exhibit a change of 33%, or one-third of protein activation, while with 99,6% almost the entire protein activation would be inhibited in the case of MUG-CC1. Concerning AKT (Fig. 9B), the biggest change in protein expression ratios between the phosphorylated and un-phosphorylated form was observed in MUG-Chor1 with 0.67 difference (0.33 remained). This was followed by a ratio of 0.41 in UM-Chor1, followed by 0.54 in U-CH2. Almost no change in protein activation was seen in MUG-CC1 with 0.92 of 100. Coming to STAT3 expression levels (Fig. 9C), MUG-CC1 did not display

STAT3 or pSTAT3 levels, neither in control nor in treated cells, suggesting a STAT3 deficiency. DMAS influence on STAT3 activation ratios was strongest in MUG-Chor1 with only 0.15 ratio remaining after treatment, followed by U-CH2 with 0.41. UM-Chor1 was least effected, still exhibiting a ratio of 0.91 (122).

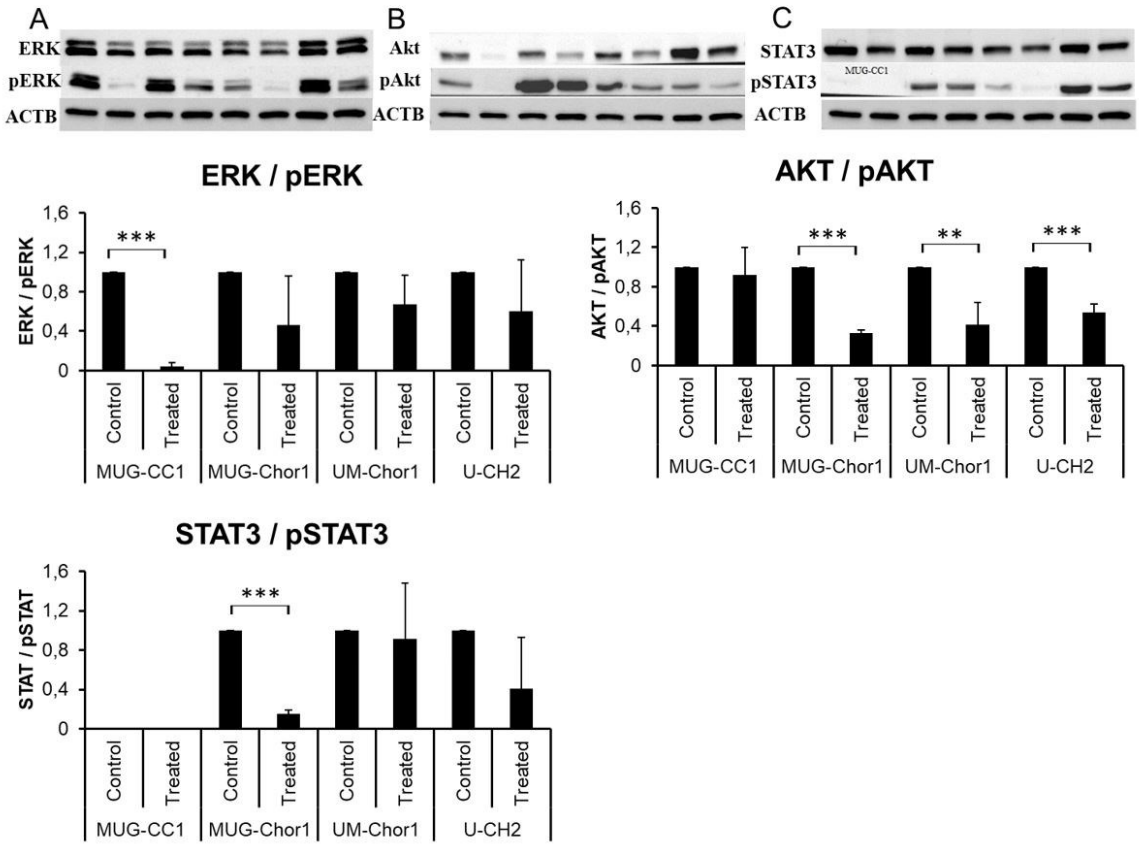

*Figure 9: Western blots of survival proteins and densitometric analysis of the ratios of un-phosphorylated vs. phosphorylated protein expression levels of A) ERK/pEKR, B) AKT/pAKT and C) STAT3/pSTAT3 (Tyr705). The x-axis contains the different cell lines, the y-axis depicts the ratio between phosphorylated and un-phosphorylated form. **p<0.01, ***p<0.001. Reproduced from (122) with permission of publisher Elsevier.*

Table 7: Summary of all expression level ratios of the examined survival proteins including standard deviations.

		AKT/pAKT	ERK/pERK	STAT/pSTAT
MUG-CC1	Control	1 ± 0	1 ± 0	0 ± 0
	Treated	0,92 ± 0,28	0,04 ± 0,04	0 ± 0
MUG-Chor1	Control	1 ± 0	1 ± 0	1 ± 0

	Treated	0,33 ± 0,03	0,46 ± 0,5	0,15 ± 0,04
UM-Chor1	Control	1 ± 0	1 ± 0	1 ± 0
	Treated	0,41 ± 0,23	0,67 ± 0,3	0,91 ± 0,57
U-CH2	Control	1 ± 0	1 ± 0	1 ± 0
	Treated	0,54 ± 0,08	0,6 ± 0,52	0,41 ± 0,52

3.3 MELANOMA

3.3.1 Influence of DMAS Treatment on Melanoma Cell Viability

3.3.1.1 EZ4U Assay

Elucidation of DMAS induced effects on melanoma cell viability was examined using the EZ4U cell proliferation and cytotoxicity assay (Biomedica) on five melanoma cell lines (MUG-Mel1, MUG-Mel2, Sbcl2, WM164, WM793) with different mutational profiles (App. Tab. 1) as well as on MCR-5 fibroblasts and juvenile melanocytes. DMAS incubation was performed for 24h, 48h and 72h to be able to assess whether DMAS induced viability reduction is time-dependent. MRC-5 fibroblasts and juvenile melanocytes, serving as control cells, were only treated for 24h. Melanocytes were chosen as control cells as natural counterpart to the tumorigenic melanoma cells. MRC-5 fibroblasts, on the other hand, were chosen to provide information about wide spread effects of DMAS on the body (123).

Thereby, DMAS was found to reduce cell viability in a dose- and time dependent manner. The exact IC_{50} values for each cell line and time points are shown in Table 8. Additionally, Figure 10A depicts a comparison of all IC_{50} values of the used melanoma cell lines as well as MRC-5 fibroblasts and juvenile melanocytes. Black bars represent 24h, light grey bars 48h and dark grey bars 72h of DMAS treatment. DMAS concentrations in µM are shown on the x-axis, cell lines on the y-axis. Comparing the different cell lines, WM793 cells seem to be more susceptible to DMAS treatment than any other cell line, with IC_{50} values of 1.17µM (24h), 0.81µM (48h) and 0.66µM (72h) (Fig. 10B. 5). This is closely followed by

MUG-Mel1 and Sbcl2, with IC_{50} value ranges of 1.9µM to 0.96µM and 1.89µM to 1.14µM, respectively (Fig. 10B. 1 and 3). In contrast, MUG-Mel2 and WM164, having IC_{50} ranges of 5.13µM to 1.68µM and 3.82µM to 2.42µM (Fig. 10B. 2 and 4), were far less susceptible to DMAS treatment. Interestingly, juvenile melanocytes were with 1.87µM IC_{50} DMAS concentration as susceptible to DMAS treatment as MUG-Mel1 and Sbcl2, which needed to be treated with the lowest DMAS concentrations among the used melanoma cell lines to achieve a 50% viability reduction. In contrast, MRC-5 fibroblasts were more robust than any other cell line tested, with 9.49µM DMAS needed to significantly lower cell viability. Comparing the time dependent effects of DMAS on cell viability, a steady decrease in IC_{50} concentrations could be observed for all cell lines except Sbcl2, which depicted a lower 48h IC_{50} then 72h IC_{50} value. However, the Sbcl2 IC_{50} values were close enough that the calculated standard deviations overlap, therefore their comparison yields an insignificant difference, hence not influencing the overall trend. Furthermore, the IC_{50} concentration reduction between 24h and 72h treatments varies among the cell lines, with some cell lines experiencing drastic changes while others depict more stable concentrations. For instance, MUG-Mel2 IC_{50} concentrations drop from 5.13µm to 1.68µM, which is a 3-fold decline, while Sblc2 values decline from 1.89µM to 1.23µM, showing a mere 1.5-fold decline. Figure 10B contains the summary of viability curves obtained with all cell lines and all time points. Figure 10C contains the scatter blots for healthy control cells MRC-5 and adult human fibroblasts after 24h (123). Taken together, Figure 10 and Table 8 show that DMAS treatment effects cell viability over a longer timer period, but at least for 72h, in a dose and time dependent manner (123).

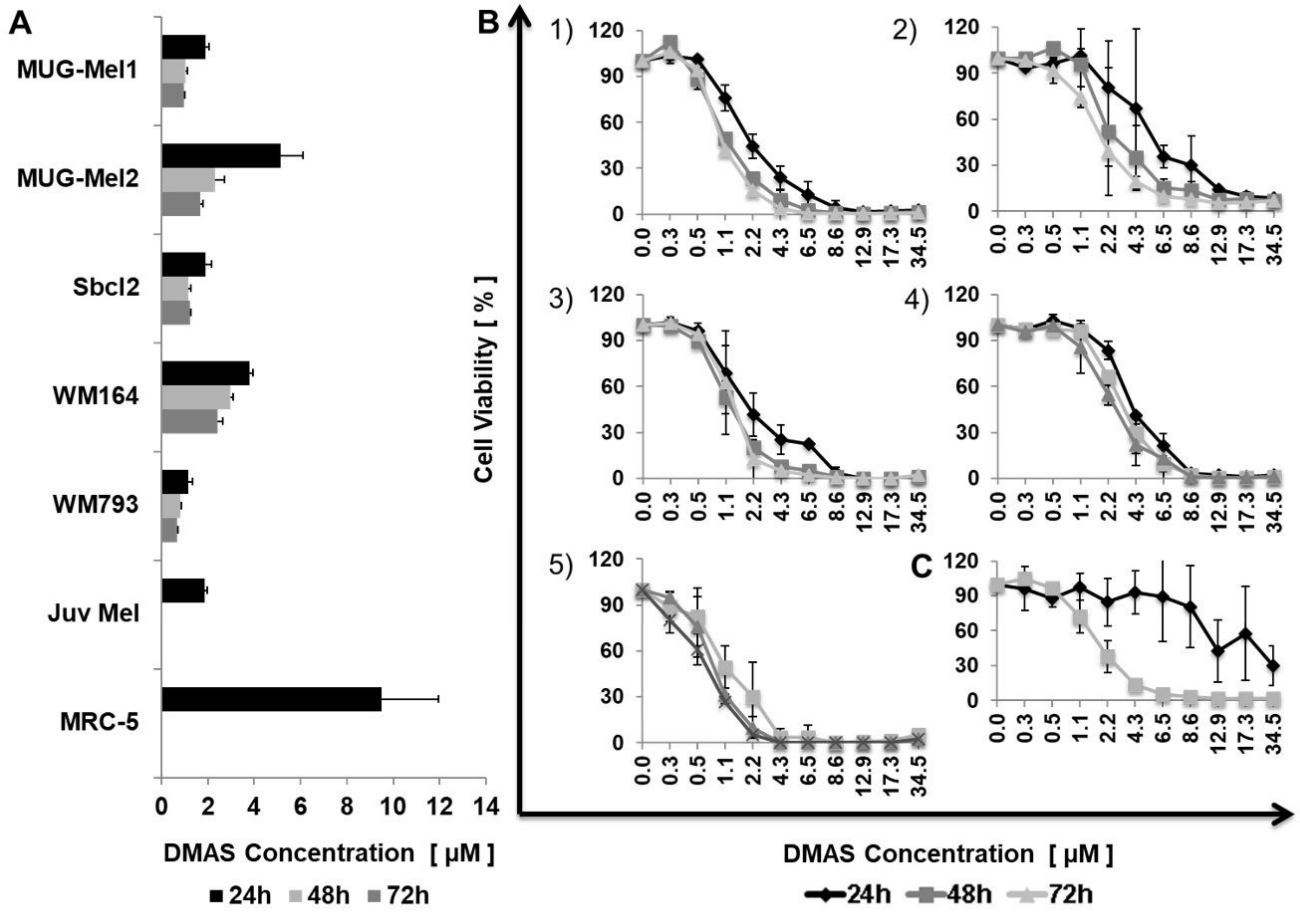

Figure 10: EZ4U viability assay of melanoma cells. A) shows a summary of calculated IC50 values of all used cell lines in respect to treatment times, with 24h shown in black, 48h in light grey and 72h in dark grey. DMAS IC50 concentrations are displayed on the x-axis, cell lines on the y-axis. B) shows the respective scatter blots, organised in cell lines and treatment times, with 1) MUG-Mel1, 2) MUG-Mel2, 3) Sbcl2, 4) WM164 and 5) WM793. The x-axis depicts the used DMAS concentrations in µM, the y-axis cell viability in percent. The colour scheme is similar to A). C) shows the respective EZ4U assays after 24h for MRC-5 fibroblasts (black) and juvenile melanocytes (light grey) (123).

Table 8: Calculated DMAS IC50 Concentrations in µM for the used melanoma cell lines MUG-Mel1, MUG-Mel2, Sbcl2, WM164 and WM793 after 24h, 48h and 72h DMAS treatment. Additionally, IC50 DMAS values of the healthy control cells MCR-5 fibroblasts and juvenile melanocytes after 24h treatment are depicted in the table. All values are shown with the respective standard deviations (123).

IC_{50} DMAS [µM]

Cell Lines	24h	48h	72h
MUG-Mel1	1.9 ± 0.14	1.06 ± 0.07	0.98 ± 0.03
MUG-Mel2	5.13 ± 0.96	2.32 ± 0.40	1.68 ± 0.09
Sbcl2	1.89 ± 0.26	1.14 ± 0.12	1.23 ± 0.03
WM164	3.82 ± 0.12	2.96 ± 0.13	2.42 ± 0.21
WM793	1.17 ± 0.16	0.81 ± 0.05	0.66 ± 0.04
Juv Mel	1.87 ± 0.10	n/a	n/a
MRC-5	9.49 ± 2.48	n/a	n/a

3.3.1.2 Annexin V / SYTOX Green Assay

Differentiation between DMAS induced apoptosis or necrosis was done with Annexin V Pacific Blue (Biolegend) and SYTOX Green (Life Technologies) staining after 6h and 24h DMAS treatment with the respective 24h IC_{50} concentrations (Tab. 9). Figure 11 A-E shows the calculated Annexin V positive cells (early apoptotic cells) as well as cells stained with Annexin V and SYTOX Green (late apoptotic cells) in percent for A) MUG-Mel1, B) MUG-Mel2, C) Sbcl2, D) WM164 and E) WM793. The graphs show the time points and the separation between early and late apoptotic cells on the x-axis while apoptotic cells in percent are depicted on the y-axis. Grey bars indicate control (C), black bars treated (T) cells. Figure 11 F) shows the respective FACS raw data dot blots for each cell line, time point and treatment. The high x-axis shows the cell lines, the right y-axis the treatment and time. The left y-axis shows necrosis, the lower x-axis apoptosis. Yellow dots represent cells negatively stained for Annexin V and SYTOX Green, indicting viable cells. Green dots show early apoptotic cells, positively staining for Annexin V, while purple cells display necrosis, being SYTOX green positive. At last, blue dots indicate late apoptotic cells, stained positively for both Annexin V and SYTOX Green. As no significant number of necrotic cells could be observed at any timepoint, those cells were not depicted in parts A-E. (123).

MUG-Mel1 and WM793 show more early apoptotic cells then late apoptotic ones. In contrast, MUG-Mel2 as well as Sbcl2 depict more late apoptotic cells, and WM164 show a balanced amount. Therefore, no clear pattern was observable regarding DMAS induced effects after 6h or 24h. Concerning the used cell lines, the strongest effect of DMAS was seen with Sbcl2, showing 76% and 84% apoptotic cells after 6h and 24h treatment, respectively. Late apoptotic cells accounted with 65% (6h) and 67% (24h) the majority of all apoptotic cells. This was followed by MUG-Mel2 with 27% after 6h and 57% apoptotic cells after 24h treatment. The difference between 6h and 24h was mainly caused by an increase of late apoptotic cells, which rose from 17% after 6h to 44% after 24h treatment. A strong effect was also observed in MUG-Mel1 after 24h with 51% of all cells showing early apoptosis, compared to only 6% early apoptotic cells after 6h treatment. In contrast to Sbcl2 and MUG-Mel2, few late apoptotic cells were observed, making up 2% of all apoptotic cells after 6h treatment and 8% after 24h treatment. The least effected cells were WM164 (11% after 6h and 25% after 24h) and WM793 (10% after 6h and 22% after 24h) (123). In WM164, early and late apoptotic cells differed after 6h treatment (2% early- and 9% late apoptotic cells), but were almost equal after 24h treatment, with early apoptotic cells accounting for 12% and late apoptotic cells accounting for 13% of all

apoptotic cells. In contrast, WM793 depicted with 6% after 6h and 18% after 24h more early apoptotic cells compared to late apoptotic ones, which made up only 4% at both time points (123).

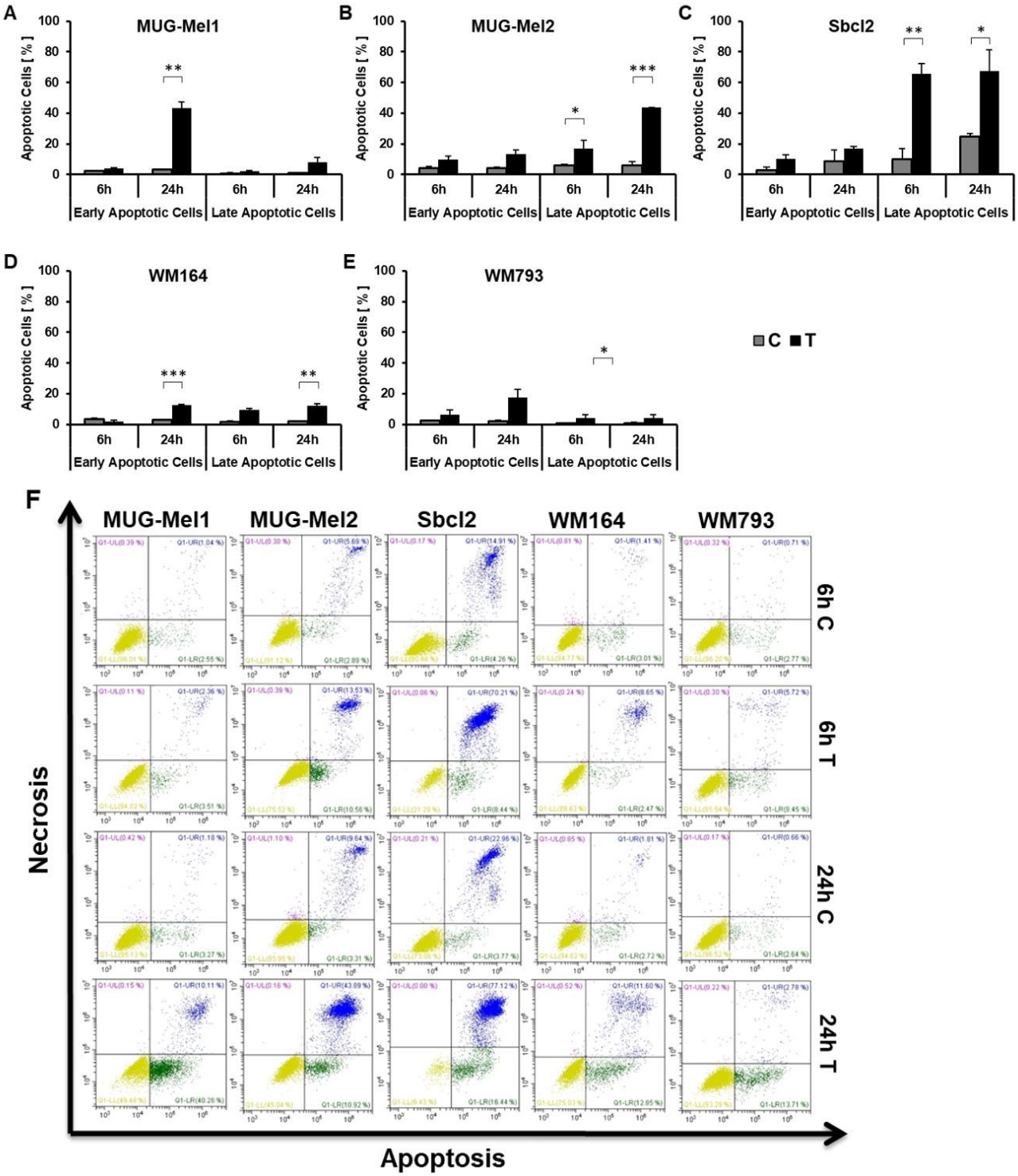

*Figure 11: Annexin V Pacific Blue / SYTOX green assay. A-E shows the summery of early and late apoptotic cells with A) MUG-Mel1, B) MUG-Mel2, C) Sbcl2, D) WM164 and E) WM793, while F) contains the respective representative FACS dot plots. Concerning the summary, vehicle treated cells are shown in grey, DMAS treated ones in black. The x-axis shows the time points and the y-axis apoptotic cells in percent. For the dot plots, viable cells are shown in yellow, early apoptotic cells in green, late apoptotic ones in blue and necrotic ones in purple. Asterixis indicate significance with *p<0.05, **p<0.01 and ***p<0.001, C = control, T = treated (123).*

Table 9: Calculated averages and standard deviations of melanoma cells in the Annexin V Pacific Blue / SYTOX green assay after 6h and 24h DMAS respective IC50 treatment.

		Early Apoptotic Cells [%]		Late Apoptotic Cells [%]		Overall Apoptosis [%]	
Cell Line	**Treatment**	**6h**	**24h**	**6h**	**24h**	**6h**	**24h**
MUG-Mel1	Control	2,2 ± 0,5	3,5 ± 0,3	0,7 ± 0,5	0,9 ± 0,4	2,9	4,4
	Treated	4 ± 0,7	43,2 ± 4,1	2,1 ± 0,3	8,1 ± 2,8	6,1	51,3
MUG-Mel2	Control	4,3 ± 0,8	4,2 ± 0,6	5,9 ± 0,7	6 ± 2,2	10,2	10,2
	Treated	9,9 ± 2,2	13,5 ± 2,4	17 ± 5,3	43,8 ± 0	26,9	57,3
Sbcl2	Control	3 ± 1,8	8,8 ± 7,1	10,1 ± 6,8	24,6 ± 2,3	13,1	33,4
	Treated	10,2 ± 2,5	17,1 ± 1	65,5 ± 6,7	67,3 ± 14	75,7	84,4
WM164	Control	3,5 ± 0,7	3 ± 0,4	1,8 ± 0,5	2 ± 0,3	5,3	5
	Treated	1,9 ± 0,8	12,7 ± 0,2	9,4 ± 1,2	12,3 ± 1,1	11,3	25
WM793	Control	2,4 ± 0,5	1,9 ± 1,1	0,6 ± 0,2	0,9 ± 0,3	3	2,8
	Treated	6,2 ± 3,1	17,5 ± 5,4	3,9 ± 2,5	4,3 ± 2,2	10,2	21,9

3.3.1.3 Caspase-3

To validate the apoptotic effect caused by DMAS in melanoma cells, active caspase-3 was measured by flow cytometry. Cells were treated with the respective DMAS IC_{50} concentrations for 24h, then stained with fluorophore labelled anti-active caspase-3 antibodies and measured by FACS (Fig. 12A, B and Tab. 10A). To ensure that caspase-3 activity was solely induced by DMAS, samples of two cell lines (MUG-Mel1 and WM793) were additionally treated with caspase-3 inhibitor (Fig. 12C and Tab. 10B). Thereby, all used cell lines were found to exhibit significant amounts of active caspase-3 after DMAS treatment, thus verifying the results gained by the Annexin V / SYTOX Green assay. Sbcl2 and MUG-Mel1 were with 58% and 47% active caspase-3 the most effected cell lines, followed by MUG-Mel2 with 43% and WM164 with 24% active caspase-3 depicting cells, respectively. WM793 was the least effected with only 9% of all cells showing caspase-3 activity (Fig. 12A). Concerning the inhibitor controls, both tested cell lines showed a decrease of caspase-3 activity under DMAS treatment when caspases were simultaneously inhibited artificially. The activities declined by 43% for MUG-Mel1 and 11% for WM793. However, due to too high error bars, only MUG-Mel1 results were found to be statistically significant. Interestingly, overall caspase-3 activity in WM793 also differed between inhibitor and normal experiments, while no such change was seen in MUG-Mel1

(123). Overall, the strength of DMAS induced effects seen in the Annexin V Pacific Blue / SYTOX Green for each used cell line was reflected in the caspase-3 assay, thereby validating the results (123).

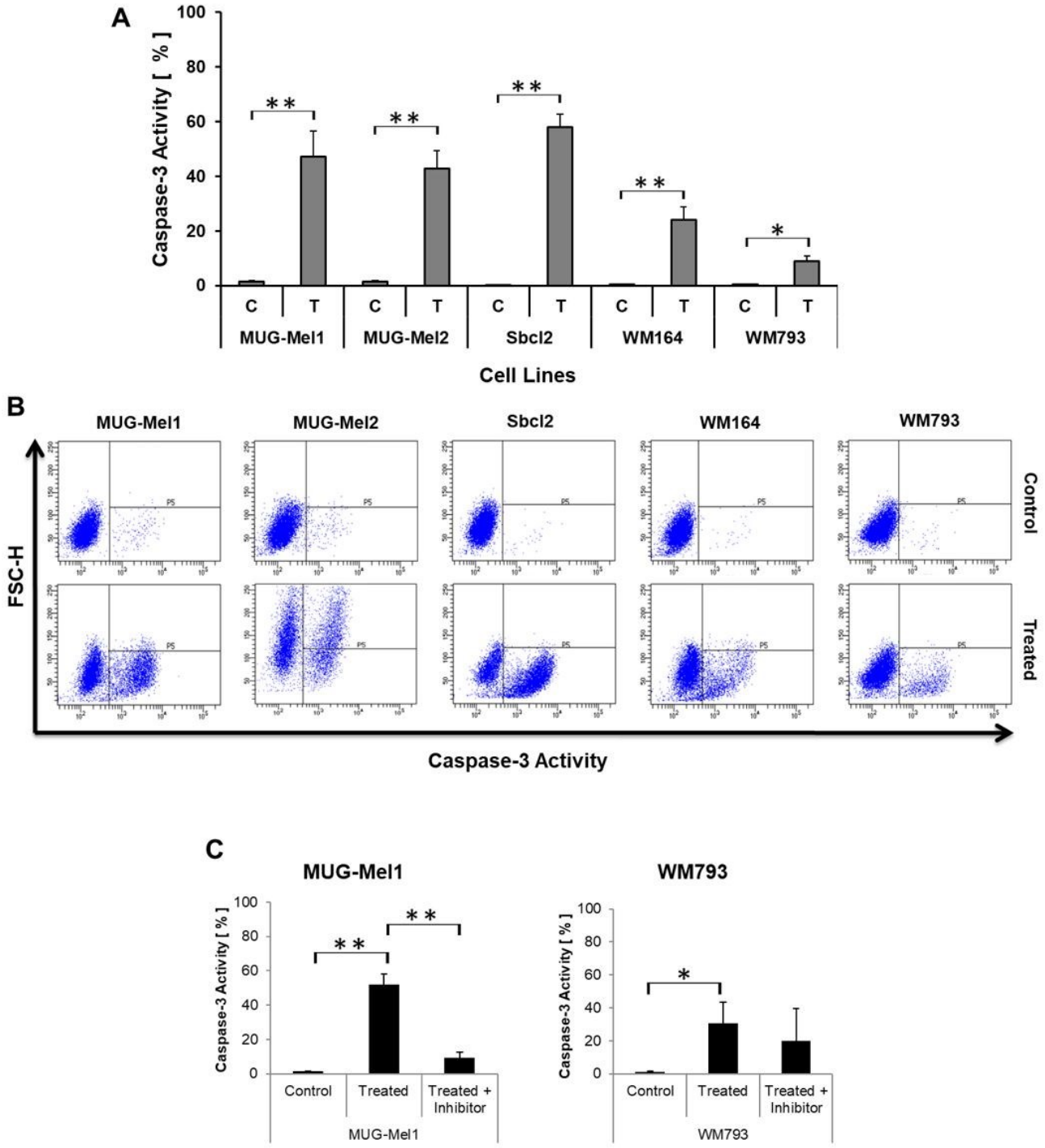

*Figure 12: Active caspase-3 assay. A) shows the summary of all used cells depicting caspase-3 activity in the FACS analysis. The x-axis presents the cell lines and the treatment (C = control, T = treated), the y-axis the caspase-3 activity in percent. B) shows the respective FACS scatter plots. The high x-axis contains the cell lines, the low x-axis shows caspase-3 activity. The left y-axis depicts forward scatter height, the right y-axis the treatment. C) exhibits the MUG-Mel1 and WM793 control caspase-3 assays including the inhibitor controls. Axis are similar to A) *p < 0.05, **p < 0.01 (123).*

Table 10: Summary of all calculated values and standard deviation of the caspase-3 assay. A) shows the normal experiments, B) the inhibitor controls.

A

		Active Caspase-3 depicting Cells [%]
MUG-Mel1	Control	1,4 ± 0,3
	Treated	47,1 ± 9,3
MUG-Mel2	Control	1,3 ± 0,6
	Treated	42,9 ± 6,5
Sbcl2	Control	0,2 ± 0,1
	Treated	58 ± 4,6
WM164	Control	0,5 ± 0,1
	Treated	24 ± 4,7
WM793	Control	0,5 ± 0,1
	Treated	8,9 ± 2

B

		Active Caspase-3 depicting Cells [%]
MUG-Mel1	Control	1,3 ± 0,1
	Treated	51,9 ± 6,3
	Treated + Inhibitor	9,2 ± 3,5
WM793	Control	1,2 ± 0,4
	Treated	30,6 ± 12,7
	Treated + Inhibitor	19,8 ± 20

3.3.2 Cell Cycle

To elucidate whether DMAS treatment influences the cell cycle of melanoma cell lines, cells were fixed and stained with propidium iodide 24h and 48h after DMAS treatment and measured by flow cytometry. Small differences in cell cycle distribution between control and treated cells as well as between the different time points could be observed in all cell lines. However, only MUG-Mel1 cells depicted statistically significant results in the G1 and S phase (Fig. 13A). After 24h DMAS treatment, MUG-Mel1 G1 cell amounts declined by around 19%, while cells in S phase increased by 12% and G2/M cells by 7%. After 48h, the decrease in MUG-Mel1 G1 cells was merely 14%, while the increase in S phase cells was about 20%. G2/M cells, in contrast to the 24h values, decreased by 6.5%. Therefore, between 24h and 48h DMAS treatment, the cell cycle distribution in MUG-Mel1 cells shifted from a primarily G1 phase-oriented change to a S phase change between control and treated cells. The results can be observed in the table and figure below (Fig. 13 and Tab. 11) (123).

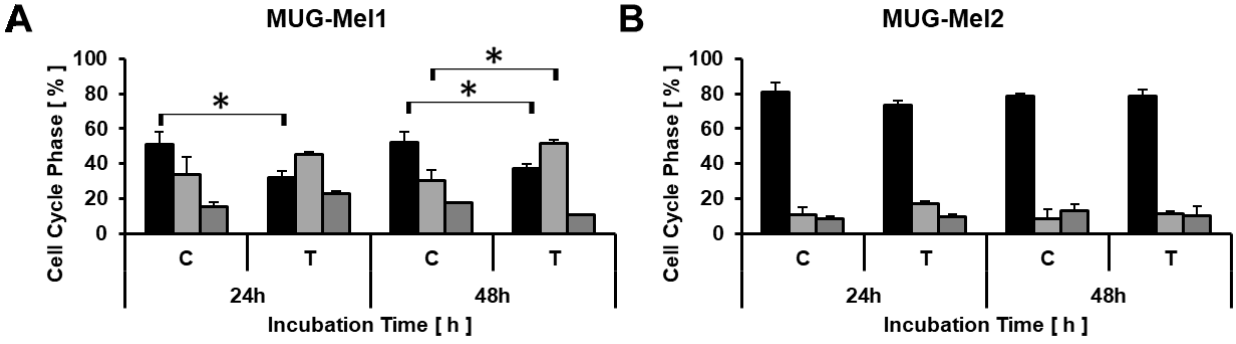

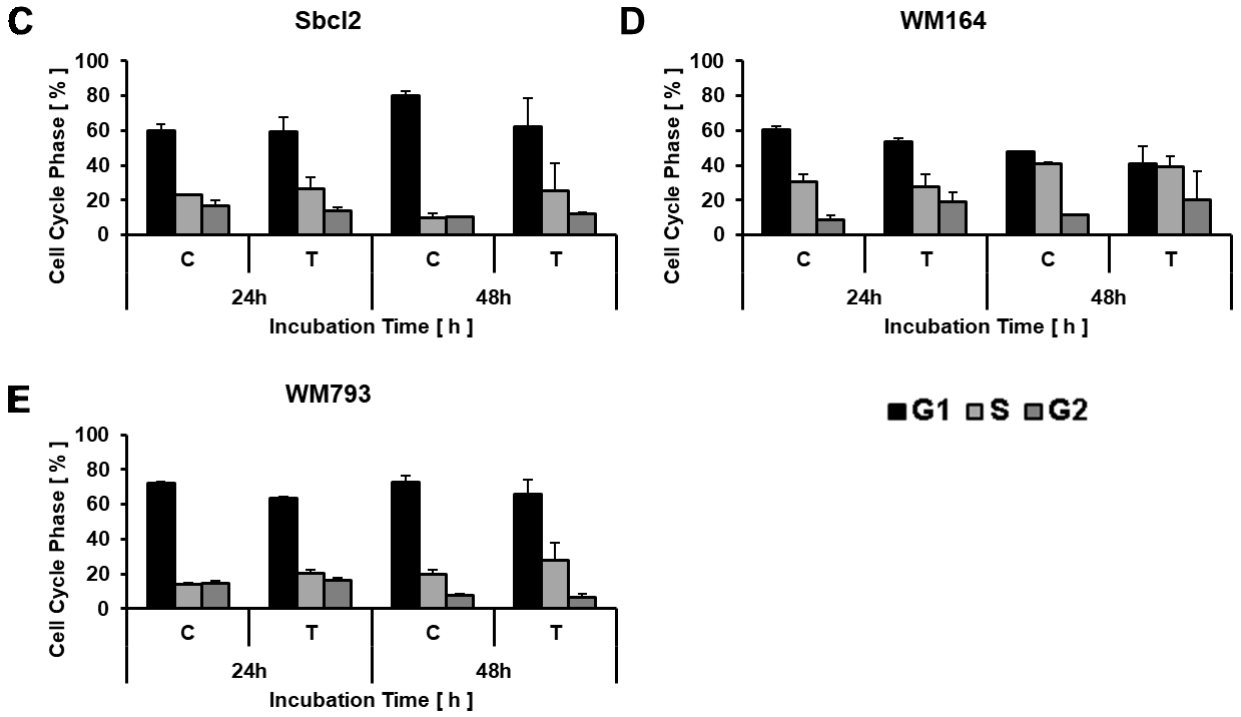

*Figure 13: Cell cycle analysis of DMAS IC50 treated A) MUG-Mel1, B) MUG-Mel2, C) Sbcl2, D) WM164 and E) WM793 cells. The x-axis depicts the incubation time in hours as well as the treatment (C = control, T = treated), the y-axis the cell cycle phase of the cell lines in percent. Black bars represent G1, light grey bars S and dark grey bars cells in G2/M phase. *p < 0.05 (123).*

Table 11: Calculated averages of cell cycle distributions including standard deviations of all five tested melanoma cell lines after 24h and 48h DMAS IC50 treatment.

			Cell Cycle Phase [%]		
Cell Line	**Time**	**Treatment**	**G1**	**S**	**G2/M**
MUG-Mel1	24h	Control	51,1 ± 7,3	33,6 ± 10	15,3 ± 2,7
		Treated	32,2 ± 3,3	45 ± 1,7	22,8 ± 1,6
	48h	Control	52 ± 6,1	30,5 ± 5,7	17,5 ± 0,4
		Treated	37,4 ± 2,2	51,6 ± 2,2	11 ± 0
MUG-Mel2	24h	Control	80,8 ± 5,5	10,7 ± 4,3	8,6 ± 1,1
		Treated	73,4 ± 2,9	17,2 ± 1,2	9,4 ± 1,7
	48h	Control	78,8 ± 1,5	8,5 ± 5,5	12,8 ± 4
		Treated	78,7 ± 3,9	11,2 ± 1,8	10,1 ± 5,6
Sbcl2	24h	Control	60,2 ± 3,4	23,2 ± 0,3	16,7 ± 3,1
		Treated	59,5 ± 8,3	26,7 ± 6,2	13,8 ± 2,1

	48h	Control	80 ± 2,9	9,8 ± 2,6	10,3 ± 0,3
		Treated	62,1 ± 16,3	25,5 ± 15,8	12,4 ± 0,5
WM164	24h	Control	60,6 ± 1,6	30,7 ± 4	8,7 ± 2,4
		Treated	53,8 ± 1,9	27,4 ± 7,6	18,8 ± 5,7
	48h	Control	47,8 ± 0,6	40,8 ± 1	11,4 ± 0,4
		Treated	40,7 ± 10,4	39,1 ± 6,1	20,2 ± 16,5
WM793	24h	Control	72,2 ± 1,1	13,9 ± 1,1	14,3 ± 1,5
		Treated	63,6 ± 0,7	20,2 ± 2,2	16,2 ± 1,6
	48h	Control	72,7 ± 3,6	19,8 ± 2,5	7,6 ± 1
		Treated	65,7 ± 8,4	27,8 ± 10,1	6,8 ± 2,1

3.3.3 DMAS Treatment changes mRNA Expression Profiles in Melanoma Cells

After assessment of DMAS induced apoptotic effects in the used melanoma cells, possible pathways responsible for the observed effects were examined by mRNA sequencing. First, Sbcl2 and WM164 cells were treated for 24h with DMAS IC_{50} concentrations, then RNA extracted, reverse transcribed to cDNA and measured using next generation Illumina sequencing. The results were interpreted with DeSeq 2, DAVID and WebGestalt.

Thereby, 7891 differentially expressed genes were found in Sbcl2 and 6033 in WM164 (Cut off: Benjamini-Hochberg (BH) corrected p-value < 0.1). Of those, only genes with a fold change (f) bigger than one or smaller than minus one $\{f \in \mathbb{R} \,/\, -1 > f < 1\}$ were considered for further analysis, yielding 2417 genes for Sbcl2 and 1312 genes for WM164. The results obtained with those genes after a five-step analysis are depicted in Figure 13. Steps 1-3 (Fig. 14A) depict the organising and sorting of the genes. On top, data analysis with differentially expressed genes of Sbcl2 and WM164 with DAVID and WebGestalt is shown. Of the 100 most significant GO Terms found in each cell line, 66 were overlapping between both software packages for Sbcl2 and 69 for WM164. These overlapping GO terms were used in the next step (Fig 14A middle), were they were compared between cell lines. In total, 30 GO terms were found to be overexpressed in both cell lines. Those GO terms were analysed again (last Venn diagram) in a more refined comparison, resulting in 188 genes which were significantly overexpressed. The resulting genes were sorted in step 4 into pathways (Fig. 14B), of which the “Apoptosis Signaling Pathway”, the “p53 Pathway” and the “p38 MAPK Pathway” were considered

most promising for containing candidate genes. Looking into those pathways (step 5), *FOS*, *JUN*, *TNF* and *BAG3* were found for the Apoptosis Signaling Pathway and *PMAIP1*, also known as *NOXA*, for the p53 Pathway. For the p38 MAPK pathway, *MAPK13* was found (Fig. 14C). Based on these findings, it was decided to focus on the mitochondrial-, p53 driven apoptosis pathway, and its representative *NOXA* (Fig. 14D). NOXA showed a 1.37-fold upregulation under treatment in Sbcl2 with a BH corrected p-value of $2.7x10^{-16}$, while in WM164 it was 1.6-fold upregulated with a BH corrected p-value of 10^{-4} (123).

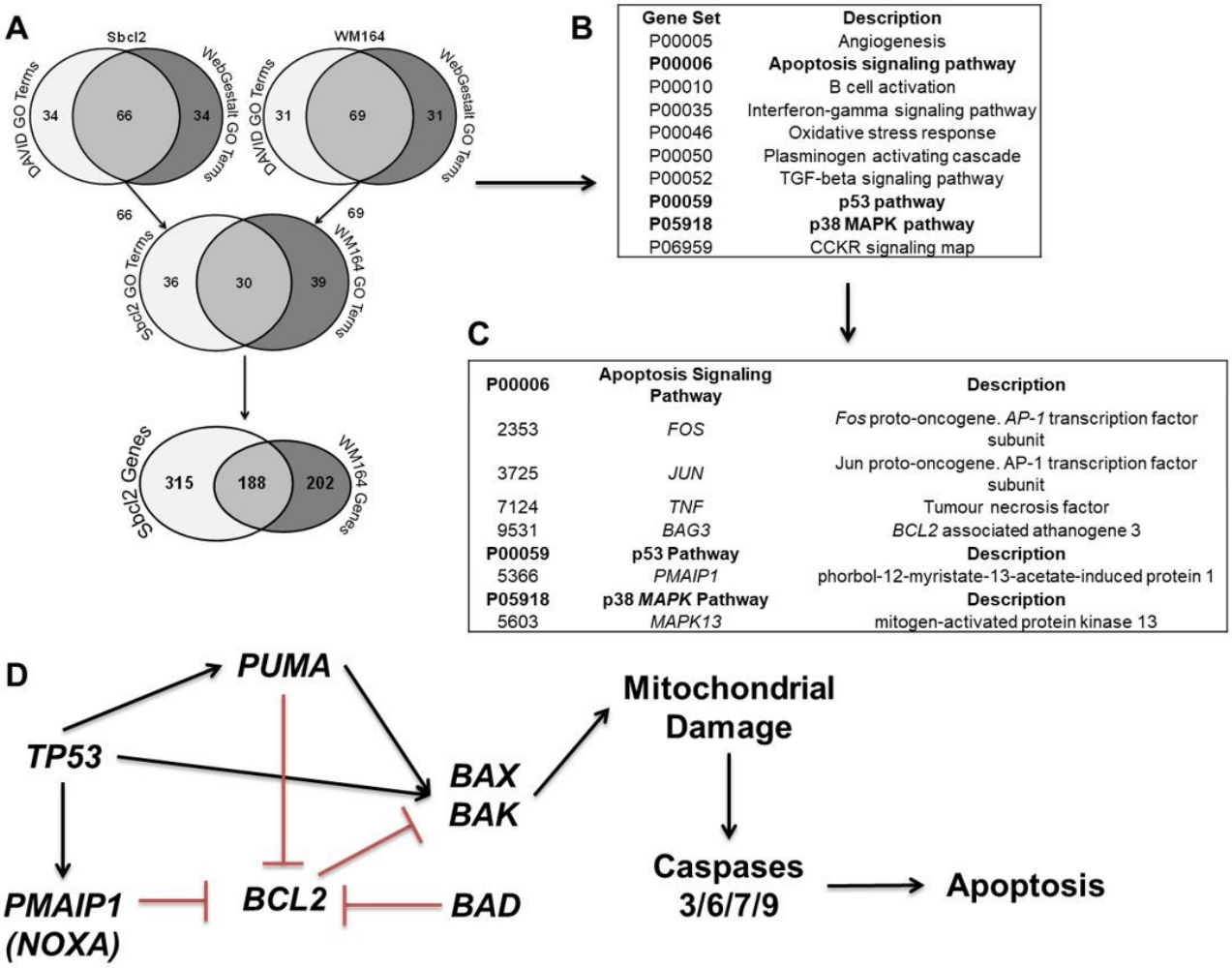

Figure 14: mRNA sequencing results of Sbcl2 and WM164, shown within a five-step process of data readout. A) contains the sorting and organising of cells with DAVID and WebGestalt, B) the resulting pathways. C) shows the genes chosen from the resulting pathways of B). E) shows NOXA in the context of the mitochondrial p53 driven apoptosis pathway (123).

3.3.4 DMAS influences Expression Levels of Apoptosis Genes in RT-qPCR Experiments

Following up on the decision made after mRNA sequencing, the p53 dependent mitochondrial pathway was examined more closely. Therefore, RT-qPCR experiments of genes related to this pathway, namely *BAD, BAX, BCL2, NOXA* and *PUMA* were performed with all five cell lines after 6h and 24h of DMAS respective IC_{50} treatment. *GAPDH* and *ACTB* were used as housekeeping genes (Fig. 15, Tab. 12, App. Tab. 2). No changes in *BAD* or *BAX* expression levels under DMAS treatment could be observed in any of the cell lines. Additionally, *BCL2* only showed significant overexpression after 6h (2-fold) and 24h (4-fold) in Sbcl2. *PUMA* was found to be overexpressed in two cell lines, namely MUG-Mel1 (6h, 3-fold) and WM164 (6h, 3.4-fold). Interestingly, overexpression was only significant after 6h treatment, declining again after 24h. This trend could also be observed in MUG-Mel2 were the small overexpression value of 1.2-fold (MUG-Mel2) declined to 0.9-fold after 24h. Sbcl2 showed no change in *PUMA* expression levels, and WM793 only an insignificant change after 24h, therefore *PUMA* was not considered a main driver of DMAS induced apoptosis. However, *NOXA* was found to be significantly overexpressed in all cell lines except WM793 after 6h and 24h, making it a suitable candidate for further investigation. The highest *NOXA* overexpression was seen in MUG-Mel2 with a 7.5-fold expression after 6h and a 5.7-fold expression after 24h. This was followed by WM164 with 4.7-fold and 4.3-fold overexpression after 6h and 24h, respectively. Sbcl2 *NOXA* expression levels were raised 2.4-fold (6h) and 3.6-fold (24h), while MUG-Mel1 showed a steady 2.4-fold overexpression at both time points. Concerning WM793, *NOXA* overexpression was observed (1,4-fold for 6h, 3-fold for 24h), but insignificant due to too high error bars. Comparing time points, no clear pattern could be observed for *NOXA* overexpression, as MUG-Mel2 and WM164 showed higher expression after 6h treatment, while Sbcl2 *NOXA* levels peaked after 24h treatment and MUG-Mel1 levels remained stable. Taken together, the obtained results make *NOXA* the most promising candidate for DMAS induced apoptosis (123).

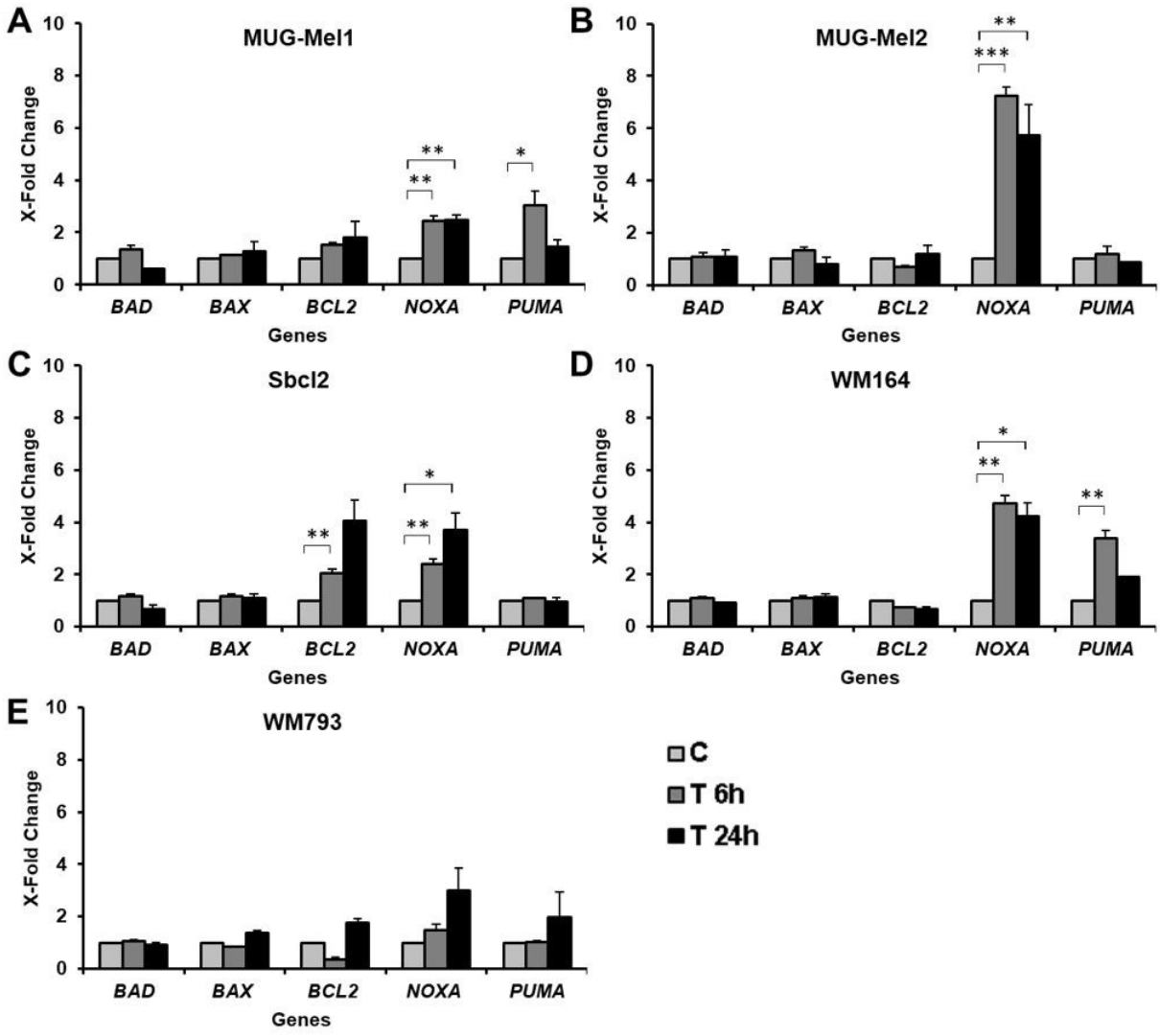

*Figure 15: RT-qPCR expression levels of A) MUG-Mel1, B) MUG-Mel2, C) Sbcl2, D) WM164 and E) WM793 after 6h and 24h of DMAS treatment. Results were obtained using the ΔΔCT method. The x-axis the contains genes and the y-axis shows the x-fold change. Light grey bars indicated controls, dark grey bars 6h DMAS IC50 treatment and black bars 24h DMAS IC50 treatment. C = control, T 6h = treated with DMAS IC50 for 6h, T 24h = treated with DMAS IC50 for 24h. *p < 0.05, **p < 0.01, ***p < 0.001 (123).*

Table 12: Calculated averages of RT-qPCR fold changes including standard errors of the mean for MUG-Mel1, MUG-Mel2, Sbcl2, WM164 and WM793 after 6h and 24h DMAS IC50 treatment.

Cell Line	Treatment	BAD	BAX	BCL2	NOXA	PUMA
MUG-Mel1	Treated 6h	1,4 ± 0,1	1,1 ± 0	1,5 ± 0,1	2,4 ± 0,2	3 ± 0,6
	Treated 24h	0,6 ± 0	1,3 ± 0,4	1,8 ± 0,6	2,5 ± 0,2	1,4 ± 0,3

MUG-Mel2	Treated 6h	1,1 ± 0,1	1,3 ± 0,1	0,7 ± 0,1	7,3 ± 0,3	1,2 ± 0,3
	Treated 24h	1,1 ± 0,3	0,8 ± 0,3	1,2 ± 0,3	5,7 ± 1,1	0,9 ± 0
Sbcl2	Treated 6h	1,2 ± 0,1	1,2 ± 0,1	2 ± 0,2	2,4 ± 0,2	1,1 ± 0
	Treated 24h	0,7 ± 0,1	1,1 ± 0,2	4,1 ± 0,8	3,7 ± 0,7	1 ± 0,1
WM164	Treated 6h	1,1 ± 0,1	1,1 ± 0,1	0,7 ± 0	4,7 ± 0,3	3,4 ± 0,3
	Treated 24h	0,9 ± 0	1,1 ± 0,1	0,7 ± 0,1	4,2 ± 0,5	1,9 ± 0
WM793	Treated 6h	1 ± 0,1	0,8 ± 0	0,4 ± 0,1	1,5 ± 0,2	1 ± 0
	Treated 24h	0,9 ± 0,1	1,4 ± 0,1	1,8 ± 0,2	3 ± 0,9	2 ± 1

3.3.5 DMAS Treatment influences Protein Expression Levels of Apoptosis Genes

To validate the results gained by RT-qPCR and to gain some new insight to DMAS induced effects on protein level, western blots were performed with all five melanoma cell lines after 24h of DMAS IC_{50} treatment (Fig. 16 and Tab. 13). Antibodies were used against BAK, BAX, BCL2, NOXA, p53 and PUMA. GAPDH was used as loading control. Thereby, except for NOXA (Fig. 16D), no significant changes in expression levels of any of the proteins under DMAS treatment could be observed. Interestingly, p53 levels (Fig. 16G) were low in all cell lines, both in control and treated cell lines. Furthermore, MUG-Mel1 depicted a p53 deficiency. NOXA, however, showed significant differences in all cell lines except for WM793. Despite of being not significant, changes of NOXA expression in WM793 were clearly visible on the blots. The insignificance was caused by the high error bar. The strongest NOXA overexpression was observed in Sbcl2 (2.8-fold), closely followed by MUG-Mel1 (2.4-fold). MUG-Mel2 and WM164 depicted both a 1.4-fold overexpression, while WM793 showed an (insignificant) 1.7-fold overexpression. Overall, these results verify the RT-qPCR experiments and clearly point towards a NOXA dependent DMAS working mechanism (123).

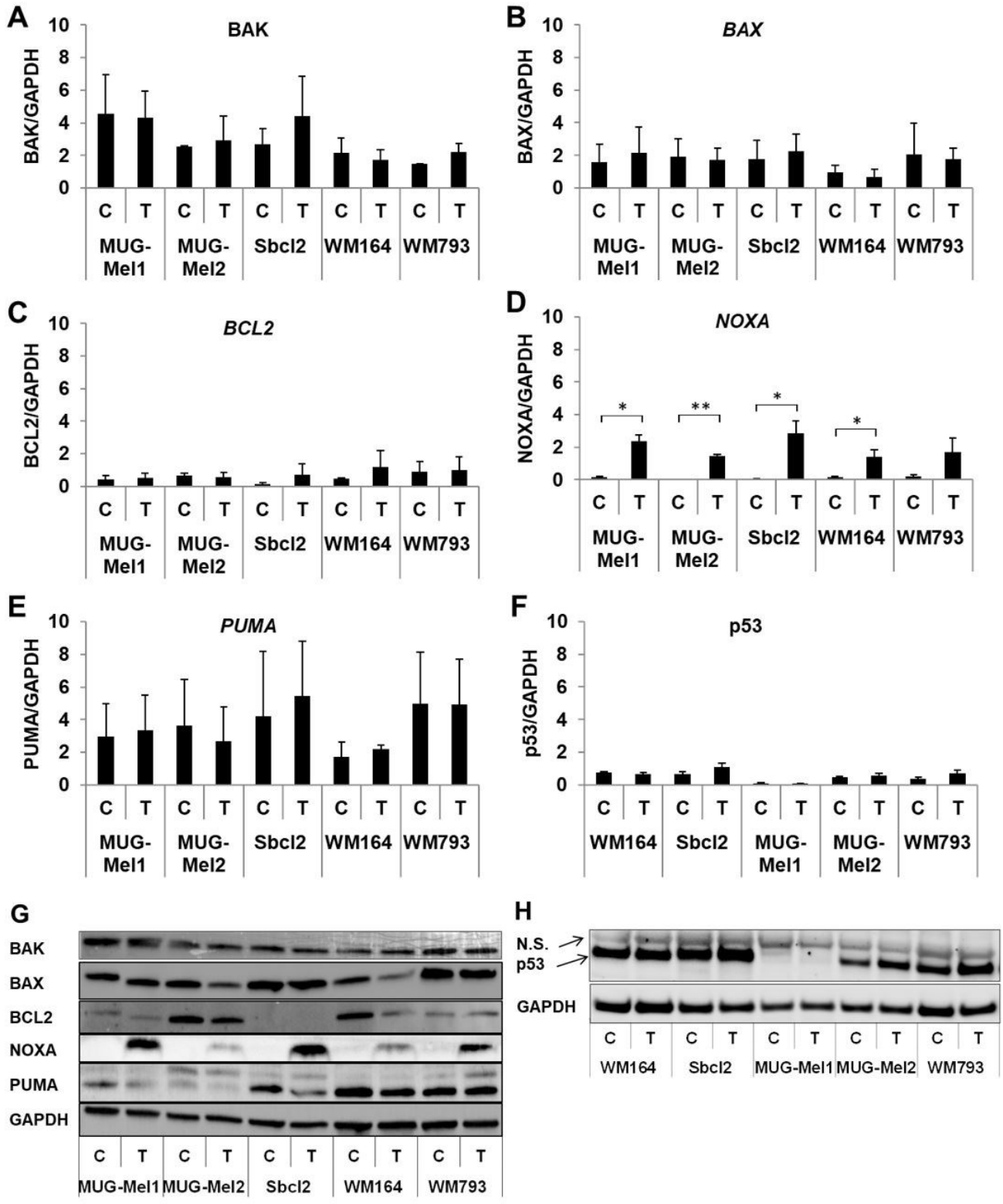

*Figure 16: Densitometric analysis of western blots of A) BAK, B) BAX, C) BCL2, D) NOXA and E) PUMA in respect to GAPDH expression. The x-axis depicts the cell lines and treatment, with "C" being control cells and "T" representing DMAS IC50 treated cells. The y-axis shows the relative protein expression compared to the respective GADPH expression. F) contains representative western blots with proteins shown on the y-axis and cell lines including treatments on the x-axis. G) shows the densitometric analysis of p53 western blots, H) the respective western blot membrane. N.S. refers to a non-specific band. This band occurs naturally when using this antibody, according to the manufacturer´s protocol. *p < 0.05, **p < 0.01 (123).*

<

Table 13: Averages and standard errors of the mean of relative protein expressions (to GAPDH) of BAK, BAX, BCL2, NOXA, p53 and PUMA as comparison of control and DMAS IC50 treated cells.

Cell Line	Treatment	BAK	BAX	BCL2	NOXA	p53	PUMA
MUG-Mel1	Control	4,5 ± 2,4	1,6 ± 1,1	0,4 ± 0,3	0,2 ± 0	0,1 ± 0,1	3 ± 2
	Treated	4,3 ± 1,6	2,2 ± 1,6	0,5 ± 0,3	2,4 ± 0,4	0,1 ± 0	3,3 ± 2,2
MUG-Mel2	Control	2,5 ± 0,1	1,9 ± 1,1	0,7 ± 0,2	0 ± 0	0,4 ± 0,1	3,6 ± 2,9
	Treated	2,9 ± 1,5	1,7 ± 0,7	0,6 ± 0,3	1,4 ± 0,1	0,6 ± 0,1	2,7 ± 2,1
Sbcl2	Control	2,7 ± 1	1,8 ± 1,1	0,1 ± 0,1	0,1 ± 0	0,7 ± 0,1	4,2 ± 4
	Treated	4,4 ± 2,4	2,3 ± 1	0,7 ± 0,7	2,8 ± 0,8	1,1 ± 0,2	5,5 ± 3,4
WM164	Control	2,2 ± 0,9	1 ± 0,4	0,5 ± 0	0,1 ± 0,1	0,8 ± 0,1	1,7 ± 0,9
	Treated	1,7 ± 0,6	0,7 ± 0,5	1,2 ± 1	1,4 ± 0,4	0,6 ± 0,1	2,2 ± 0,2
WM793	Control	1,5 ± 0	2 ± 1,9	0,9 ± 0,6	0,2 ± 0,1	0,4 ± 0,1	5 ± 3,1
	Treated	2,2 ± 0,5	1,8 ± 0,7	1 ± 0,8	1,7 ± 0,9	0,7 ± 0,2	4,9 ± 2,8

3.3.6 Apoptosis Induction of DMAS is dependent on NOXA Overexpression

3.3.6.1 Pilot Studies

Following up on the hypothesis that DMAS induced apoptosis is NOXA dependent, NOXA knockdown experiments were performed in Sbcl2 and WM164 cells. For that, the knockdown was first established by optimization of the needed transfection reagent amount as well as the NOXA siRNA amount using flow cytometry.

Thereby it was found that none of the used DharmaFECT-2 concentrations had a significant effect on transfection efficiency. Additionally, the control containing only siRNA, but no DharmaFECT-2, showed equal transfection efficiency compared to all other

samples (Fig 17A, B, D). Testing whether transfection efficiency would rise after siRNA concentration elevation, the 4-fold siRNA concentration was used on Sbcl2 in a follow up experiment. Hereby, all samples, independent of DharmaFECT-2 concentration (and including again the siRNA control), depicted almost 100% transfected cells (Fig 17C). Hence, DharmaFECT-2 did not affect transfection significantly, in contrast to siRNA concentration. It was therefore decided that the lowest amount of DharmaFECT-2 would be used for all further experiments (123).

Trying to optimize the NOXA siRNA amount needed for sufficient NOXA knockdown, different NOXA siRNA concentrations (10nM to 80nM) were applied on Sbcl2 cells after NOXA induction by DMAS IC_{50} treatment. Subsequently, proteins were isolated and subjected to western blot. Hereby it was found that the NOXA Knockdown was efficient, as the non-transfected, but DMAS treated cells (NT) depicted higher NOXA levels on the western blot than the transfected and DMAS treated cells. Furthermore, the knockdown was almost 100% efficient, independent of the used NOXA siRNA concentrations. The negative control (NC), being neither transfected nor DMAS treated, exhibited no NOXA protein expression. This was expected as untreated cells do not have high NOXA expression levels. Concluding, the smallest siRNA concentration (10nM) and the smallest DharmaFECT-2 concentration (0.25µl/ml) was used for all NOXA knockdown experiments (Fig 17E) (123).

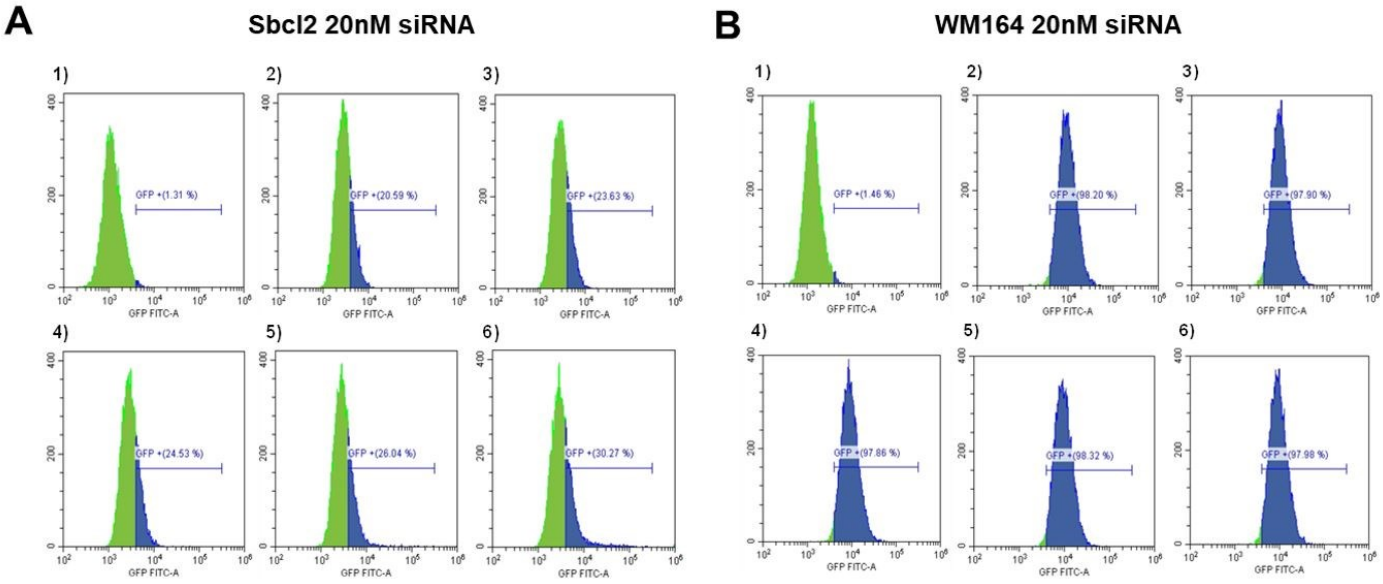

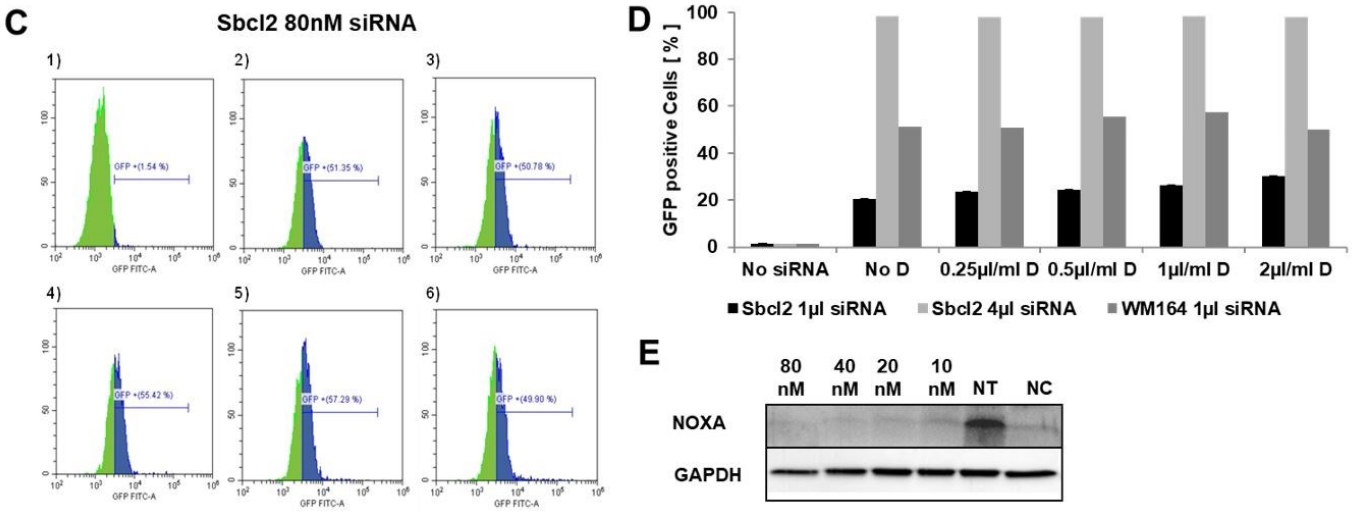

Figure 17: Flow cytometry analysis of allstar neg siRNA AF488 transfected cells. The transfection amounts of siRNA were A) 20nM Sbcl2, B) 20nM for WM164 and C) 80nM for Sbcl2. The x-axis shows GFP positive cells, the y-axis the counts. 1) contains transfected samples without siRNA. With 2) marked plots contain samples with siRNA, but no DharmaFECT-2. All other samples show increasing concentrations of DharmaFECT-2, while siRNA levels remain constant, with 3) 0.25µl/ml 4) 0.5µl/ml 5) 1µl/ml and 6) 2µl/ml DharmaFECT-2. The bar chart D) exhibits the summary of all FACS dot plots, with the x-axis depicting the different samples/DharmaFECT-2 concentrations and the y-axis showing the amount of GFP positive cells. Furthermore, Western blots of Sbcl2 cells after transfection and DMAS treatment are shown in E). NT describes cells which were not transfected but treated with DMAS. NC is the negative control, without transfection or DMAS treatment. All other samples contain different amounts of NOXA siRNA after 24h DMAS treatment, from 10nM to 80mM (123).

3.3.6.2 NOXA Knockdown

First, NOXA was silenced using the established NOXA siRNA and DharmaFECT-2 concentrations. Then, DMAS treatment was done for 24h. The knockdown was verified by western blots and its effect on DMAS induced apoptosis examined by flow cytometry measurements of active capase-3 (Fig. 18 and Tab. 14). Hereby, western blots confirmed a successful NOXA knockdown. The densitometric analysis of Sbcl2 and WM164 showed a significant knockdown between treated scrambled siRNA cells and treated NOXA siRNA cells. Additionally, in Sblc2, the differences between only treated cells and treated NOXA siRNA cells was also significant. Furthermore, no NOXA expression was found in any of the three controls (all controls were vehicle treated, the differences were as follows: no siRNA control, scrambled siRNA control, NOXA siRNA control). This indicates that NOXA overexpression is caused by DMAS treatment, and that NOXA overexpression levels are lower under NOXA knockdown (Fig. 18A-B and D-E) (123).

The caspase-3 assay exhibited small, but significant differences in DMAS induced apoptosis between scrambled siRNA treated cells and NOXA siRNA treated cells. Furthermore, in WM164, the difference between only DMAS treated cells and NOXA siRNA treated cells was also significant (Fig. 18C, F). Additionally, the results fit to the

formerly conducted caspase-3 experiments. Overall, this assay confirms that NOXA knockdown diminishes DMAS induced apoptosis significantly (123).

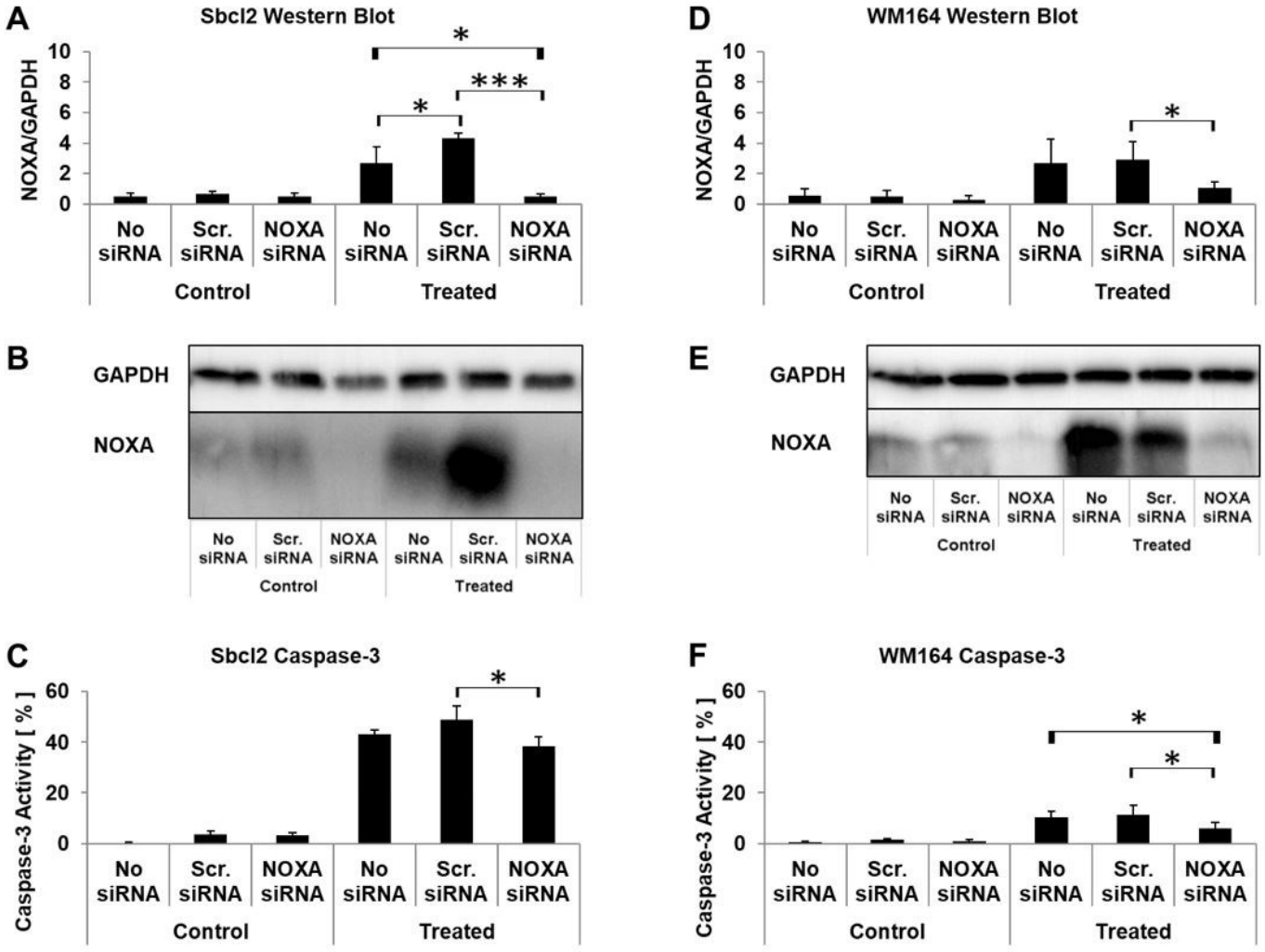

*Figure 18: Western blots and caspase-3 assays of DMAS treated Sbcl2 (A-C) and WM164 (D-F) cells under NOXA knockdown. A) and D) contain the densitometric analysis of NOXA western blots in respect to GAPDH expression. The x-axis depicts the different samples, the y-axis the relative protein expression. B) and E) exhibit representative western blots. C) and F) contain the active caspase-3 assays. The x-axis shows the respective samples, the y-axis depicts the percentage of cells with caspase-3 activity. *p < 0.05, ***p < 0.001 (123).*

Table 14: Averages of active caspase-3 depicting cells and NOXA expression levels in caspase-3 assays and western blots, respectively, including standard deviations. Assays were conducted with DMAS treatment and NOXA silencing.

Cell Line	Treatment	Transfection	Caspase-3 Activity [%]	NOXA Western Blot
Sbcl2	Control	No siRNA	0,3 ± 0,1	0,5 ± 0,2
		Scrambeled siRNA	3,5 ± 1,5	0,6 ± 0,2
		NOXA siRNA	3,2 ± 1,1	0,5 ± 0,2
	Treated	No siRNA	43 ± 1,7	2,7 ± 1
		Scrambled siRNA	49 ± 5,4	4,3 ± 0,3
		NOXA siRNA	38,4 ± 3,9	0,5 ± 0,1
WM164	Control	No siRNA	0,5 ± 0,4	0,6 ± 0,4
		Scrambeled siRNA	1,5 ± 0,4	0,5 ± 0,4
		NOXA siRNA	1 ± 0,5	0,3 ± 0,3
	Treated	No siRNA	10,3 ± 2,5	2,7 ± 1,6
		Scrambled siRNA	11,4 ± 3,7	2,9 ± 1,2
		NOXA siRNA	6 ± 2,5	1 ± 0,4

3.3.7 DMAS Treatment induces Apoptosis, Necrosis and Regression of Melanoma *In-Vivo*

3.3.7.1 Pilot Studies

Before mouse experiments with large animal cohorts were started, pilot studies were performed to elucidate whether those experiments could be successful. Therefore, mice were injected with WM164 or Sbcl2, the tumours treated with DMAS and subsequently harvested together with the mice organs. Tumours were stained with H&E. *In-Vivo*

analysis of Sbcl2 (Fig. 19A, D) and WM164 (Fig. 19B, C, E) tumours in nude mice with DMAS treatment showed a colouring effect of DMAS on tumours. Furthermore, tumours depicted apoptotic and necrotic areas under DMAS treatment, while the surrounding tissue was not affected, indicating that DMAS did not diffuse out of the tumour. Overall, the results point towards a general apoptosis or necrosis inducing effect of DMAS, irrespective of the cell line, but concealed locally to the injection point. Therefore, DMAS could be used for local tumour treatment (123).

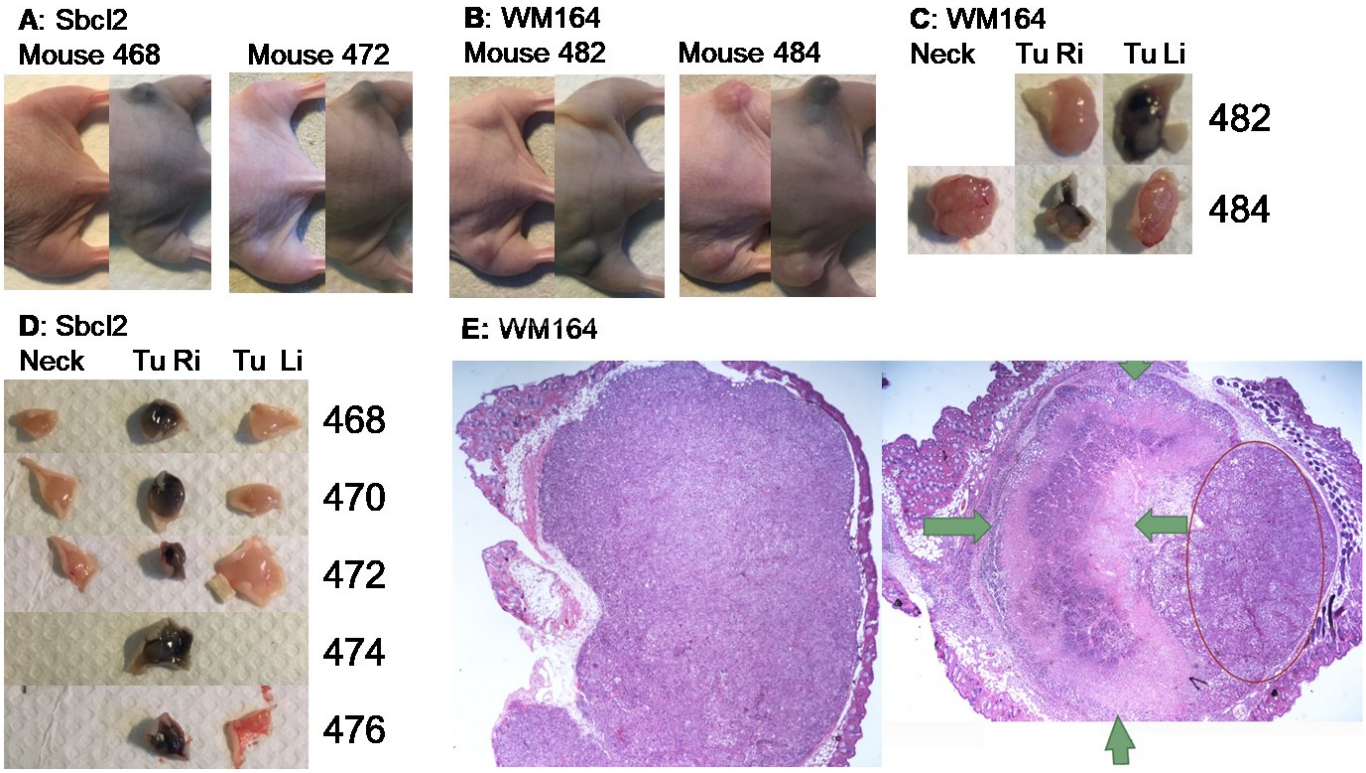

Figure 19: Pilot in-vivo experiments with DMAS. A) shows Sbcl2 and B) WM164 tumours in mice, respectively. C) depicts the harvested tumour pieces after the last DMAS application for WM164 tumours, while D) shows the same for Sbcl2 tumours. E) shows the H&E staining of the WM164 tumours in mouse 482, left side untreated, right side treated. The green arrows in picture E) indicate apoptotic/necrotic areas, the circle viable cells (123).

3.3.7.2 *In-Vivo* Trials

Subsequently to pilot studies, two cohorts of each twenty NU(NCr)-Foxn1 immunodeficient mice were injected with Sbcl2 or WM164. After the tumour size exceeded 5mm², tumours were injected with DMAS according to the treatment plan. Hereafter, mice were sacrificed and tumours as well as organs harvested. H&E staining was performed to differentiate viable from dead tissue, allowing an observation of DMAS induced effects. KI67 staining was performed to examine the influence of DMAS on cell proliferation. Thereby DMAS was found to induce a variety of effects within both Sbcl2 and WM164 derived tumours. Apoptotic and necrotic areas where observed as well as fibrosis. The pathologist analysing the tumour slides referred to both apoptotic as well as necrotic areas as “necrotic”, therefore this term will be used for both. In Sbcl2 tumours, necrosis and regression, taking up between 10% to 50% of the entire tumour tissue could be observed. WM164 tumours were treated with 1mg/kg DMAS showed up to 60% necrosis and regression, 2mg/kg treated tumours up to 50%. WM164 tumours treated with 4mg/kg depicted up to 30% necrotic tissue. DMAS influence on tumours was strongly fluctuating for both cell lines, with some tumours only exhibiting 5% necrosis, while in others, more than half of the tumour tissues were necrotic (Tab. 15-16). The representative mouse slices are shown in Fig. 20 depict the variety of effects observed in mouse tumours. On the left side (Fig. 20A, D, G) the untreated tumours are shown, in the middle (Fig. 20B, E, H) the treated once and on the right side specific areas within the treated tumours (Fig. 20C, F, I). In the zoomed-in areas, the diverse effects are displayed, with Fig. 20C showing a necrotic area in the right upper part, separated by a small fibrosis from viable cells on the left lower part. Fig. 19F shows a large part of the tumour with all effects running in circles around a viable centre on the lower left border of the tumour. Fig. 20I shows a region dominated by fibrosis which slowly repairs the necrotic parts. Overall, the tumours depict a variety of DMAS induced effects, with apoptosis, necrosis and fibrosis being present side-by-side within the same tumour (123).

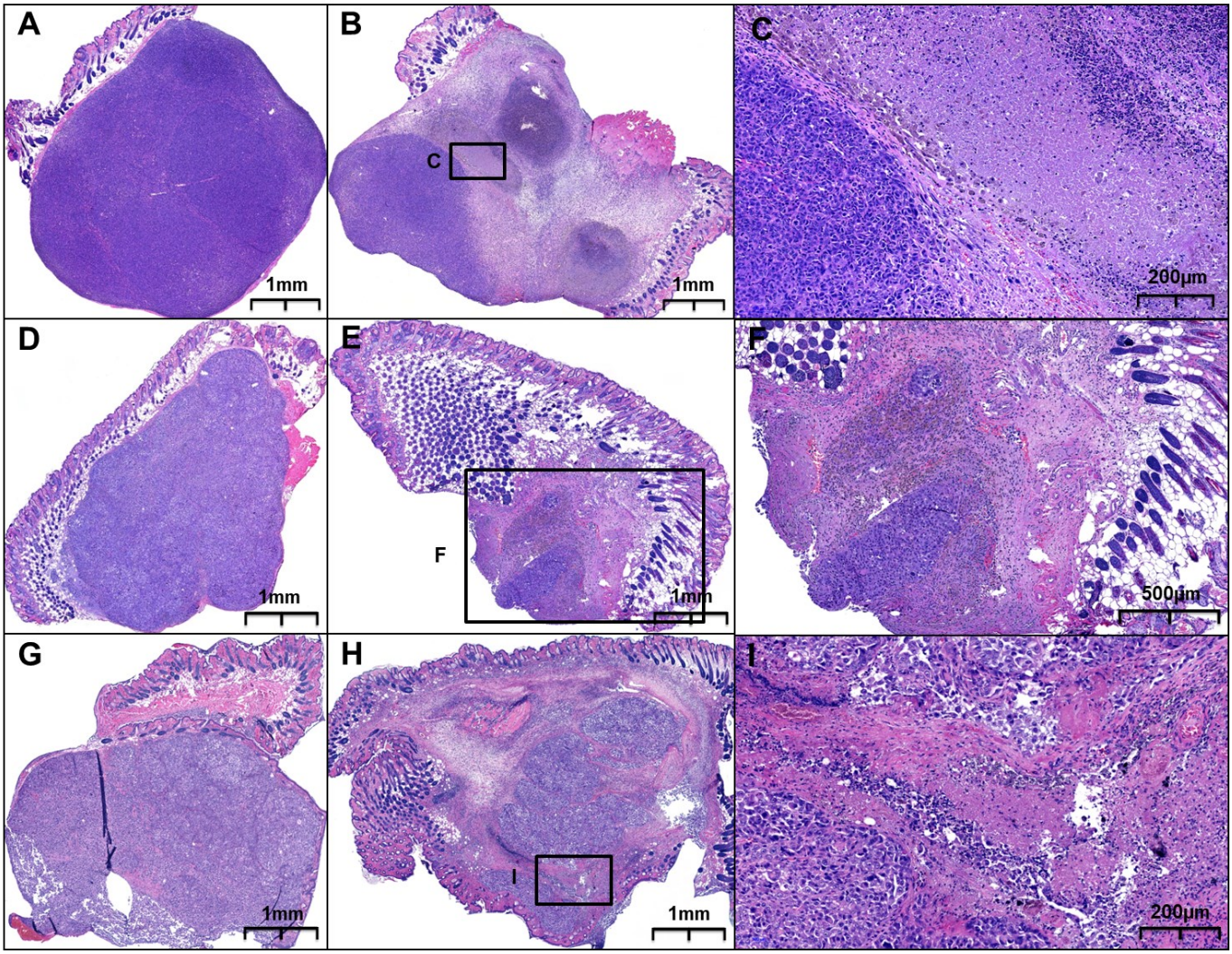

Figure 20: H&E stained images of mouse xenograft experiments from NU(NCr)-Foxn1 immunodeficient mice. A-C depict Sbcl2 derived tumours, with A) showing the vehicle control, B) depicting the 4mg/kg DMAS treatment and C) being a zoomed-in area of B), showing viable (deep purple) and necrotic (rose/pink) areas, mixed with fibrotic ones. D-I show WM164 derived tumours, with each D-F and G-I belonging to one mouse. D) and G) depict control tumours, while E) and H) show 2mg/kg and 4mg/kg treated tumours, respectively. F) and I) show again zoomed-in areas of E) and H). (123).

Table 15: Sbcl2 mouse data showing H&E as well as KI67 staining results.

Sbcl2 Control Mice. only vehicle treatment				
Mouse Nr.	**Tissue**	**Data Read Out H&E**	**Treatment**	**KI67 positive Cells**
1	Tumour Right	Vital Tumour Tissue	Vehicle	not stained
2	Tumour Right	Vital Tumour Tissue	Vehicle	not stained
3	Tumour Right	Vital Tumour Tissue	Vehicle	not stained
4	Tumour Right	Vital Tumour Tissue	Vehicle	not stained
Sbcl2				
Mouse Nr.	**Tissue**	**Data Read Out H&E**	**Treatment**	**KI67 positive Cells**
1	Tumour Left	10% Regression	4mg/kg DMAS	80%
	Tumour Right	Vital Tumour Tissue	Vehicle	40-50%

2	Tumour Left	Vital Tumour Tissue	Vehicle	40%
	Tumour Right	15% Regression	4mg/kg DMAS	50%
3	Tumour Left	20% Regression & Necrosis	4mg/kg DMAS	60%
	Tumour Right	Vital Tumour Tissue	Vehicle	50-60%
4	Tumour Left	40% Regression & Necrosis	4mg/kg DMAS	40-50%
	Tumour Right	Vital Tumour Tissue	Vehicle	50%
5	Tumour Left	Vital Tumour Tissue	Vehicle	not stained
	Tumour Right	50% Regression & Necrosis	4mg/kg DMAS	not stained
6	Tumour Left	15% Regression & focal Necrosis	4mg/kg DMAS	not stained
	Tumour Right	Vital Tumour Tissue	Vehicle	not stained

Table 16: WM164 mouse data showing H&E as well as KI67 staining results.

WM164				
Mouse Nr.	**Tissue**	**Data Read Out H&E**	**Treatment**	**KI67 positive Cells**
1	Tumour Left	Vital Tumour Tissue	Vehicle	not stained
	Tumour Right	60% Regression & Necrosis	1 mg/kg DMAS	not stained
2	Tumour Left	Vital Tumour Tissue	Vehicle	not stained
	Tumour Right	Vital Tumour Tissue	1 mg/kg DMAS	not stained
3	Tumour Left	Vital Tumour Tissue	Vehicle	not stained
	Tumour Right	5% Necrosis	1 mg/kg DMAS	not stained
4	Tumour Left	Vital Tumour Tissue	Vehicle	not stained
	Tumour Right	Vital Tumour Tissue	1 mg/kg DMAS	not stained
5	Tumour Left	Vital Tumour Tissue	Vehicle	not stained
	Tumour Right	15% Regression	2 mg/kg DMAS	not stained
6	Tumour Left	Vital Tumour Tissue	Vehicle	not stained
	Tumour Right	30% Regression & Necrosis	2 mg/kg DMAS	not stained
7	Tumour Left	Vital Tumour Tissue	Vehicle	not stained
	Tumour Right	30% Fibrosis & Regression	2 mg/kg DMAS	not stained
8	Tumour Left	Vital Tumour Tissue	Vehicle	not stained

	Tumour Right	15% Regression & Necrosis	2 mg/kg DMAS	not stained
9	Tumour Left	Vital Tumour Tissue	Vehicle	not stained
	Tumour Right	50% Regression & Necrosis	2 mg/kg DMAS	not stained
10	Tumour Left	10% Regression	4 mg/kg DMAS	80%
	Tumour Right	Vital Tumour Tissue	Vehicle	80%
	Heart	no Tumour. vital Tissue		not stained
	Lung	no Tumour. vital Tissue		not stained
	Liver	no Tumour. vital Tissue		not stained
	Kidney	no Tumour. vital Tissue		not stained
	Spleen	no Tumour. vital Tissue		not stained
11	Tumour Left	10% Regression	4 mg/kg DMAS	60-70%
	Tumour Right	Vital Tumour Tissue	Vehicle	60%
12	Tumour Left	30% Regression & Necrosis	4 mg/kg DMAS	60%
	Tumour Right	Vital Tumour Tissue	Vehicle	60-70%
13	Tumour Left	5% Regression	4 mg/kg DMAS	70-80%
	Tumour Right	Vital Tumour Tissue	Vehicle	80-90%

Interestingly, no significant reduction of the tumour area could be observed, as regression

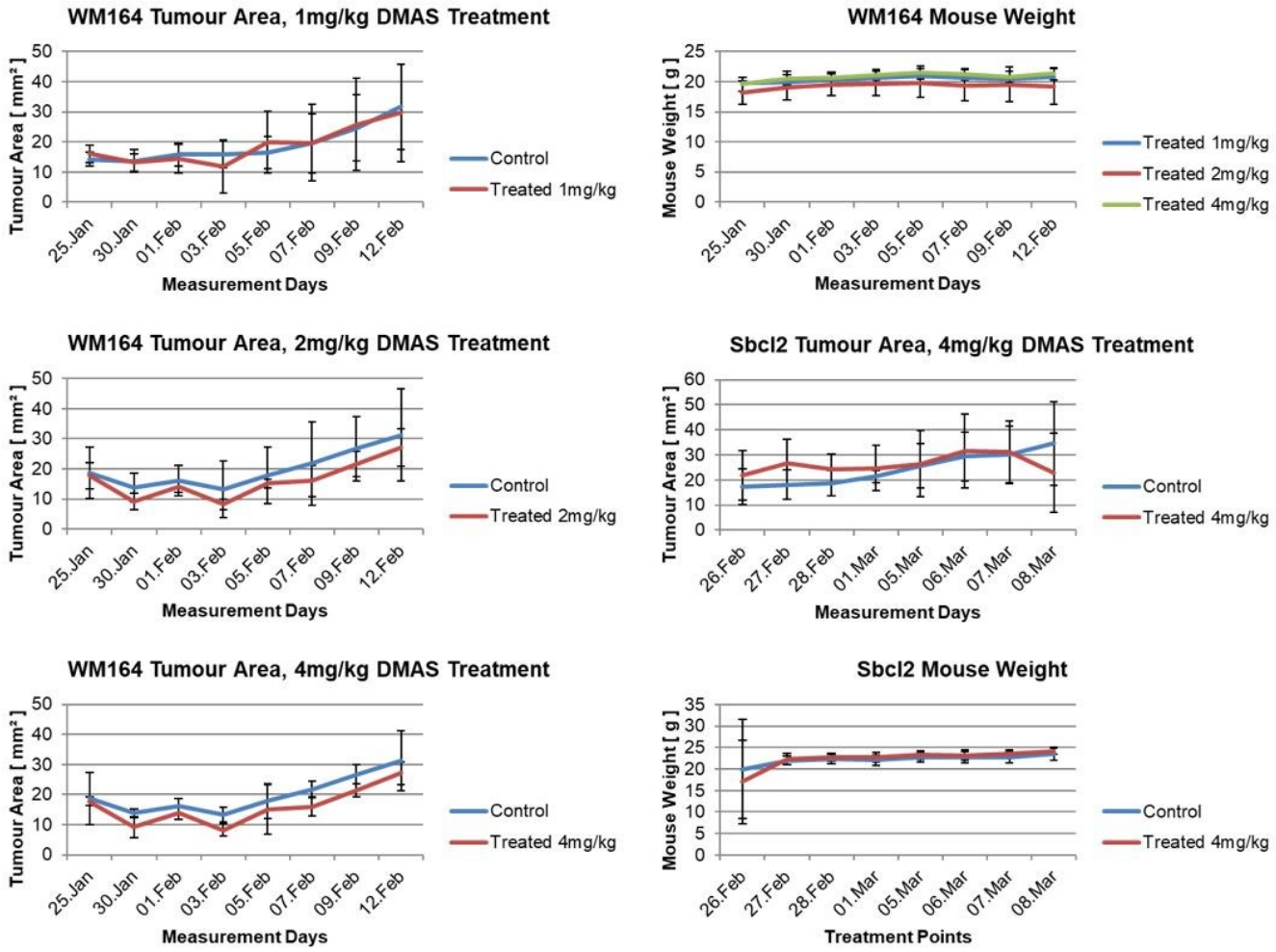

Figure 21: Tumour area and mouse weight of Sbcl2 and WM164 injected mice throughout the experiment. The DMAS application dates are displayed on the x-axis, tumour area or mouse weight on the y-axis. The charts resemble arithmetic averages of the mouse population, with: Control Sbcl2: n=5, Treated Sbcl2: n=8. For WM164, control tumours rather than control mice were used, with n=5 for each concentration in control as well as treated tumours (123).

took place within the tumour, without affecting its overall size. Additionally, organs and control tumours displayed no necrotic tissue or any other possible DMAS induced effects. Furthermore, no significant differences concerning mouse weight could be observed under DMAS treatment, therefore it can be assumed that DMAS induced side effects are not severe when DMAS is injected directly into the tumour (Fig 21). Overall, the *in-vivo* results resembled the *in-vitro* results in terms of apoptosis (123).

Coming to KI67, most of the stained control tumours as well treated tumours were strongly positive for KI67. In Sbcl2 (Fig. 22A, B), between 40% to 80% KI67 positive cells could be observed, in WM164 (Fig 22C, D) derived tumours between 60% to 90% (Tab. 15-16). Taken together, DMAS induces necrosis and regression in melanoma tumours in mice but

has no influence on cell proliferation (123).

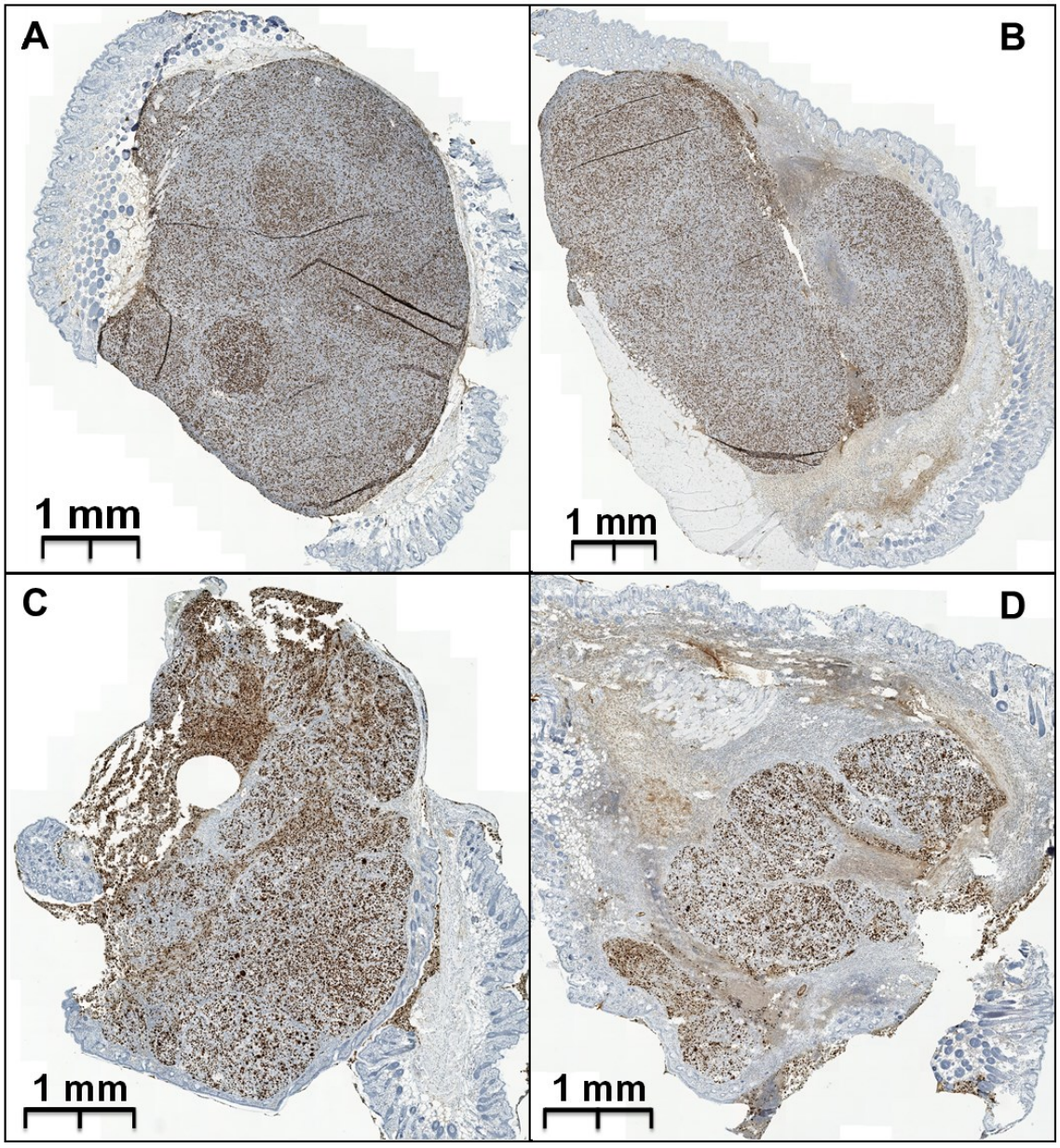

Figure 22: KI67 staining of mouse xenograft models featuring NU(NCr)-Foxn1 immunodeficient mice. A) and B) show vehicle and 4mg/kg DMAS treated Sbcl2 derived tumours, respectively. WM164 control tumour is depicted in C), while a 4mg/kg DMAS treated tumour is shown in D) (123).

4 DISCUSSION

β-β-Dimethylacrylshikonin, a shikonin derivative isolated from *Onosma paniculata* Bureau & Franchet (Boraginaceae), was shown to have strong anti-cancer effects in several different cancer types, among which are colorectal cancer (108), breast cancer (112), and lung adenocarcinoma (111). However, the effects of DMAS on chordoma and melanoma cells are still unknown. Experiments were conducted with the aims to 1) elucidate whether DMAS induces apoptosis *in-vitro*, 2) to find DMAS affected pathways and 3) to see whether DMAS induced effects in melanoma *in-vitro* could be reproduced *in-vivo*.

In this chapter, the results obtained about DMAS effects in both chordoma and melanoma are discussed. Despite the strict separation of both cancer types in the result section, discussion of some of the DMAS effects will be combined here. The reason is that publications concerning DMAS as well as the basis for discussion of the used methods are similar and would therefore lead to repetition if both cancer types would be discussed separately. Whenever assays and backgrounds for discussion were overlapping, the major discussion was done solely in the melanoma part. However, a small note or summery was made in the chordoma part to address the core issues. This concerns the following assays: viability assay (EZ4U for melanoma and MTS for chordoma), Annexin V / SYTOX Green assay, active caspase-3 assay, RT-qPCR and western blots.

4.1 Chordoma

4.1.1 Viability Assay

DMAS cytotoxicity on chordoma cells was examined using the MTS assay on four different chordoma cell lines of which two were clival (MUG-CC1 and UM-Chor1) and two were sacral (MUG-Chor1 and U-Ch2). The MTS assay was conducted 48h after DMAS treatment with different concentrations. Thereby it was found that DMAS reduces chordoma cell viability in a dose dependent manner. The differences between DMAS IC_{50} values of sacral and clival chordoma cells was minimal, showing that the location of the cancer does not change treatment efficiency. However, this observation is only based on comparison of three of the cell lines, as the UM-Chor1 error bar was too high, so this result was not taken into account. The error bar was primarily caused by difficulties concerning the MTS assay with UM-Chor1 cells and did not occur in any other assay performed with this cell line. MTS, a tetrazolium salt and an analogue to MTT, is used to measure metabolic activity, proliferation and viability in cell culture (127). It is known that

MTS, MTT and other assays based on this technology yield different results, dependent on the cell line, growth conditions and other factors. Therefore, it is possible that the high error bar in case of UM-Chor1 was caused by internal cell processes which rendered the use of the MTS assay itself useless (128,129). Another reason for the high error bar is the four-parameter logistic curve used for IC_{50} calculation. This equation assumes a sigmoidal shape of tumour viability in respect to increasing treatment concentrations. When the curve is not sigmoidal, the assumed graph does not fit, leading to high error bars in the IC_{50} calculation, as was the case with UM-Chor1. However, as for chordoma cells the decision was made to treat all cell lines for all further experiments with 2.2µM DMAS, the MTS result did not affect other experiments. Furthermore, results gained with UM-Chor1 in the Annexin V / SYTOX Green as well as the active caspase-3 assay were close to those obtained with MUG-CC1 and MUG-Chor1, therefore it can be assumed that UM-Chor1 susceptibility to DMAS treatment is similar to these two cell lines (122).

Comparing chordoma cells to adult human fibroblasts which were used as healthy control cells, it was found that fibroblasts were less susceptible to DMAS treatment, therefore DMAS might be more specific towards chordoma- then healthy cells. The EZ4U assays with MRC-5 fibroblasts and melanoma cell lines yielded a similar result. This finding is further strengthened by a study from Hasenoehrl et. al. 2017(130), showing that DMAS and other shikonin derivatives have a lower toxicity towards human HF-SAR fibroblasts in comparison to thyroid carcinoma cells. (122,130).

4.1.2 Apoptosis Induction by DMAS in Chordoma Cells

To elucidate the type of DMAS induced cell death in chordoma cells, Annexin V / SYTOX Green assays and active caspase-3 assays were performed after 2.2µM DMAS treatment of chordoma cells for 24h. Not surprisingly, MUG-CC1, UM-Chor1 and MUG-Chor1, for which the IC_{50} DMAS concentration was higher than 2.2µM, showed less than 50% overall apoptosis, while U-CH2 with an IC_{50} concentration of 1.9µM depicted 71% apoptosis. Interestingly, the clival cell lines MUG-CC1 and UM-Chor1 showed more early apoptotic cells, while the sacral chordoma cell lines MUG-Chor1 and U-CH2 exhibited equal amounts of early and late apoptotic cells. Late apoptotic cells cannot be differentiated from necrotic cells in the Annexin V /SYTOX Green Assay (131–133), an issue further discussed in the Annexin V /SYTOX Green chapter in melanoma cells. Therefore, it is unclear in case of sacral chordoma cell lines whether DMAS solely induces apoptosis or also necrosis. Further elucidation of DMAS induced effects in those tumours is necessary to find the reasons for the shift of early to late apoptotic cells. The active caspase-3 assay

confirmed the apoptosis inducing effect of DMAS, showing approximately the same trend, with U-CH2 being more susceptible to DMAS treatment than the other cell lines (122).

4.1.3 RT-qPCR and Western Blots of apoptotic Genes and Proteins in Chordoma Cell Lines

The apoptosis inducing effect of DMAS could be caused by activation of the intrinsic or the extrinsic apoptosis pathway or a combination of both. Both pathways are largely independent from each other and unify only in the caspase cascades, leading to disintegration of the cells by formation of apoptotic bodies (113,134). There is evidence suggesting that DMAS works over the mitochondrial apoptosis pathway. Xiong et al., 2013 (112) reported DMAS induced apoptosis over BCL2 and NF-kB, which was confirmed for BCL2 by Wu et al 2012 (109) in hepatocellular carcinoma. Additionally, Kwak et al 2014 (110) showed apoptosis induction over DNA damage by DMAS induced formation of reactive oxygen species. Taking these findings into consideration, the intrinsic or mitochondrial apoptosis pathway was chosen for further studies, with BCL2, NOXA and PUMA yielding significant results. NOXA was found to be upregulated in all tested chordoma cell lines, while PUMA was just upregulated in MUG-Chor1 and BCL2 only in U-CH2 cells. In the conducted western blot experiments to confirm the results, no significant differences could be found in protein expression of BCL2. For PUMA, only UM-Chor1 and MUG-CC1 showed significant upregulation. However, in case of MUG-CC1, the significance was a mere statistical effect, but due to the small basis amount likely not relevant for cell behaviour, leaving UM-Chor1 as the only cell line which might be affected by PUMA upregulation. Concerning cytochrome-c, a member of the inner mitochondrial membrane which is release towards the end of the intrinsic apoptosis pathway (135–137), no significant differences could be found between control and treated cells. Therefore, DMAS might not act primarily over this protein either (122). These findings showed similarities to those obtained in melanoma cell lines, especially concerning NOXA. Therefore, apoptosis genes and possible mechanisms are discussed in the melanoma chapter. The same accounts for western blot experiments conducted to confirm the RT-qPCR experiments (122).

4.1.4 Western Blots of Survival or Proliferative Proteins in Chordoma Cells

To test whether DMAS has an effect not only on apoptosis, but also survival and proliferative genes, western blots were performed with AKT/pAKT, ERK/pEKR and

STAT/pSTAT (Tyr705). Thereby, changes in ratios between phosphorylated and unphosphorylated proteins were observed between control and treated cells. Overall, the ratios of all three proteins were lower in treated samples compared to untreated samples, suggesting that DMAS has a negative influence on phosphorylation of survival and proliferative genes. This is not surprising, as DMAS was shown to induce apoptosis in chordoma cells in this work. Once the apoptotic process has started, proliferative and survival genes are often downregulated (138,139). Moreover, inhibition of those pathways might be necessary for successful apoptosis induction (122,140,141).

The investigated proteins belong to some of the major regulating pathways within cells, namely the TKR/RAS/ERK (MAPK)-, TKR/PI3K/AKT- and the JAK/STAT pathway. These pathways have been shown to play a critical role not just for proliferation, transcription or survival, but also for apoptosis in cells (139,142). Many of the proteins within those pathways require phosphorylation to get activated or deactivated, therefore changes in their phosphorylation ratios under DMAS treatment should be investigated in more detail. Inhibition of phosphorylation could have occurred by downregulation of upstream kinases or their inhibition. Another possibility would be the upregulation of tumour suppressor genes like PTEN, P38 or p53 (143), of which the latter was shown not to be significantly influenced by DMAS in melanoma cells in this work. In case of AKT/pAKT, an upregulation of PTEN as well as a downregulation of PDK1 or PI3K could have caused the ratio shift (144). In ERK/pEKR, however, inhibition of upstream kinases like RAS or RAF could have led to the decrease of pEKR under DMAS treatment (142). However, also rising PTEN or PI3K levels could have caused this effect. Furthermore, the decrease in pSTAT3 (Tyr705) expression could have been an effect of JAK or SRC level reductions (145,146). Overall, the possibilities and diversity of effects that could have caused the ratio changes under DMAS treatment need to be investigated further to elucidate the exact mechanisms behind the changes. However, this would be beyond the scope of this work (122).

4.2 Melanoma

4.2.1 DMAS Influence on Viability in Melanoma Cells

To elucidate the effects of DMAS on melanoma, five cell lines with different mutational profiles were examined with various assays. Juvenile melanocytes and MRC-5 fibroblasts were used as healthy control cell lines. Here, MUG-Mel2 and Sbcl2, two melanoma cell lines with NRAS driver mutation, were compared with WM164 and WM793, which feature

a BRAF mutation. Additionally, MUG-Mel1, having neither BRAF nor NRAS, were used as wild type control. BRAF and NRAS are the most important driver mutations in melanoma. While there are treatments prolonging the live of patients suffering of BRAF mutated melanoma, little can be done against NRAS mutated forms (34,123,147).

The viability assays conducted after 24h, 48h and 72h of DMAS treatment with different concentrations, revealed that DMAS influenced cell viability in a dose- and time dependent manner. The lowest DMAS IC_{50} concentration was found in WM793, followed closely by MUG-Mel1 and Sbcl2. WM793 and Sbcl2 were both derived from primary metastasis, while MUG-Mel1 was established using a brain metastasis, suggesting that DMAS has the potential to work equally effective on metastasized as well as primary tumours. However, Sbcl2 is a non-metastatic cell line, and MUG-Mel1 does not have any of the prominent driver mutations like BRAF or NRAS (148). Therefore, one can assume that DMAS does not work selectively on highly aggressive cell lines. This was further emphasized as juvenile melanocytes, being the healthy counterpart of melanoma cells, were equally affected by DMAS as Sbcl2 and MUG-Mel1. Furthermore, WM164 and MUG-Mel2, two highly aggressive metastatic cell lines, needed to be treated with higher DMAS concentrations to achieve significant cell viability reduction. Overall, this suggests that DMAS treatment efficacy is not primarily dependent on BRAF or NRAS mutations. Possible other DMAS target candidates would be the RAS-RAF-MEK downstream target ERK as shown by Shen et al 2012 (117) in gastric cancer, or BCL2 and NF-kB in case of breast cancer (112). Both papers point towards the mitochondrial apoptosis pathway as general working mechanism for DMAS, a hypothesis gaining more and more support by several papers in the last years (108,111,117). If indeed DMAS would work solely by activation of mitochondrial apoptosis genes, it would be independent of BRAF and NRAS mutations. Thus, DMAS would provide the unique opportunity to treat also highly aggressive NRAS mutated melanoma, which is unsuccessful with the currently available drugs (34). Therefore, assays concerning the mitochondrial apoptosis pathway are discussed later in this chapter (123).

Despite the low IC_{50} concentration for juvenile melanocytes, suggesting that DMAS might be toxic for the human body, MRC-5 fibroblasts were less affected by DMAS treatment than any other cell line used. Furthermore, the IC_{50} value of MRC-5 was comparable to the IC_{50} obtained with adult human fibroblasts, which were used in chordoma experiments for comparison. It can therefore be assumed that DMAS has a strong effect on all melanoma cell lines and melanocytes but is less toxic for fibroblasts. This is further supported by a study from Hasenoehrl et al 2017 (130), which examined DMAS treatment

influence on medullary thyroid carcinoma and human HF-SAR fibroblasts, finding also no negative effects on fibroblasts. Therefore, hopefully no systematic side effects may occur in potential patients.

Additionally, DMAS IC_{50} concentrations declined over time, suggesting that the substance has a long-term effect. The decrease was not uniform amongst the used cell lines, showing also the diversity of reactions of different melanoma cell lines to DMAS treatment. Compared to other cancer types, DMAS IC_{50} values were lower in melanoma cells, suggesting that the drug is more efficient in this cancer type. Wu et. al. 2012 (109) reported 40.5μM DMAS IC_{50} value for hepatocellular carcinoma, while Shen et. al. 2012 (117) found 11.89μM for gastric cancer cells and Xiong et al 2013 (112) even found 80μM for breast cancer cells. Therefore, even the relatively low IC_{50} concentration found by Shen et al. 2012 is at least double then the highest IC_{50} concentration reported for melanoma here (MUG-Mel2 IC_{50} after 34h = 5.13μM).

Taken together, DMAS effects vary strongly among the different cell lines, but differences in BRAF and NRAS mutations seem not to be the defining criteria for DMAS treatment efficacy. Furthermore, DMAS is cytotoxic towards juvenile melanocytes, but not towards MRC-5 fibroblasts, thus it might not show general cytotoxicity (123).

4.2.2 Apoptosis Induction by DMAS in Melanoma Cells

To study the type of cell death induced by DMAS, melanoma cells were treated and subsequently stained with Annexin V / SYTOX Green. Additionally, active caspase-3 was measured. Thereby it was found in the Annexin V / SYTOX Green assay that DMAS induced apoptosis, but not necrosis, in melanoma cells. The apoptosis inducing effect was confirmed in the active caspase-3 assay. Interestingly, the calculated 24h DMAS IC_{50} values used for treatment were not always reflected in the Annexin V / SYTOX Green assay, with just MUG-Mel1, MUG-Mel2 and WM164 depicting an amount of dying cells close to 50%. Sbcl2 showed a far higher amount of dying cells after both 6h and 24h treatment than would be expected, while WM793 were less susceptible. However, as the EZ4U cell viability assay examined mainly metabolism, differences between the assays are not surprising. Comparing cell lines, both MUG-Mel1 and WM793 showed clear apoptotic effects, with more than 40% of cells in early apoptosis in MUG-Mel1 and up to 20% in WM793 after 24h treatment. In contrast, late apoptotic cells were more common in MUG-Mel2 after 6h and 24h treatment, suggesting a stronger effect of DMAS on this cell line. Sbcl2 showed by far the highest response at both time points, suggesting that DMAS

might be toxic for those cells. As Sbcl2 is less aggressive than the other cell lines and had a rather low IC_{50} value in EZ4U Assays, this is surprising and contradicting some of the conclusions made based on the EZ4U assay. Overall, no clear pattern could be observed between cell lines and time points, suggesting once more that DMAS has a rather individual effect, largely differing between cell lines (123).

However, in all cell lines, but especially in MUG-Mel2 and Sbcl2, a certain amount of late apoptotic cells could also be observed. Late apoptotic cells cannot be properly differentiated from necrotic cells within Annexin V / SYTOX Green staining due to the working mechanisms of SYTOX Green. While Annexin V binds to phosphatidylserine, a membrane component flipping from the cytosolic to the extracellular membrane side during apoptosis (131,132), SYTOX Green binds to nucleic acids (133). Once the cell membrane is damaged by necrosis inducing factors, SYTOX Green enters the cell to bind DNA and other nucleic acids. Therefore, in late apoptosis, where both phosphatidylserine is displayed on the outside of the cell and the cell membrane is porous, allowing SYTOX Green inside, cells are stained positive for both dyes. Hence, late apoptotic cells cannot be differentiated from necrotic cells within this assay. Therefore, DMAS might induce apoptosis as well as necrosis in the used tumour cell lines (123).

4.2.3 Cell Cycle

Determining the effects of DMAS treatment on the melanoma cell cycle, it was found that only MUG-Mel1 was significantly affected, showing a shift from G1 to S phase. All other used cell lines were unaffected, thus DMAS might not primarily act over the cell cycle. This stands in strong contrast to previous works like Wu et. al. 2012 (109), who showed a G2/M cell cycle arrest in SMMC-7721 after 24h DMAS treatment. Interestingly, MUG-Mel1 was the cell line showing no *BRAF* nor *NRAS* mutation, and therefore being used as a wild type control. Furthermore, MUG-Mel1 was shown later in this work to be p53 deficient. p53 has a negative regulatory effect on the cell cycle in case of DNA damage, leading to cell cycle arrest (149). The p53 deficiency of MUG-Mel1, together with the observed cell cycle shift, might point towards an altogether different working mechanism of DMAS in this cell line. Furthermore, as MUG-Mel1 had one of the lowest IC_{50} concentrations in the here conducted viability assay, DMAS induced apoptosis might be p53 independent, a hypothesis discussed further in section 4.2.5. However, this effect could not be investigated with any of the assays used in this work and would require further studies, which is beyond the scope of this work (123).

4.2.4 mRNA Sequencing

The apoptosis inducing effect of DMAS was shown with the Annexin V / SYTOX Green assay and verified by active caspase-3 staining. However, those assays did not give a hint which apoptosis pathways were involved.

The two major apoptotic pathways, namely the extrinsic or death receptor pathway and the intrinsic or mitochondrial apoptosis pathway, are activating a caspase cascade leading to disintegration of the cell by formation of apoptotic bodies (134). However, both pathways are independent from each other and therefore require different activation and signal transduction. The extrinsic pathway is activated over cell surface receptors when bound by specific agonists. The intrinsic pathway, in contrast, needs for activation internal signals from certain tumour suppressor genes like p53 or PTEN. It is primarily a reaction of the cell to stress which is too big to handle, for instance in case of unrepairable DNA damage (114,123).

To get a hint towards the pathways involved in DMAS mediated apoptosis as well as further pathways influenced by it, mRNA sequencing was performed with Sbcl2 and WM164 cells. 7891 differentially expressed genes were found in Sbcl2 and 6033 differentially expressed genes were found in WM164. They were sorted out using BH corrected p-values and a cut-off for fold changes. Subsequently they were organized into a few overrepresented pathways and genes, namely the “Apoptosis Signaling Pathway” with its members *FOS*, *JUN*, *TNF* and *BAG3*, the “p53 Pathway” represented by *NOXA* and the “p38 MAPK Pathway” with *MAPK13*.

JUN and *FOS* are oncogenes, driving tumour development (150) and therefore irrelevant for the apoptosis inducing effect of DMAS. *BAG3* is a co-chaperon interacting with heat shock protein 70 and involved in many biological processes, ranging from apoptosis and autophagy induction to cell proliferation. The role of *BAG3* in apoptosis induction is controversial, as upregulation of this gene promotes apoptosis in several tumours while inhibiting it in others (151). Therefore, *BAG3* was not considered for further investigation, leaving *TNF*, *MAPK13* and *NOXA* for further in-depth studies. *MAPK13* and *NOXA* are proteins of the p38 and the p53 intrinsic apoptosis pathways, respectively, (134,141,152), whereas *TNF* is a member of the extrinsic apoptosis pathway (153). DMAS was shown to work over the intrinsic apoptosis pathway by Xiong et al 2013 (112), Wu et al 2012 (109) as well as Shen et al 2012 (117). Therefore, the p53 pathway, including *NOXA*, was chosen for further analysis, rather than the extrinsic apoptosis pathway with *TNF*. Analysis

of the p53 as well as the p38 pathway would go beyond the scope of this work, therefore examination *MAPK13* upregulation was not further pursued. However, Wang and Ma 2015 (111) showed that DMAS induced apoptosis over the mitochondrial pathway by activation of *p38*. Thus, investigation of an involvement of *p38* in DMAS induced apoptosis would be an interesting objective for further studies. Furthermore, *TNF* is responsible not just for apoptosis but also necrosis (154). This would also be an interesting research objective to possibly explain the late apoptotic cells found in the Annexin V / SYTOX assay as well as the necrosis observed in tumour tissues in mouse experiments (123).

4.2.5 RT-qPCR and Western Blots of Melanoma Cells

Following up on the results obtained by mRNA sequencing, RT-qPCR and western blots were performed with apoptosis genes related to the mitochondrial apoptosis pathway. In RT-qPCR, *BAD*, *BAX*, *BCL2*, *NOXA* and *PUMA* were examined, while in western blots, BAK, BAX, BCL2, NOXA, p53 and PUMA were looked upon. NOXA overexpression could be observed in both RT-qPCR and western blots, while PUMA and BCL2 were only overexpressed in some cell lines in RT-qPCR, but not in western blots. Interestingly, p53 was not overexpressed in any cell line, but MUG-Mel1 exhibited p53 deficiency (123).

The obtained results indicated that DMAS induced apoptosis is NOXA dependent. NOXA, a member of the BH3 only proteins, induces apoptosis via the intrinsic mitochondrial pathway by inhibiting BCL2, which is an inhibitor of apoptosis (113). Furthermore, as claimed by Dai et al 2011(155), NOXA might also be able to directly activate BAX and BAK, without the need for BCL2 inhibition. BCL2, a pro-survival gene, is known to inhibit activation of mitochondrial driven apoptosis, and thus should be inhibited for apoptosis induction. Interestingly, no significant differences could be found in BCL2 expression western blots. In RT-qPCR, only Sbcl2 depicted a significant change, an upregulation of BCL2 levels, which would contradict NOXA induced BCL2 inhibition (156). However, as Sbcl2 were the most susceptible cells to DMAS treatment according to viability and apoptosis assays and taken the fact into account that BCL2 was not overexpressed in western blots, the BCL2 overexpression in RT-qPCR might not play a role in DMAS induced apoptosis in this case (123).

Furthermore, NOXA and PUMA are direct downstream targets of p53, which activates both via phosphorylation (113). PUMA was not significantly changed, except in MUG-Mel1 and WM164 cells in RT-qPCR experiments, so it is unlikely that it plays a major role in DMAS induced apoptosis. As NOXA was upregulated, a change in p53 levels would be

expected, which would be necessary for NOXA activation. However, p53 did not depict upregulation in any of the cell lines and was even depleted in MUG-Mel1 cells. Taken together with the high NOXA levels, this could lead to two different conclusions: First, p53 could have undergone an internal shift of the unphosphorylated, inactive form, towards the phosphorylated form without the change of expression levels. This would enable NOXA activation, however, at smaller levels than observed, as NOXA expression is dependent on p53 (157). Anyhow, p53 was depleted in MUG-Mel1 cells, which depicted significant NOXA overexpression and a low IC_{50} concentration, thereby contradicting this hypothesis. Alternatively, DMAS could lead to direct NOXA activation, circumventing p53. Looking at p53 levels, this is more likely and was therefore examined in NOXA silencing experiments in this work. Thus, DMAS would be an interesting candidate drug for treatment of p53 deficient tumours. Looking at the other investigated genes and proteins, namely BAD; BAX and BAK (only western blots), no significant differences could be found in any of the cell lines. Therefore, involvement of those genes or proteins in DMAS mediated apoptosis is unlikely. BAD, an inhibitor of BCL2, would not be needed for apoptosis in case of NOXA overexpression, as NOXA is sufficient for BCL2 inhibition (123,155).

BAX and BAK, on the other hand, are important drivers of the mitochondrial apoptosis pathway, activating the caspase cascade. Both are activated by PUMA or p53 and inhibited by BCL2 (152,158). In case of a NOXA driven apoptosis with no significant overexpression of PUMA or p53, unchanged BAK/BAX levels can only be explained with BCL2 inhibition. Normal BAK, BAX, p53 and PUMA levels would, in case of BCL2 inhibition, be sufficient for induction of apoptosis (118,159,160). Interestingly, publications concerning DMAS induced apoptosis in other cancer types reported BAD, BAX or BCL2 ratios as its primary drivers (109,161,162). Taken, together, this suggests that NOXA upregulation by DMAS might be the sole driver of DMAS induced apoptosis, without the need for changes of other apoptotic proteins.

The hypothesis that NOXA alone is sufficient to induce apoptosis gained support over the last years, making this working mechanism likely. DMAS would not be the first therapeutic using NOXA as primary target for apoptosis induction. In 2012, Kelly et al(163) showed that reovirus therapy induced NOXA expression indirectly via endoplasmic reticulum stress, leading to apoptosis in multiple myeloma cells. Additionally, NOXA was found to mediate cytotoxic effects of various chemotherapeutics (164). In melanoma, the therapeutic effects of bortezomib, a protease inhibitor, could be linked to induced changes of NOXA and Mcl-1 expression levels by the drug (165–167). Interestingly, also MG-132, lactacytsin and epoxomicin, three potent protease inhibitors, induce apoptosis via the

mitochondrial apoptosis pathway, making an involvement of NOXA likely (168). Overall, NOXA seems to be a potent apoptosis inducer, with several therapeutics using it as primary target. NOXA induction was also shown to be linked to apoptosis in this work. Therefore, DMAS induced apoptosis via NOXA overexpression is more than a theoretical possibility (123).

4.2.6 NOXA Knockdown

Examination of NOXA dependent apoptosis induction by DMAS was done by NOXA knockdown experiments. First, western blot analysis confirmed a successful silencing, with NOXA protein expression levels compared between scrambled siRNA and NOXA siRNA transfected cells. Then, active caspase-3 assays were performed to examine whether NOXA knockdown diminishes DMAS treatment efficiency. Cells, treated with DMAS, but no siRNA (No siRNA cells) were compared with DMAS treated cells which were also transfected with scrambled siRNA (Scr. siRNA cells) or NOXA siRNA (NOXA siRNA cells)

Thereby, NOXA knockdown was confirmed to reduce active caspase-3 depicting cells significantly. However, the differences were smaller than expected, especially as the knockdown almost completely diminished NOXA expression levels in “NOXA siRNA cells”. A possible explanation would be that DMAS, apart from NOXA induced apoptosis, also uses the TNF driven extrinsic apoptosis pathway for apoptosis induction, as was found in mRNA sequencing analysis. However, till date, no publications found a connection of DMAS and the extrinsic apoptosis pathway (123).

Another interesting effect was the discrepancy between “No siRNA cells” and “Scr. siRNA cells”. The scrambled siRNA transfected cells depicted slightly higher NOXA levels in western blots and subsequently more apoptosis in the active caspase-3 assay. This difference could have been caused by the transfection itself. The transfection process is rather stressful for cells, thereby making them vulnerable to other stress inducing factors like drugs. As shown in several publications (169,170), only a certain amount of cells survives transfection, and those need a resting time before being used for further experiments. In case of DMAS treatment, no cells were killed during transfection as seen in the controls, but the conducted experiments would not be able to show stress induction levels which do not lead to immediate apoptosis of the cells. Therefore, cell stress upon transfection is likely to be the reason for the different apoptosis values (123).

However, although small, the differences in active caspase-3 depicting cells between “Src siRNA cells” and “NOXA siRNA cells” are significant, confirming that DMAS induced apoptosis via NOXA upregulation.

4.2.7 *In-Vivo* Experiments

Human melanoma xenograft mouse models were used with the aim to find out whether the observed *in-vitro* results could be replicated *in-vivo*. First, pilot experiments were done using 2mg/kg DMAS treatment, followed by the main experiment with bigger mouse cohorts and different DMAS concentrations. Tumours and organs were stained with H&E and KI67 for cell viability and proliferation, respectively.

In the pilot as well as the main experiment, DMAS was found to induce apoptosis / necrosis and sometimes also fibrosis in both Sbcl2 and WM164 derived tumours. The necrotic effect was strongly varying among treated mice. As described above (sections 3.2.2 and 3.3.2), no necrotic effects could be observed in 2D experiments, but necrotic and late apoptotic cells cannot be differentiated in the Annexin V / SYTOX Green assay (as discussed in section 4.2.2). Therefore, it is likely that the late apoptotic cells observed in 2D experiments are necrotic, which would reflect the results gained *in-vivo*. A possible explanation for the necrotic effect of DMAS is treatment time (123).

The 2D Annexin V / SYTOX Green assay showed a shift from apoptotic to late apoptotic cells from 6h to 24h, therefore mouse experiments with DMAS treatment over several weeks would possibly shift the balance towards necrotic cells.

Interestingly, several papers published about DMAS treatment in other cancer types describe only an apoptotic effect of this substance *in-vitro* and *in-vivo* without showing a necrotic effect (108,109). However, Wu et al 2012(109) proved the apoptotic effect of DMAS by showing only a small selected area within the tumour which depicted 100% caspase-3 positive cells. Conveniently, the rest of the tumour was not shown, making a full analysis of its morphology impossible. In contrast, the here presented complete mouse tumour slices showed mixed apoptotic / necrotic areas as well as areas with fibroses and viable tissue.

Furthermore, Fan et al 2012(108) based the apoptosis inducing effect of DMAS on BCL2 and BAX positive tumours but did not show the apoptotic effect directly by H&E or caspase-3 staining. Additionally, Kwak et al 2014(110), showing tumour regression upon

DMAS and irradiation combination treatment, did not specify the type of induced cell death. Overall, the currently available papers make it difficult to confirm a pure apoptosis inducing effect of DMAS, therefore a more diverse working profile, with apoptotic, necrotic and fibrotic areas as shown in this thesis is possible.

Interestingly, no significant differences in tumour area could be observed upon DMAS treatment. Therefore, DMAS led to internal tumour regression, seen by apoptotic / necrotic areas, but did not affect overall tumour size. A possible explanation is fibrosis, which was seen in several tumours. Instead of shrinking, necrotic areas within the tumour could have been replaced with fibroblasts, therefore the overall tumour size would remain constant, leading to the illusion that the tumour was unaffected (123).

Additionally, KI67 staining, performed in several of the main tumours, showed proliferative activity of all non-necrotic areas. As each tumour showed a certain amount of viable KI67 positive areas as well as necrotic areas, a better distribution method delivering the drug to all tumour cells needs to be found to enable more efficient treatment.

Organs were found not to be affected by DMAS, indicating that DMAS has limited side effects if administered directly into the tumour tissue. This hypothesis was also strengthened by measurements of the mouse weight, which was stable throughout the experiments, and mouse behaviour observation, yielding no atypical behaviour.
However, no prediction concerning DMAS side effects, once the drug is administered systemically, can be derived from the conducted assays. Interestingly, no publications till date addressed the issue of side effects, be it in mice or patients. Therefore, it is necessary to conduct further studies focused on those effects (123).

4.3 Conclusion and Outlook

DMAS was applied on chordoma and melanoma cell lines to elucidate its therapeutic potential. Thereby it was found that DMAS reduced cell viability in both cancer types in a dose- dependent manner, in melanoma additionally in a time dependent one. Furthermore, DMAS induced apoptosis in both melanoma and chordoma cells. Concerning affected pathways, only NOXA was significantly upregulated in both cancer types on genetical as well as protein level, with PUMA and BCL2 as possible candidates only for certain cell lines. NOXA knockdown diminished DMAS treatment efficiency in melanoma cells, therefore DMAS induces apoptosis *in-vitro* in a NOXA dependent manner. The results obtained *in-vitro* could be partially reproduced in melanoma human

xenograft models, with an additional strong effect of DMAS on both Sbcl2 and WM164 derived tumours. No side effects of DMAS *in-vivo* could be observed when DMAS was injected directly into the tumour, with organs being unaffected and the mouse weight remaining stable under treatment. However, the necrotic effects of DMAS *in-vivo* need further investigation, as do the affected pathways to fully understand DMAS induced effects in chordoma and melanoma. Taken together, DMAS is a possible new cancer therapeutic for both cancer types.

5 REFERENCES

1. Hanahan D, Weinberg RA. The Hallmarks of Cancer. Cell. 2000;100(1):57–70.
2. WHO. Cancer [Internet]. 2018. Available from: http://www.who.int/en/news-room/fact-sheets/detail/cancer
3. Torre LA, Siegel RL, Ward EM, Jemal A. Global cancer incidence and mortality rates and trends - An update. Cancer Epidemiol Biomarkers Prev. 2016;25(1):16–27.
4. American Cancer Society. Cancer Facts and Figures 2018. ACS. 2018;
5. WHO. Cancer Control and Prevention. 2007;2–13. Available from: http://apps.who.int/iris/bitstream/10665/43575/1/9241547111_eng.pdf
6. NCI. Cancer Stat Facts: Melanoma of the Skin [Internet]. 2016. Available from: http://seer.cancer.gov/%0Astatfacts/html/melan.html
7. Cancer Research UK. Types of cancer [Internet]. 2017. Available from: https://www.cancerresearchuk.org/what-is-cancer/how-cancer-starts/types-of-cancer
8. Bray F, Ferlay J, Soerjomataram I, Siegel R, Torre S, Jemal A. Global Cancer Statistics 2018: GLOBOCAN Estimates of Incidence and Mortality Worldwide for 36 Cancers in 185 Countries. CA CANCER J CLIN. 2018;(1):1–31.
9. Ferlay J, Soerjomataram I, Ervik M, Dikshit R, Eser S, Mathers C, et al. Cancer Incidence and Mortality Worldwide. Int Agency Res Cancer, World Heal Organ. 2013;52(7):405–11.
10. Chordoma Foundation. Understanding Cordoma [Internet]. 2018. Available from: https://www.chordomafoundation.org/understanding-chordoma/
11. National Cancer Institute. Cancer Stat Facts: Bone and Joint Cancer. National Cancer Institute. 2018.
12. Lomas A, Leonardi-Bee J, Bath-Hextall F. A systematic review of worldwide incidence of nonmelanoma skin cancer. Br J Dermatol. 2012;(166):1069–80.

13. Apalla Z, Nashan D, Weller RB, Castellsagué X. Skin Cancer: Epidemiology, Disease Burden, Pathophysiology, Diagnosis, and Therapeutic Approaches. Dermatol Ther (Heidelb). 2017;7:5–19.
14. American Cancer Society. Cancer Facts and Fibures 2008. Am Cancer Soc. 2008;
15. American Cancer Society. Special Section: Rare Cancers in Adults. Amerincan Cancer Soc. 2017;
16. Fitzmaurice C, Allen C, Barber RM, Barregard L, Bhutta ZA, Brenner H, et al. Global, regional, and national cancer incidence, mortality, years of life lost, years lived with disability, and disability-adjusted life-years for 32 cancer groups, 1990 to 2015: A Systematic Analysis for the Global Burden of Disease Study Global Burden . JAMA Oncol. 2017;3(4):524–48.
17. American Cancer Society. What Are Basal and Squamous Cell Skin Cancers? [Internet]. 2018. Available from: https://www.cancer.org/cancer/basal-and-squamous-cell-skin-cancer/about/what-is-basal-and-squamous-cell.html#references
18. Canadian Cancer Society. Types of Non-Melanoma Skin Cancer [Internet]. 2018. Available from: http://www.cancer.ca/en/cancer-information/cancer-type/skin-non-melanoma/non-melanoma-skin-cancer/types-of-non-melanoma/?region=on
19. Lewis K, Weinstock M. Nonmelanoma Skin Cancer Mortality (1988-2000). Arch Dermatol. 2014;140(7):837–42.
20. Samarasinghe V, Madan V. Nonmelanoma Skin Cancer. J Cutan Aesthet Surg. 2012;5(1):3–10.
21. Boukamp P. Non-melanoma skin cancer: What drives tumor development and progression? Carcinogenesis. 2005;26(10):1657–67.
22. Koh HK, Geller AC, Miller DR, Grossbart TA, Lew RA. Prevention and early detection strategies for melanoma and skin cancer - Current status. Arch Dermatol. 1996;132(4):436–43.
23. Parkin DM, Mesher D, Sasieni P. Cancers attributable to solar (ultraviolet) radiation exposure in the UK in 2010. Br J Cancer. 2011;105:66–9.
24. Corrie P, Hategan M, Fife K, Parkinson C. Management of melanoma. Br Med Bull. 2014;111(1):149–62.
25. Xie J, Murone M, Luoh SM, Ryan A, Gu Q, Zhang C, et al. Activating Smoothened mutations in sporadic basal-cell carcinoma. Nature. 1998;391(6662):90–2.
26. Johnson RL, Rothman AL, Xie J, Goodrich L V., Bare JW, Bonifas JM, et al. Human homolog of patched, a candidate gene for the basal cell nevus syndrome. Science (80-). 1996;272(5268):1668–71.
27. McGillis ST, Fein H. Topical treatment strategies for non-melanoma skin cancer

and precursor lesions. Semin Cutan Med Surg. 2004;23(3):174–83.
28. Aamdal S. Current approaches to adjuvant therapy of melanoma. Eur J Cancer. 2011;47(S3):336–7.
29. National Cancer Institute. Cancer Stat Facts: Melanoma of the Skin [Internet]. National Cancer Institute. 2018. Available from: https://seer.cancer.gov/statfacts/html/melan.html
30. Welch HG, Woloshin S, Schwartz LM. Skin biopsy rates and incidence of melanoma: Population based ecological study. Br Med J. 2005;331(7515):481–4.
31. Erdmann F, Lortet-Tieulent J, Schüz J, Zeeb H, Greinert R, Breitbart EW, et al. International trends in the incidence of malignant melanoma 1953-2008-are recent generations at higher or lower risk? Int J Cancer. 2013;132(2):385–400.
32. Linos E, Swetter SM, Cockburn MG, Colditz GA, Clarke CA. Increasing burden of melanoma in the United States. J Invest Dermatol. 2009;129(7):1666–74.
33. Ugurel S, Becker JC. Therapie des inoperabel metastasierten Melanoms. Hautarzt. 2011;62(6):423–9.
34. Maverakis E, Cornelius LA, Bowen GM, Phan T, Patel FB, Fitzmaurice S, et al. Metastatic melanoma – A review of current and future treatment options. Acta Derm Venereol. 2015;95(5):516–24.
35. Yamamoto T, Ueta E, Osaki T. Apoptosis induction by interleukin-2-activated cytotoxic lymphocytes in a squamous cell carcinoma cell line and Daudi cells - Involvement of reactive oxygen species-dependent cytochrome c and reactive oxygen species-independent apoptosis-inducing factors. Immunology. 2003;110(2):217–24.
36. Winder M, Virós A. Mechanisms of Drug Resistance in Melanoma. In: Handbook of Experimental Pharmacology. Springer, Berlin, Heidelberg; 2017.
37. Wilkerson BL. Malignant melanoma. Plast Surg Nurs. 2011;
38. Hayward NK, Wilmott JS, Waddell N, Johansson PA, Field MA, Nones K, et al. Whole-genome landscapes of major melanoma subtypes. Nature. 2017;545(7653):175–80.
39. Hanahan D, Weinberg RA. Hallmarks of cancer: The next generation. Cell. 2011;144(5):646–74.
40. Hodis E, Watson IR, Kryukov G V., Arold ST, Imielinski M, Theurillat JP, et al. A landscape of driver mutations in melanoma. Cell. 2012;150(2):251–63.
41. Flaherty KT, Hodi FS, Fisher DE. From genes to drugs: Targeted strategies for melanoma. Nat Rev Cancer [Internet]. 2012;12(5):349–61. Available from: http://dx.doi.org/10.1038/nrc3218
42. Zhang W, Liu HT. MAPK signal pathways in the regulation of cell proliferation in

mammalian cells. Cell Res. 2002;12(1):9–18.

43. Papp T, Pemsel H, Zimmermann R, Bastrop R, Weiss DG, Schivmann D. Mutational analysis of the N-ras, p53, p16 INK4a , CDK4, and MC1R genes in human congenital melanocytic naevi. J Med Genet. 1999;36(8):610–4.
44. Heppt M V., Siepmann T, Engel J, Schubert-Fritschle G, Eckel R, Mirlach L, et al. Prognostic significance of BRAF and NRAS mutations in melanoma: a German study from routine care. BMC Cancer. 2017;17(1):536.
45. Bastian BC, Kashani-Sabet M, Hamm H, Godfrey T, Moore DH, Bröcker E-B, et al. Gene Amplifications Characterize Acral Melanoma and Permit the Detection of Occult Tumor Cells in the Surrounding Skin. Cancer Res [Internet]. 2000 Apr 1;60(7):1968 LP-1973. Available from: http://cancerres.aacrjournals.org/content/60/7/1968.abstract
46. Tan C, Du X. KRAS mutation testing in metastatic colorectal cancer. World J Gastroenterol. 2012;18(37):5171–80.
47. Dietrich P, Kuphal S, Spruss T, Hellerbrand C, Bosserhoff AK. Wild-type KRAS is a novel therapeutic target for melanoma contributing to primary and acquired resistance to BRAF inhibition. Oncogene. 2018;37(7):897–911.
48. Eskandarpour M, Kiaii S, Zhu C, Castro J, Sakko AJ, Hansson J. Suppression of oncogenic NRAS by RNA interference induces apoptosis of human melanoma cells. Int J Cancer. 2005;115(1):65–73.
49. Gajewski TF, Salama AKS, Niedzwiecki D, Johnson J, Linette G, Bucher C, et al. Phase II study of the farnesyltransferase inhibitor R115777 in advanced melanoma (CALGB 500104). J Transl Med. 2012;10(1).
50. Smalley KSM, Xiao M, Villanueva J, Nguyen TK, Flaherty KT, Letrero R, et al. CRAF inhibition induces apoptosis in melanoma cells with non-V600E BRAF mutations. Oncogene. 2009;28(1).
51. Dhomen N, Marais R. New insight into BRAF mutations in cancer. Curr Opin Genet Dev. 2007;17(1):31–9.
52. Davies H, Bignell GR, Cox C, Stephens P, Edkins S, Clegg S, et al. Mutations of the BRAF gene in human cancer. Nature. 2002;417(6892):949–54.
53. Heidorn SJ, Milagre C, Whittaker S, Nourry A, Niculescu-Duvas I, Dhomen N, et al. Kinase-Dead BRAF and Oncogenic RAS Cooperate to Drive Tumor Progression through CRAF. Cell. 2010;140(2):209–21.
54. Van 't Veer LJ, Burgering BMT, Versteeg R, Boot AJM, Ruiter DJ, Osanto S, et al. N-ras Mutations in Human Cutaneous Melanoma from Sun-Exposed Body Sites. 1989;9(7):3114–6.
55. National Toxicology Program. Ultraviolet-Radiation-Related Exposures Exposure to

Sunlamps or Sunbeds Ultraviolet-Radiation-Related Exposures Studies on Mechanisms of Carcinogenesis. Ultraviolet-Radiation-Related Expo. 2002;(2000).

56. WHO. Solar Ultraviolet Radiation: Global burden of disease from solar ultraviolet radiation. World Heal Organ. 2006;
57. Daya-Grosjean L, Dumaz N, Sarasin A. The specificity of p53 mutation spectra in sunlight induced human cancers. J Photochem Photobiol B Biol [Internet]. 1995;28(2):115–24. Available from: http://www.sciencedirect.com/science/article/pii/101113449507130T
58. Maldonado JL, Fridlyand J, Patel H, Jain AN, Busam K, Kageshita T, et al. Determinants of BRAF Mutations in Primary Melanomas. JNCI J Natl Cancer Inst. 2003;95(24):1878–90.
59. Pollock PM, Harper UL, Hansen KS, Yudt LM, Stark M, Robbins CM, et al. High frequency of BRAF mutations in nevi. Nat Genet. 2003;33(1):19–20.
60. Saldanha G, Purnell D, Fletcher A, Potter L, Gillies A, Pringle JH. High BRAF mutation frequency does not characterize all melanocytic tumor types. Int J Cancer. 2004;111(5):705–10.
61. Cymerman RM, Shao Y, Wang K, Zhang Y, Murzaku EC, Penn LA, et al. De Novo vs Nevus-Associated Melanomas: Differences in Associations With Prognostic Indicators and Survival. J Natl Cancer Inst. 2016;108(10).
62. Jafari M, Papp T, Kirchner S, Kiener U, Henschler D, Burg G, et al. Analysis of ras mutations in human melanocytic lesions: activation of the ras gene seems to be associated with the nodular type of human malignant melanoma. J Cancer Res Clin Oncol. 1995;121(1):23–30.
63. Masters JRW. Human cancer cell lines: fact and fantasy. Nat Rev Mol Cell Biol [Internet]. 2000 Dec 1;1:233. Available from: https://doi.org/10.1038/35043102
64. Lammers T, Kiessling F, Hennink WE, Storm G. Drug targeting to tumors: Principles, pitfalls and (pre-) clinical progress. J Control Release. 2012;161(2).
65. Holliday DL, Speirs V. Choosing the right cell line for breast cancer research. Breast Cancer Res [Internet]. 2011 Aug;13(4):215. Available from: https://doi.org/10.1186/bcr2889
66. Vincent KM, Postovit L-M. Investigating the utility of human melanoma cell lines as tumour models. Oncotarget [Internet]. 2017;8(6):10498–509. Available from: www.impactjournals.com/oncotarget
67. Burdall SE, Hanby AM, Lansdown MRJ, Speirs V. Breast cancer cell lines: Friend or foe? Breast Cancer Res. 2003;5(2):89–95.
68. Dorfman H., Czerniak B, Kotz R, Vanel D, Park Y., Unni K. WHO classification of tumours of bone: Introduction. In: World Health Organization classification of

tumors pathology and genetics of tumors of soft tissue and bone. IARC, Lyon; 2002. p. 226–32.

69. Bone Cancer Research Trust. About Bone Cancer [Internet]. 2014. Available from: https://www.bcrt.org.uk/information/about-bone-cancer/
70. Dorfman HD, Czerniak B. Bone cancers. Cancer. 1995;75(1 S):203–10.
71. Fletcher CD., Bridge J., Hogendoorn P, Mertens F. WHO Classification of Tumours of Soft Tissue and Bone. 4th ed. IARC Press; 2013.
72. Gerrand C, Athanasou N, Brennan B, Grimer R, Judson I, Morland B, et al. UK guidelines for the management of bone sarcomas. Clin Sarcoma Res [Internet]. 2016;6(1):7. Available from: https://doi.org/10.1186/s13569-016-0047-1
73. Wilkins RM, Pritchard DJ, Omer EB, Unni KK. Ewing's sarcoma of bone. Experience with 140 patients. Cancer. 1986;58(11):2551–5.
74. Eriksson B, Gunterberg B, Kindblom LG. Chordoma: A clinicopathologic and prognostic study of a swedish national series. Acta Orthop. 1981;52(1):49–58.
75. Damron T. Dahlin's Bone Tumors: General Aspects and Data on 10,165 Cases. 6th ed. Bone. 2010;
76. Fletcher CDM, Unni KK, Mertens F. World Health Organization Classification of Tumours Pathology and Genetics of Tumours of Soft Tissue and Bone. Cancer. 2002;177(3):96–100.
77. Horten BC, Montague SR. In vitro characteristics of a sacrococcygeal chordoma maintained in tissue and organ culture systems. Acta Neuropathol. 1976;35(1):13–25.
78. Ramesh T, Nagula S V, Tardieu GG, Saker E, Shoja M, Loukas M, et al. Update on the Notochord Including its Embryology, Molecular Development, and Pathology: A Primer for the Clinician. Cureus [Internet]. 2017;9(4). Available from: http://www.cureus.com/articles/6504-update-on-the-notochord-including-its-embryology-molecular-development-and-pathology-a-primer-for-the-clinician
79. Healey JH, Lane JM. Chordoma: a critical review of diagnosis and treatment. Orthop Clin North Am [Internet]. 1989;20(3):417—426. Available from: http://europepmc.org/abstract/MED/2662114
80. Stiller CA, Trama A, Serraino D, Rossi S, Navarro C, Chirlaque MD, et al. Descriptive epidemiology of sarcomas in Europe: Report from the RARECARE project. Eur J Cancer [Internet]. 2013;49(3):684–95. Available from: http://www.sciencedirect.com/science/article/pii/S0959804912007253
81. Stacchiotti S, Sommer J. Building a global consensus approach to chordoma: A position paper from the medical and patient community. Lancet Oncol [Internet]. 2015;16(2):e71–83. Available from: http://dx.doi.org/10.1016/S1470-

2045(14)71190-8

82. McMaster ML, Goldstein AM, Bromley CM, Ishibe N, Parry DM. Chordoma: Incidence and survival patterns in the United States, 1973-1995. Cancer Causes Control. 2001;12(1):1–11.
83. Wiacek MP, Kaczmarek K, Sulewski A, Kubaszewski L, Kaczmarczyk J. Unusual location of chordoma metastasis. Pol Orthop Traumatol. 2014;79(June):47–9.
84. Stacchiotti S, Gronchi A, Fossati P, Akiyama T, Alapetite C, Baumann M, et al. Best practices for the management of local-regional recurrent chordoma: A position paper by the Chordoma Global Consensus Group. Ann Oncol. 2017;28(6):1230–42.
85. Walcott BP, Nahed B V., Mohyeldin A, Coumans JV, Kahle KT, Ferreira MJ. Chordoma: Current concepts, management, and future directions. Lancet Oncol [Internet]. 2012;13(2):e69–76. Available from: http://dx.doi.org/10.1016/S1470-2045(11)70337-0
86. Higinbotham NL, Phillips RF, Farr HW, Hustu HO. Chordoma. Thirty-five-year study at memorial hospital. Cancer. 1967;20(11):1841–50.
87. Hindi N, Casali PG, Morosi C, Messina A, Palassini E, Pilotti S, et al. Imatinib in advanced chordoma: A retrospective case series analysis. Eur J Cancer [Internet]. 2015;51(17):2609–14. Available from: http://www.sciencedirect.com/science/article/pii/S0959804915007443
88. Stacchiotti S, Longhi A, Ferraresi V, Grignani G, Comandone A, Stupp R, et al. Phase II study of imatinib in advanced chordoma. J Clin Oncol. 2012;30(9):914–20.
89. NIH. A Phase 2, Single Arm, European Multi-center Trial Evaluating the Efficacy of Afatinib as First-line or Later-line Treatment in Advanced Chordoma. 2018. p. ClinicalTrials.gov Identifier: NCT03083678.
90. Scheil-Bertram S, Kappler R, Von Baer A, Hartwig E, Sarkar M, Serra M, et al. Molecular profiling of chordoma. Int J Oncol. 2014;44(4):1041–55.
91. Choy E, MacConaill LE, Cote GM, Le LP, Shen JK, Nielsen GP, et al. Genotyping cancer-associated genes in chordoma identifies mutations in oncogenes and areas of chromosomal loss involving CDKN2A, PTEN, and SMARCB1. PLoS One. 2014;9(7).
92. Yakkioui Y, Temel Y, Creytens D, Jahanshahi A, Fleischeuer R, Santegoeds RGC, et al. A Comparison of Cell-Cycle Markers in Skull Base and Sacral Chordomas. World Neurosurg [Internet]. 2014;82(1):e311–8. Available from: http://www.sciencedirect.com/science/article/pii/S1878875013003197
93. Hu Y, Mintz A, Shah SR, Quinones-Hinojosa A, Hsu W. The FGFR/MEK/ERK/brachyury pathway is critical for chordoma cell growth and

survival. Carcinogenesis. 2014;35(7):1491–9.

94. Tamborini E, Virdis E, Negri T, Orsenigo M, Brich S, Conca E, et al. Analysis of receptor tyrosine kinases (RTKs) and downstream pathways in chordomas. Neuro Oncol. 2010;12(8):776–89.
95. De Castro CV, Guimaraes G, Aguiar S, Lopes A, Baiocchi G, Da Cunha IW, et al. Tyrosine kinase receptor expression in chordomas: Phosphorylated AKT correlates inversely with outcome. Hum Pathol. 2013;44(9):1747–55.
96. Newman DJ, Cragg GM. Natural Products as Sources of New Drugs from 1981 to 2014. J Nat Prod. 2016;79(3):629–61.
97. Li-Weber M. New therapeutic aspects of flavones: The anticancer properties of Scutellaria and its main active constituents Wogonin, Baicalein and Baicalin. Cancer Treat Rev. 2009;35(1):57–68.
98. Lomovskaya N, Otten SL, Doi-Katayama Y, Fonstein L, Liu XC, Takatsu T, et al. Doxorubicin overproduction in Streptomyces peucetius: Cloning and characterization of the dnrU ketoreductase and dnrV genes and the doxA cytochrome P-450 hydroxylase gene. J Bacteriol. 1999;181(1):305–18.
99. Zhongzhen Z. An illustrated Chinese materia medica in Hong Kong. School of Chinese Med. Hong Kong Baptist Univ.; 2004.
100. Chen X, Yang L, Zhang N, Turpin JA, Buckheit RW, Osterling C, et al. Shikonin, a component of Chinese herbal medicine, inhibits chemokine receptor function and suppresses human immunodeficiency virus type 1. Antimicrob Agents Chemother. 2003;47(9):2810–6.
101. Chen X, Yang L, Oppenheim JJ, Zack Howard OM. Cellular pharmacology studies of shikonin derivatives. Phyther Res. 2002;16(3):199–209.
102. Andujar I, Recio M, Giner R, Ríos J. Traditional Chinese Medicine Remedy to Jury: The Pharmacological Basis for the Use of Shikonin as an Anticancer Therapy. Curr Med Chem. 2013;
103. Jeung YJ, Kim HG, Ahn J, Lee HJ, Lee SB, Won M, et al. Shikonin induces apoptosis of lung cancer cells via activation of FOXO3a/EGR1/SIRT1 signaling antagonized by p300. Biochim Biophys Acta - Mol Cell Res. 2016;1863(11):2584–93.
104. Trivedi R, Müller GA, Rathore MS, Mishra DP, Dihazi H. Anti-leukemic activity of shikonin: Role of ERP57 in shikonin induced apoptosis in acute myeloid leukemia. Cell Physiol Biochem. 2016;39(2):604–16.
105. He G, He G, Zhou R, Pi Z, Zhu T, Jiang L, et al. Enhancement of cisplatin-induced colon cancer cells apoptosis by shikonin, a natural inducer of ROS in vitro and in vivo. Biochem Biophys Res Commun. 2016;469(4):1075–82.

106. Kretschmer N, Rinner B, Deutsch AJA, Lohberger B, Knausz H, Kunert O, et al. Naphthoquinones from Onosma paniculata induce cell-cycle arrest and apoptosis in melanoma cells. J Nat Prod. 2012;75(5):865–9.
107. Rinner B, Kretschmer N, Knausz H, Mayer A, Boechzelt H, Hao XJ, et al. A petrol ether extract of the roots of Onosma paniculatum induces cell death in a caspase dependent manner. J Ethnopharmacol [Internet]. 2010;129(2):182–8. Available from: http://dx.doi.org/10.1016/j.jep.2010.02.006
108. Fan Y, Jin S, He J, Shao Z, Yan J, Feng T, et al. Effect of β,β-dimethylacrylshikonin on inhibition of human colorectal cancer cell growth in vitro and in vivo. Int J Mol Sci. 2012;13(7):9184–93.
109. Wu Y, Wan L, Zheng X, Shao Z, Chen J, Chen X, et al. Inhibitory Effects of β,β-Dimethylacrylshikonin on Hepatocellular Carcinoma In Vitro and In Vivo. Phyther Res. 2012;26(5):764–71.
110. Kwak SY, Jeong YK, Kim BY, Lee JY, Ahn HJ, Jeong JH, et al. B,B-Dimethylacrylshikonin Sensitizes Human Colon Cancer Cells To Ionizing Radiation Through the Upregulation of Reactive Oxygen Species. Oncol Lett. 2014;7(6):1812–8.
111. Wang HB, Ma XQ. β, β-Dimethylacrylshikonin induces mitochondria-dependent apoptosis of human lung adenocarcinoma cells in vitro via p38 pathway activation. Acta Pharmacol Sin. 2015;36(1):131–8.
112. Xiong Y, Ma XY, Zhang Z, Shao ZJ, Zhang YY, Zhou LM. Apoptosis induced by β,β-dimethylacrylshikonin is associated with Bcl-2 and NF-κB in human breast carcinoma MCF-7 cells. Oncol Lett. 2013;6(6):1789–93.
113. Happo L, Strasser A, Cory S. BH3-only proteins in apoptosis at a glance. J Cell Sci [Internet]. 2012;125(5):1081–7. Available from: http://jcs.biologists.org/cgi/doi/10.1242/jcs.090514
114. Elmore S. Apoptosis: A Review of Programmed Cell Death. Toxicol Pathol. 2007;35(4):495–516.
115. Martinvalet D, Zhu P, Lieberman J. Granzyme A Induces Caspase-Independent Mitochondrial Damage, a Required First Step for Apoptosis. Immunity [Internet]. 2005;22(3):355–70. Available from: http://www.sciencedirect.com/science/article/pii/S1074761305000683
116. Wajant H, Pfizenmaier K, Scheurich P. TNF-related apoptosis inducing ligand (TRAIL) and its receptors in tumor surveillance and cancer therapy. Apoptosis [Internet]. 2002;7(5):449–59. Available from: https://doi.org/10.1023/A:1020039225764
117. Shen XJ, Wang HB, Ma XQ, Chen JH. β,β-dimethylacrylshikonin induces

mitochondria dependent apoptosis through ERK pathway in human gastric cancer SGC-7901 cells. PLoS One. 2012;7(7):1–8.

118. Cory S, Adams JM. The BCL2 family: Regulators of the cellular life-or-death switch. Nat Rev Cancer. 2002;2:647–656.
119. Gellner V, Tomazic PV, Lohberger B, Meditz K, Heitzer E, Mokry M, et al. Establishment of clival chordoma cell line MUG-CC1 and lymphoblastoid cells as a model for potential new treatment strategies. Sci Rep [Internet]. 2016;6(April):1–9. Available from: http://dx.doi.org/10.1038/srep24195
120. Rinner B, Froehlich EV, Buerger K, Knausz H, Lohberger B, Scheipl S, et al. Establishment and detailed functional and molecular genetic characterisation of a novel sacral chordoma cell line, MUG-Chor1. Int J Oncol. 2012;40(2):443–51.
121. Rinner B, Gandolfi G, Meditz K, Frisch MT, Wagner K, Ciarrocchi A, et al. MUG-Mel2, a novel highly pigmented and well characterized NRAS mutated human melanoma cell line. Sci Rep. 2017;7(1).
122. Jahanafrooz Z, Stallinger A, Anders I, Kleinegger F, Lohberger B, Durchschein C, et al. Influence of silibinin and β-β-dimethylacrylshikonin on chordoma cells. Phytomedicine. 2018;49:32–40.
123. Stallinger A, Kleinegger F, Brvar L, Liegl-Atzwanger B, Prokesch A, Durchschein C, et al. β-β-Dimethylacrylshikonin induces Apoptosis in Melanoma Cell Lines by NOXA Upregulation. Manuscr Submitt.
124. Love MI, Huber W, Anders S. Moderated estimation of fold change and dispersion for RNA-seq data with DESeq2. Genome Biol. 2014;15(12).
125. Huang DW, Sherman BT, Lempicki RA. Systematic and integrative analysis of large gene lists using DAVID bioinformatics resources. Nat Protoc. 2009;4(1):44–57.
126. Wang J, Vasaikar S, Shi Z, Greer M, Zhang B. WebGestalt 2017: A more comprehensive, powerful, flexible and interactive gene set enrichment analysis toolkit. Nucleic Acids Res. 2017;45(W1):W130–7.
127. Cory AH, Owen TC, Barltrop JA CJ. Use of an aqueous soluble tetrazolium/formazan assay for cell growth assays in culture. Cancer Commun. 1991;3(7):207–12.
128. Plumb JA, Milroy R, Kaye SB. Effects of the pH Dependence of 3-(4,5-Dimethylthiazol-2-yl)-2,5-diphenyltetrazolium Bromide-Formazan Absorption on Chemosensitivity Determined by a Novel Tetrazolium-based Assay. Cancer Res. 1989;49(16):4435–40.
129. Wang P, Henning SM, Heber D. Limitations of MTT and MTS-based assays for measurement of antiproliferative activity of green tea polyphenols. PLoS One. 2010;5(4).

130. Hasenoehrl C, Schwach G, Ghaffari-Tabrizi-Wizsy N, Fuchs R, Kretschmer N, Bauer R, et al. Anti-tumor effects of shikonin derivatives on human medullary thyroid carcinoma cells. Endocr Connect [Internet]. 2017;6(2):53–62. Available from: http://www.endocrineconnections.com/lookup/doi/10.1530/EC-16-0105
131. Van Engeland M, Nieland LJW, Ramaekers FCS, Schutte B, Reutelingsperger CPM. Annexin V-affinity assay: A review on an apoptosis detection system based on phosphatidylserine exposure. Cytometry. 1998;31(1):1–9.
132. van Genderen H, Kenis H, Lux P, Ungeth L, Maassen C, Deckers N, et al. In vitro measurement of cell death with the annexin A5 affinity assay. Nat Protoc. 2006;1(1):363–7.
133. Lebaron P, Catala P, Parthuisot N. Effectiveness of SYTOX green stain for bacterial viability assessment. Appl Environ Microbiol. 1998;64(7):2697–700.
134. Borner C. The Bcl-2 protein family: Sensors and checkpoints for life-or-death decisions. Mol Immunol. 2003;39(11):615–47.
135. Liu X, Kim CN, Yang J, Jemmerson R, Wang X. Induction of apoptotic program in cell-free extracts: Requirement for dATP and cytochrome c. Cell. 1996;86(1):147–57.
136. Yang J, Liu X, Bhalla K, Kim CN, Ibrado AM, Cai J, et al. Prevention of apoptosis by Bcl-2: Release of cytochrome c from mitochondria blocked. Science (80-). 1997;275(5303):1129–32.
137. Kluck RM, Bossy-Wetzel E, Green DR, Newmeyer DD. The release of cytochrome c from mitochondria: A primary site for Bcl- 2 regulation of apoptosis. Science (80-). 1997;275(5303):1132–6.
138. Chang F, Lee JT, Navolanic PM, Steelman LS, Shelton JG, Blalock WL, et al. Involvement of PI3K/Akt pathway in cell cycle progression, apoptosis, and neoplastic transformation: A target for cancer chemotherapy. Leukemia. 2003;17(3):590–603.
139. Cagnol S, Chambard JC. ERK and cell death: Mechanisms of ERK-induced cell death - Apoptosis, autophagy and senescence. FEBS J. 2010;277(1):2–21.
140. Liu L, Cao Y, Chen C, Zhang X, McNabola A, Wilkie D, et al. Sorafenib blocks the RAF/MEK/ERK pathway, inhibits tumor angiogenesis, and induces tumor cell apoptosis in hepatocellular carcinoma model PLC/PRF/5. Cancer Res. 2006;
141. Berra E, Diaz-Meco MT, Moscat J. The activation of p38 and apoptosis by the inhibition of Erk is antagonized by the phosphoinositide 3-kinase/Akt pathway. J Biol Chem. 1998;273(17):10792–7.
142. McCubrey JA, Steelman LS, Abrams SL, Bertrand FE, Ludwig DE, Bäsecke J, et al. Targeting survival cascades induced by activation of Ras/Raf/MEK/ERK,

PI3K/PTEN/Akt/mTOR and Jak/STAT pathways for effective leukemia therapy. Leukemia [Internet]. 2008 Mar 13;22:708. Available from: https://doi.org/10.1038/leu.2008.27

143. Freeman DJ, Li AG, Wei G, Li HH, Kertesz N, Lesche R, et al. PTEN tumor suppressor regulates p53 protein levels and activity through phosphatase-dependent and -independent mechanisms. Cancer Cell. 2003;3(2):117–30.
144. Vanhaeserbroeck B, Alessi DR. The PI3K–PDK1 connection: more than just a road to PKB. Biochem J. 2000;346(3):561.
145. Haura EB. SRC and STAT Pathways. J Thorac Oncol [Internet]. 2006 Jun 1;1(5):403–5. Available from: https://doi.org/10.1016/S1556-0864(15)31601-4
146. Rawlings JS, Rosler KM, Harrison DA. The JAK/STAT signaling pathway. J Cell Sci [Internet]. 2004 Mar 15;117(8):1281 LP-1283. Available from: http://jcs.biologists.org/content/117/8/1281.abstract
147. Muñoz-Couselo E, Adelantado EZ, Ortiz C, García JS, Perez-Garcia J. NRAS-mutant melanoma: Current challenges and future prospect. Onco Targets Ther. 2017;10:3941–7.
148. Sini MC, Doneddu V, Paliogiannis P, Casula M, Colombino M, Manca A, et al. Genetic alterations in main candidate genes during melanoma progression. Oncotarget. 2018;9(9).
149. Chen J. The Cell-Cycle Arrest and Apoptotic and Progression. 2016;1–16.
150. Angel P, Karin M. The role of Jun, Fos and the AP-1 complex in cell-proliferation and transformation. BBA - Rev Cancer. 1991;1072(2–3):129–57.
151. Rosati A, Graziano V, De Laurenzi V, Pascale M, Turco MC. BAG3: a multifaceted protein that regulates major cell pathways. Cell Death &Amp; Dis [Internet]. 2011 Apr 7;2:e141. Available from: https://doi.org/10.1038/cddis.2011.24
152. Shamas-Din A, Brahmbhatt H, Leber B, Andrews DW. BH3-only proteins: Orchestrators of apoptosis. Biochim Biophys Acta - Mol Cell Res. 2011;1813(4):508–20.
153. Ouyang L, Shi Z, Zhao S, Wang FT, Zhou TT, Liu B, et al. Programmed cell death pathways in cancer: A review of apoptosis, autophagy and programmed necrosis. Cell Prolif. 2012;45(6):487–98.
154. Chu W-M. Mini-review Tumor necrosis factor. Cancer Lett. 2013;328(2):222–5.
155. Dai H, Smith A, Meng XW, Schneider PA, Pang YP, Kaufmann SH. Transient binding of an activator BH3 domain to the Bak BH3-binding groove initiates Bak oligomerization. J Cell Biol. 2011;194(1):39–48.
156. Karim CB, Michel Espinoza-Fonseca L, James ZM, Hanse EA, Gaynes JS, Thomas DD, et al. Structural Mechanism for Regulation of Bcl-2 protein Noxa by

phosphorylation. Sci Rep [Internet]. 2015;5:1–10. Available from: http://dx.doi.org/10.1038/srep14557

157. Oda E, Ohki R, Murasawa H, Nemoto J. Noxa, a BH3-Only Member of the Bcl-2 Family and Candidate Mediator of p53-Induced Apoptosis. Science (80-) [Internet]. 2000;288(80):1053–6. Available from: http://www.sciencemag.org/cgi/content/full/288/5468/1053%5Cnhttp://www.sciencemag.org/cgi/content/full/288/5468/1053#otherarticles%5Cnhttp://www.sciencemag.org/cgi/collection/cell_biol
158. Reed JC. Regulation of apoptosis by bcl-2 family proteins and its role in cancer and chemoresistance. Curr Opin Oncol. 1995;7(6):541–546.
159. Yin C, Knudson CM, Korsmeyer SJ, Van Dyke T. Bax suppresses tumorigenesis and stimulates apoptosis in vivo. Nature. 1997;385(6617):637–40.
160. McCurrach ME, Connor TM, Knudson CM, Korsmeyer SJ, Lowe SW. bax-deficiency promotes drug resistance and oncogenic transformation by attenuating p53-dependent apoptosis. ProcNatlAcadSciUSA. 1997;94(6):2345–9.
161. Green DR, Evan GI. A matter of life and death. Cancer Cell. 2002;1(1):19–30.
162. Adams JM, Cory S. Life-or-death decisions by the Bcl-2 protein family. Trends Biochem Sci. 2001;26(1):61–6.
163. Kelly KR, Espitia CM, Mahalingam D, Oyajobi BO, Coffey M, Giles FJ, et al. Reovirus therapy stimulates endoplasmic reticular stress, NOXA induction, and augments bortezomib-mediated apoptosis in multiple myeloma. Oncogene. 2012;31(25):3023–38.
164. Albert MC, Brinkmann K, Kashkar H. Noxa and cancer therapy: Tuning up the mitochondrial death machinery in response to chemotherapy. Mol Cell Oncol. 2014;1(1).
165. Wolter KG, Verhaegen M, Fernández Y, Nikolovska-Coleska Z, Riblett M, Martin de la Vega C, et al. Therapeutic window for melanoma treatment provided by selective effects of the proteasome on Bcl-2 proteins. Cell Death Differ. 2007;14(9):1605–16.
166. Reuland SN, Goldstein NB, Partyka KA, Smith S, Luo Y, Fujita M, et al. ABT-737 synergizes with Bortezomib to kill melanoma cells. Biol Open. 2012;1(2):92–100.
167. Selimovic D, Porzig BBOW, El-Khattouti A, Badura HE, Ahmad M, Ghanjati F, et al. Bortezomib/proteasome inhibitor triggers both apoptosis and autophagy-dependent pathways in melanoma cells. Cell Signal. 2013;25(1):308–18.
168. Sidor-Kaczmarek J, Cichorek M, Spodnik JH, Wójcik S, Moryś J. Proteasome inhibitors against amelanotic melanoma. Cell Biol Toxicol. 2017;33(6):557–73.
169. Kim TK, Eberwine JH. Mammalian cell transfection: The present and the future. Anal Bioanal Chem. 2010;397(8):3173–8.

170. Li LH, Sen A, Murphy SP, Jahreis GP, Fuji H, Hui SW. Apoptosis induced by DNA uptake limits transfection efficiency. Exp Cell Res. 1999;253(2):541–50.

6 APPENDIX

6.1 Appendix Table 1: Overview over all used chordoma and melanoma cell lines

(Reproduced and modified from (122) with permission of publisher Elsevier and 123)

Cell Line	Tissue Origin
MUG-CC1	Clival
MUG-Chor1	Sacral
UM-Chor1	Clival
U-CH2	Sacral

Cell Line	NRAS	BRAF
MUG-Mel1	WT	WT
MUG-Mel2	pQ61K	WT
Sbcl2	Q61l	WT
WM164	WT	V600E
WM793	WT	V600E

6.2 Appendix Table 2: RT-qPCR Primers

(Modified from 123).

Primer	F 5‘ to 3'	R 5' to 3'	Tm (F.R)
ACTB	GAACGGTGAAGGTGACAGCAG	AGGATGGCAAGGGACTTCCTG	(61.47, 61.81)
BAD	GAGGATCCGTGCTGTCTCCTTTG	AAACCCAAAACTTCCGATGGGAC	(63.08, 61.57)
BAX	ATGCGTTTTCCTTACGTGTCTG	TCAAGGTCACAGTGAGGTCAG	(59.52, 59.31)
BCL2	CGACTCCTGATTCATTGGGAAG	CAAATGCATAAGGCAACGATCC	(58.80, 58.63)
BIM 1/6	TAACGCTTACTATGCAAGGAGG	GTCTTCGGCTGCTTGGTAAT	(60.10, 58.40)
BIM 9	AACCACTATCTCAGTGCAATGG	TTGACTATGGTGGTGGCCA	(60.10, 57.50)
BID	GGAACCGTTGTTGACCTCAC	GAGGAGCACAGTGCGGAT	(60.50, 58.40)
GAPDH	TGGTATCGTGGAAGGACTCATG	AGTAGAGGCAGGGATGATGTTC	(59.57. 59.30)
NOXA	CCAGCAGAGCTGGAAGTCGAGTG	GATGCAGTCAGGTTCCTGAGCAG	(65.14. 63.33)
PUMA	GACCTCAACGCACAGTACGAG	AGGAGTCCCATGATGAGATTGT	(60.99. 58.61)

6.3 Appendix 3: Reagent Preparation for Western Blot

<u>10x TBS (1l):</u>

31.52g Tris-base

80.06g NaCl

pH 7.6

1x TBST (1l):

100ml 10x TBS

1ml Tween20

900ml dH_2O

pH 7.6

10x Transfer Buffer (1l)

58.15g Tris-base

29.3g Glycin

1l dH_2O

pH 7.4

1x Transfer Buffer (1l)

100ml 10x Transfer Buffer

100ml methanol

800ml dH_2O

pH 7.4

6.4 Appendix 4: Material List

Material and Devices

Material and Devices	Company
0.2ml PCR Tube	Eppendorf
1.4ml Mirconic tubes	Micronic
1.5% Seakem LE agarose	Lonza
1.5ml DNA Low Binding Tubes	Eppendorf
15ml Centrifugation Tubes	VWR
1x Tris-Acetate-EDTA Electrophoresis Buffer	Thermo Fisher Scientific
2100 Bioanalyzer	Agilent
2x Laemmli Sample Buffer	Bio-Rad Laboratories
50ml Centrifuge Tube	VWR
6x MassRuler DNA Loading Dye	Thermo Fisher Scientific
ABI3730 Genetic Analyzer	Applied Biosystems
Accutase	Gibco
Acetonitrile	Sigma-Aldrich

Alexa Fluor® 647 Rabbit Anti-Active Caspase-3	BD Biosciences
Annexin V Pacific Blue	BioLegend
Bovine Serum Albumin	Thermo Fisher Scientific
CASY TT	Omni Life Science
Cell Staining Buffer	Biolegend
Cell Titer 96® Aqueous Non-Radioactive Cell Proliferation Assay Kit	Promega
CFX384 Real Time Thermal Cycler	Bio-Rad Laboratories
Chamber Slides	BD Biosciences
ChemiDoc Touch	Bio-Rad Laboratories
Chloroform	Sigma-Aldrich
Cytofix/Cytoperm	BD Biosciences
CytoFLEX Flow Cytometer	Beckman Coulter
CytoFLEX flow cytometer	Beckman Coulter
DharmaFECT-2	Dharmacon
Dispase-2	Hoffmann - La Roche
DMEM	Gibco
Ethanol	Merck
EZ4U Cell Proliferation and Cytotoxicity Assay	Biomedica
Fast Ruler Low Range DNA Ladder	Thermo Fisher Scientific
Femto Maximum Sensitivity Reagent	Thermo Fisher Scientific
Fetal Bovine Serum	Biochrom
Filter Papers	Bio-Rad Laboratories
Fixation/Permeabilization Solution Kit	BD Biosciences
Glycin	Carl Roth
Hamilton STARLet	Hamilton Robotics
High-Capacity cDNA Reverse Transcription Kit	Applied Biosystems
HiSeq2500	Illumina
HMB45	Dako
Hot FirePol Evagreen qPCR Supermix	Solis Biodyne
IMDM	Gibco
Immobilon-P PVDF 0.45µM Nitrocellulose Membranes	Merck

Insulin-Transferrin-Selenium	Invitrogen
L-Glutamine	Invitrogen
LSRII Flow Cytometer	BD Biosciences
Melan-A	Dako
Melanocyte Growth Medium M2 with Supplements	Biomedica
Methanol	Merck
miRNeasy Mini Kit	Qiagen
NanoDrop2000	Thermo Fisher Scientific
Omega SPECTROstar Photometer	BMG Labtech
OneStep PCR Inhibitor Removal Kit	Zymo Research
Page Ruler Plus Prestained Protein Ladder	Thermo Fisher Scientific
Page Ruler Plus Prestained Protein Ladder	Thermo Fisher Scientific
Paraffin	Sanova
Penicillin/Streptomycin	Invitrogen
PhosSTOP	Sigma-Aldrich
Pierce BCA Protein Assay Kit	Thermo Fisher Scientific
PonceauS Solution	Sigma-Aldrich
PowerPlex 16HS System	Promega
Propidium Iodide	Sigma-Aldrich
Protease Inhibitor Cocktail	Sigma-Aldrich
QIAamp DNA Mini Kit	Qiagen
RIPA Lysis Buffer	Thermo Fisher Scientific
RNAse A	Fermentas
RNase free DNase Kit	Qiagen
RPMI	Gibco
S100	Dako
siRNA AF488	Qiagen
Skim Milk Powder	Sigma-Aldrich
SMA	Sigma-Aldrich
Sodium Citrate	Sigma-Aldrich
SybrGold	Thermo Fisher Scientific
SYTOX Green	Life Technologies
T100 Thermal Cycler	Bio-Rad Laboratories

Thermal Cycler	Bio-Rad Laboratories
Thermal Cycler	VWR
Trans-Blot SD Semi-Dry Transfer Cell	Bio-Rad Laboratories
Trans-Blot SD Semi-Dry Transfer Cell	Bio-Rad Laboratories
Tris-Base	Sigma-Aldrich
Triton X-100	Sigma-Aldrich
TruSeq Stranded mRNA Kit	Illumina, San Diego, USA
TrypLE Express	Gibco
Tween20	Sigma-Aldrich
Varian R PrepStar SD-1	Agilent Technologies
VenorGeM Mycoplasma Detection Kit for conventional PCR	Minerva Biolabs
XT Bis-Tris Protein Gels	Bio-Rad Laboratories
XT Mes 20x Running Buffer	Bio-Rad Laboratories

Mice Strains, Primary Cells and Cell Lines

Cells and Mice	**Obtained from**
Adult Human Fibroblasts	Beate Rinner, Medical University of Graz
Juvenile Melanocytes	Isolated during the project
MRC-5	ATCC
MUG-CC1	Beate Rinner, Medical University of Graz
MUG-Chor1	Beate Rinner, Medical University of Graz
MUG-Mel1	Beate Rinner, Medical University of Graz
MUG-Mel2	Beate Rinner, Medical University of Graz
NU(NCr)-Foxn1 immunodeficient mice	Charles River Laboratories
NU-Fox nu immunodeficient mice	Charles River Laboratories
Sbcl2	Helmut Schaider, Wistar Institute
U-CH2	Silke Brüderlein, University of Ulm
UM-Chor1	Chordoma Foundation
WM164	Helmut Schaider, Wistar Institute
WM793	Helmut Schaider, Wistar Institute

Software

Software	**Company or Authors**
WebGestalt 2017	Wang et al., 2017
GO View	Wang et al., 2017

FACS Diva 1.0	BD Biosciences
ABI Genemapper Software Version 4.0	Applied Biosystems
CytExpert 1.2.10.0	Beckman Coulter
ImageLab 5.2	Bio-Rad Laboratories
DeSeq2 3.6	Love, Huber and Anders, 2014
DAVID 6.8	Huang, Sherman, and Lempicki, 2009
SigmaPlot 13.0	Systat Software GmbH
Excel 16.0	Microsoft

Antibodies and Reagents

Antibodies and Reagents	**Company**	**Cat Nr.**
ACTB	Santa Cruz Biotechnology	47778
AKT	Cell Signaling Technology	9272
Annexin V Pacific Blue	Biolegend	422201
BAD	Cell Signaling Technology	9292
BAK	Cell Signaling Technology	6947
BAX	Cell Signaling Technology	5023
BCL2	Cell Signaling Technology	3498
BCL-XL	Cell Signaling Technology	2764
Caspase-3	BD Biosciences	560626
Cytochrome C	Santa Cruz BioTechnology	8385
ERK	Cell Signaling Technology	4695
GAPDH	Cell Signaling Technology	2118
Melan-a	Dako	IR633
NOXA	Thermo Fisher Scientific	MA1-41000
P53	Santa Cruz Biotechnology	Sc-126
pAKT	Cell Signaling Technology	9271
pERK	Cell Signaling Technology	4370
pSTAT3 (Tyr705)	Cell Signaling Technology	9145

PUMA	Cell Signaling Technology	4976
S100	Dako	GA50461
SMA	Sigma-Aldrich	A2547
STAT3	Cell Signaling Technology	4904
Sytox Green	Thermo Fisher Scientific	S34860
Vinculin	Thermo Fisher Scientific	PA5-29688

7 PUBLICATIONS BASED ON THIS THESIS

Part of this thesis was published in Jahanafrooz Z, Stallinger A, Anders I, Kleinegger F, Lohberger B, Durchschein C, Bauer R, Deutsch A, Rinner B, Kretscher N. 2018. Influence of silibinin and β-β-dimethylacrylshikonin on chordoma cells. Phytomedicine. 2018;49:32–40.

Part of this thesis is currently submitted for publication as Stallinger A, Kleinegger F, Brvar L, Liegl-Atzwanger B, Prokesch A, Durchschein C, Bauer R, Deutsch A, Kretschmer N, Rinner B. β-β-Dimethylacrylshikonin induces Apoptosis in Melanoma Cell Lines by NOXA Upregulation, manuscript submitted